Masters Theses   Graduate School

5-2000

Nickel-titanium shape-memory alloy reinforced aluminum composites

Glen Andrew Porter

Follow this and additional works at: https://trace.tennessee.edu/utk_gradthes

To the Graduate Council:

I am submitting herewith a thesis written by Glen Andrew Porter entitled "Nickel-titanium shape-memory alloy reinforced aluminum composites." I have examined the final electronic copy of this thesis for form and content and recommend that it be accepted in partial fulfillment of the requirements for the degree of Master of Science, with a major in Metallurgical Engineering.

                                              Peter K. Liaw, Major Professor

We have read this thesis and recommend its acceptance:

Raymond A. Buchanan, Thomas T. Meek, Terry M. Tiegs

                                              Accepted for the Council:
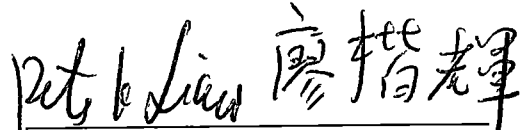   Carolyn R. Hodges

                         Vice Provost and Dean of the Graduate School

(Original signatures are on file with official student records.)

To the Graduate Council:

I am submitting herewith a thesis written by Glen Andrew Porter entitled "Nickel-Titanium Shape-Memory Alloy Reinforced Aluminum Composites". I have examined the final copy of this thesis for form and content, and recommend that it be accepted in partial fulfillment of the requirement for the degree of Master of Science, with a major in Metallurgical Engineering.

Dr Peter K Liaw, Major Professor

We have read this thesis
and recommend its acceptance:

Dr Raymond A. Buchanan

Dr Thomas T. Meek

Dr Terry N Tiegs

Accepted for the Council:

Associate Vice-Chancellor and
Dean of the Graduate School

Nickel-Titanium Shape-Memory Alloy Reinforced Aluminum Composites

A Thesis Presented for the Master of Science Degree

The University of Tennessee, Knoxville

Glen Andrew Porter

May 2000

Abstract

The purpose of the study is to create an NiTi/aluminum metal matrix composite (MMC) material which will have mechanical properties superior to those of the aluminum matrix. The goal is to fabricate a composite material by dispersing a shape-memory alloy (NiTi) in the form of a powder, into an aluminum matrix, using isostatic or hot pressing, powder-metallurgy processing techniques. The author wishes to obtain a composite material with a satisfactory density (> 97% of theoretical density), greater strength, and improved fatigue resistance, relative to the aluminum matrix.

When the shape-memory alloy particles are embedded in the matrix, the shape-memory effect is utilized by deforming the composite material below the M_s temperature, (around -20°C or -4°F), which will also deform each NiTi particle within the matrix (since the martensitic phase of NiTi has a much lower yield strength than aluminum at that temperature). Upon reheating to the austenite phase, the NiTi will return to it's original shape, (within 8-9% of deformation), embedded within the aluminum matrix which has a much lesser degree of thermal strain. This action will create residual, internal stresses around each NiTi particle, tensile stresses in the longitudinal and transverse directions, and compressive stresses in the through-thickness direction, which will strengthen the material in a similar fashion as thermal stresses strengthen a ceramic particle reinforced metal matrix composite upon cooling from the manufacturing temperature.

In order to accomplish the objective, the NiTi powder may first be reduced in size to enhance bonding and deformation characteristics. This is done through a tedious and time-consuming mechanical milling process. Also, since the shape-memory effect is so strongly dependent on the composition of the NiTi, the powder must first be treated with a coating to resist the diffusion of the matrix into the NiTi particles during pressing. Oxide and nitride coatings have been investigated with moderate success. The process of hot pressing also lends difficulty because the time at elevated pressures and temperatures results in further diffusion. However, without a sufficient pressure and temperature in hot pressing, a good density cannot be achieved. Internal voids due to poor densification may become sites for crack initiation upon loading, thus weakening the material.

Several different NiTi/Al composites have been studied. The NiTi powders have been treated in a couple different manners. One method reduces the particle sizes and roughens their shape. A heat-treatment procedure has been developed in order to produce a surface oxide coating, which helps prevent diffusion during hot pressing. Different aluminum powders have been investigated also. The size of the aluminum particles has proved to be very influential in affecting the quality of composite materials produced. This finding is important because the failure of this kind of composite has been shown to be matrix-dominated.

Some physical and mechanical properties of the NiTi/Al composite material have been characterized by Digital Scanning Calorimetry (DSC), Scanning Electron Microscopy (SEM), and through tensile and fatigue testing. There is a considerable increase in the yield strength, the ultimate strength, and the fatigue resistance due to the

addition of the NiTi powder into the matrix. However, the elastic modulus drops slightly in some materials, perhaps due to a phenomenon called *stress-induced martensite*, which is common in the NiTi shape-memory alloy.

Table of Contents

PART III.

PHYSICAL CHARACTERIZATION

PART IV.

MECHANICAL CHARACTERIZATION

PART V.

FINAL CONCLUSIONS

PART VI.

ACKNOWLEDGEMENTS

Index of Equations

Index of Figures

Index of Tables

PART I.

AN INTRODUCTION TO THE SHAPE-MEMORY EFFECT

AND COMPOSITE MATERIALS

1.1 Introduction

A shape-memory alloy (SMA) has the unique property of being able to recover its original shape after deformation has occurred. Once only regarded as a phenomenon, it has been proven that the unique shape-memory behavior is due to a phase change in the material. This phase change from a softer martensite to a harder austenite is temperature-dependent, and its micromechanism has been theoretically explained in detail by authors, such as Wayman[1] and Nishiyama.[2]

For example, if a shape-memory alloy is cooled below a certain temperature labeled as the martensitic starting temperature (M_s), a phase change to martensite occurs. If there is deformation of the material in the martensite phase before the material is heated to another specific temperature (usually higher than the M_s temperature) labeled as the austenitic starting temperature (A_s), the material will return to its original shape. Up to 6 to 10 % deformation can be recovered through this process.

The shape-memory alloy, NiTi, was discovered in the late 1950s, and the shape-memory effect was, at first, thought to occur only in this alloy. However, further research and investigations through the years have shown that many binary and ternary alloys exhibit the shape-memory effect. Some of the more common alloys include AgZn, AgCd, AuCd, CuAuZn, CuAl, CuAlNi, CuSn, CuZn, CuZnAl, CuZnGa, CuZnSi, CuZnSn, FeBe, FePt, NbTi, and NiAl.[1-3] Since their discovery, shape-memory alloys have grown in commercial use.[4] Their unique temperature-induced shape-change

2

property has led to their use in many widespread applications, including hydraulic fittings, rivets, temperature-control devices, and surgical instruments.

Tiegs,[3] at ORNL, had the idea of dispersing the shape-memory alloy, in the form of a powder, throughout an aluminum matrix in the hope of using the shape-memory effect to achieve strengthening in the aluminum matrix. Some work in this field has already been done using NiTi *fibers*,[5] but only one source[6] has been found on this subject using NiTi *powders*. Since the funding support was received at the Oak Ridge National Laboratory (ORNL) in 1996, much research has been done to bring this idea to fruition. The actual development of such a material has been lengthy and obstacle-ridden. Some of the major problems encountered in the production of the material include:

1. Insufficient sample density due to inadequate powder compaction in a die mold.

2. Brittle intermetallic compounds forming from reactions between the NiTi and the aluminum matrix.

3. Loss of the shape-memory effect due to material processing.

4. Precise and time-consuming production processes.

However, slow progress has been made in the development and subsequent testing of such a material. These difficulties have been successfully overcome by the author, as shown by the tests in the present study, who proved that the composite material had a 42% gain in strength over the matrix material, with an increased resistance to fatigue. For some materials, the fatigue life has been extended up to four orders of magnitude. The

following discourse describes the theory, problems, laboratory processing, experimental

results, and discussion of this endeavor.

1.2 Aluminum And Aluminum Alloys [7]

In our work, aluminum possessed a major volume content of the composite [90 volume percent (vol. %)]. It was chosen as a matrix material because of its high commercial use, low density, and thus, marketability. Our main goal was to increase the yield strength and the fatigue resistance of the aluminum by combining it with the NiTi shape-memory alloy in the form of a metal matrix composite.

Most composites that have an aluminum matrix are not made with pure aluminum, but with aluminum alloys. However, pure aluminum was adopted as a matrix material in an effort to avoid complications arising from the reaction of NiTi with aluminum alloying elements, such as copper. Simplifying the composition of the entire composite to three elements eliminated the problem of identifying phases and constituent elements for the initial work. Nevertheless, it is of interest to describe other forms of aluminum alloys that may be utilized, namely one that is age-hardenable.

An aluminum alloy with a copper content of 4 wt.% copper, such as Aluminum 2024, has a property known as *age hardenability*. [7-10] If this alloy is heated above 500°C (930°F), all of the copper will be dissolved in a solid solution. When the alloy is rapidly quenched in water, there is not enough time for a phase transformation to occur, leaving a supersaturated solution with the potential for precipitation. The material in this form is soft and pliable. Aging takes place if the material is left at temperatures between 20°C

5

(68°F) and 180°C (360°F) for a period of time. During aging, a series of transition phases precipitate within the matrix. Guinier-Preston zones are first formed, when the copper in solution diffuses into localized areas of higher concentration in the matrix. This is followed by the θ'' phase, which is a coherent crystal structure of a higher copper concentration. Then, the θ' phase is formed as a semi-coherent second-phase, which results from further copper diffusion. Finally, the stable phase, θ, is generated, producing an incoherent second phase of a higher copper concentration in the matrix. The precipitation of this second phase produces a higher concentration of misfit strains, which results in the hardening of the material due to the change in the crystal structure.

The composite material was subjected to a short heat treatment during the hot-pressing procedure. This heat treatment may accomplish several results if an age-hardenable aluminum alloy is used as a matrix material. First, if Aluminum 2024 [4.5 weight percent copper (wt.% Cu)] is being used, a heat treatment is conducted in order to form a solid solution in the matrix. This procedure forms a solid solution in the material and the precipitates are removed. The lack of precipitates yields a softer material, which facilitates deformation. From this, the process of age hardening, which was discussed earlier, can begin again. Also, the heat treatment promoted a controlled amount of grain growth which enhances interfacial bonding between the aluminum matrix and the NiTi particles. Fortunately, only a short amount of time is required for these processes to occur, leaving a limited extent of diffusion in the composite.

The presence of the NiTi particulates may also influence the aging characteristics of the material. Salvo, Suery, and Decomps[9] produced a silicon carbide reinforced 6061 aluminum composite using compocasting followed by a rapid complete remelting before a pressurized solidification. They found that the presence of a particulate reinforcement in this age-hardenable aluminum alloy affected the rate of aging. Generally, the presence of a reinforcement often accelerated the aging kinetics, but under a certain transition temperature, the inhibition of the GP zone formation slowed precipitation and reduced the aging rate. However, it is mentioned that Nieh and Karlack[10] found a systematic acceleration of aging in a 6061 Al reinforced with B_4C particles, produced using powder-metallurgy techniques.

Composite samples made with age-hardenable aluminum alloy matrices were developed and manufactured during the course of this study, but none were successful in retaining the shape-memory effect, due to the diffusion of copper, producing unwanted phases. As a result, this alloy was not continued to be used as a matrix material in developing a composite material and tensile test specimens. Further work needs to be done to improve surface coatings, interfaces, and diffusion barriers, before this material may be considered for use as a matrix material for a NiTi reinforced composite material.

1.3 A Short History and Current Applications of Shape-Memory Alloys[1,11]

Since the introduction of shape-memory alloys (SMAs) in the 1950s, the demand for them has been growing slower than expected. This is mainly due to the fact that the development of the alloys is still proceeding after having been introduced to industry. The cost of producing such alloys remains high. Demand for the alloy is stifled because of the lack of faith in the shape-memory effect. This is due to a limited amount of development that has taken place. As a result, there is not enough interest or revenue from industry to support the ongoing research in the further development of the alloys. A cycle of stagnation prevails. Surprisingly, even though the shape-memory effect is so remarkable in character, poor marketing and public relations have further hampered the growth of this family of alloys. However, success in marketing is slowly growing, due to a better selection of certain SMAs for specific functions, and also due to the growing volume and reliability of technical data available on the alloys. A great number of small companies are developing their own niches in a slowly steadying market. Table 1.3.1 names several of the many applications for SMAs in a plethora of fields.

Table 1.3.1: Applications of SMAs in Science and Industry[11]

1. **Aircraft and Space Exploration**
   - antenna opening
   - high damping parts
   - Hubble telescope
   - release mechanisms
   - triggering device for the separation of auxiliary fuel tanks for jet fighters

2. **Arts, Toys, and Gadgets**
   - memory box
   - model railways
   - sculptures
   - thermobile

3. **Automobile Industry**
   - cold start performance
   - fuel injection
   - rattling noise reduction
   - ventilation and climate control

4. **Composite Materials**
   - AMM (Active Modal Modification)
   - ASET (Active strain energy tuning biased actuators)

5. **Domestic Appliance Industry**
   - automatic steam vent for cooking utensils
   - electric kettle switch
   - fire shield damper
   - lamp robot with memory metal drivers, controlled by means of speech recognition

6. **Electronic Engineering**
   - circuit breakers
   - connectors
   - gas decharge switch
   - wire connectors

7. **Mechanical Engineering**
   - actuator for micro-valve control
   - bearings with adjustable lubricating oil supply
   - microactuators
   - nuclear power plant applications
   - optical fiber splice
   - robot actuators

   - rock blasting
   - reusable pseudoelastic sealing rings for use in vacuum or corrosive atmosphere

8. **Medical Applications**

   (a) *Implants*
   - adjustable dental implants
   - porous pseudoelastic tissue
   - pseudoelastic armature wire for the fixation of an artificial hip with automatic correction when bone necrosis occurs
   - pseudoelastic dental arch wires
   - pseudoelastic scoliosis correction system

   (b) *Medical Tools*
   - guide wires for catheters
   - mounting device for intraocular lenses
   - pseudoelastic catheter coils
   - remote controlled closing system for small blood vessels, etc.

   (c) *Tools for prosthesis and the disabled*
   - Braille system
   - intramedullary fixation mail
   - revalidation equipment for rheumatism patients

9. **Safety Technology**
   - gas valves
   - oil well valves
   - overheating protection system
   - removable and self-locking fire-break ceilings
   - restorable heat sensitive elements

10. **Sensors, Heating, and Ventilation Engineering**
    - adjustments of flaps or slats
    - air discharge flaps in air conditioning plants
    - automatic ventilation
    - solar actuator used for automatic adjustment of venetian blinds
    - thermomarker

9

1.4 Understanding The Nickel-Titanium Shape-Memory Behavior

It is important to establish a framework by which the reader may become accustomed to the nature of the remarkable shape-memory behavior, and its effect on the matrix. This chapter provides a basic background of shape-memory alloys (SMAs). As stated earlier, Nickel-Titanium is one of the most commonly used SMAs. A more detailed description of the specific physical properties of NiTi shape-memory alloys may be found in the following Table.

During the lengthy course of research, several physical constants were referred to on a continual basis. It became expedient to list these properties in a single place for easy reference. On the following page, (Table 1.4.1), is a compilation of such lists, which may be informative to the reader.

Martensitic Transformations in Shape-Memory Alloys

As previously stated, the remarkable performance of a shape-memory alloy is due to a martensitic phase transformation within the microstructure of the material. Upon an inspection of the microstructure of the material transforming during cooling, one may see the face-centered-cubic austenite changing to a body-centered-tetragonal martensitic crystal structure. The atomic structure of the martensite is ordered and is produced from an ordered parent (austenite) as the transformation is diffusionless. Wayman[1] states,

Table 1.4.1: The Basic Physical Properties of NiTi Powders[12]

Composition:

    For superelasticity: 49.0-49.4 at.% Ti

    For shape memory: 49.7-50.7 at.% Ti

        (If less than 49.4 at.% Ti, the crystal structure is unstable.)

$M_s = A_s - (25 \text{ to } 50°C)$

Coefficient of thermal expansion:

    for martensite: $\alpha = 6.6 \times 10^{-6} \text{m./}°C$

    for austenite: $\alpha = 11 \times 10^{-6} \text{m./}°C$

Volume change from austenite to martensite = -0.16%

    (Particles will "grow" in size from the martensite to austenite.)

Density: 6.45 - 6.5 g/cm^3 (0.233 lb./in.^{3})

Electrical resistivity:

    for martensite: $\rho = 76 \times 10^{-6}$ ohm-cm

    for austenite: $\rho = 82 \times 10^{-6}$ ohm-cm

Melting Temperature: $T_m = 1,310°C$ (2,390°F)

Poisson's ratio: $\nu = 0.33$

Ultimate Strength:

    for martensite: $\sigma_u = 120\text{-}160$ MPa (17.4-23.2 ksi) for binary alloys, and

        as low as 60-90 MPa (8.7-13.1 ksi) for NiTiCu alloys

Yield strength:

    for martensite: $\sigma_y = 70\text{-}140$ MPa (10-20 ksi)

    for austenite: $\sigma_y = 195\text{-}690$ MPa (28-100 ksi)

Young's Modulus:

    for martensite: E = 40 GPa (5.8 Msi)

    for austenite: E = 75 GPa (10.8 Msi)

...the various shape-memory materials are found to have common characteristics, such as atomic ordering, a thermoelastic martensitic transformation that is crystallographically reversible, and a martensite phase that forms in a self-accommodating manner.

Figure 1.4.1 explains the behavior of the crystallographic and physical changes that take place under the transformation. This figure shows a plot of property change vs. temperature for shape-memory alloys. As a SMA cools, it follows the A_f M_s M_f curve, forming martensite in the process, where A_f is the austenitic finishing temperature, M_s is the martensitic starting temperature, and M_f is the martensitic finishing temperature.
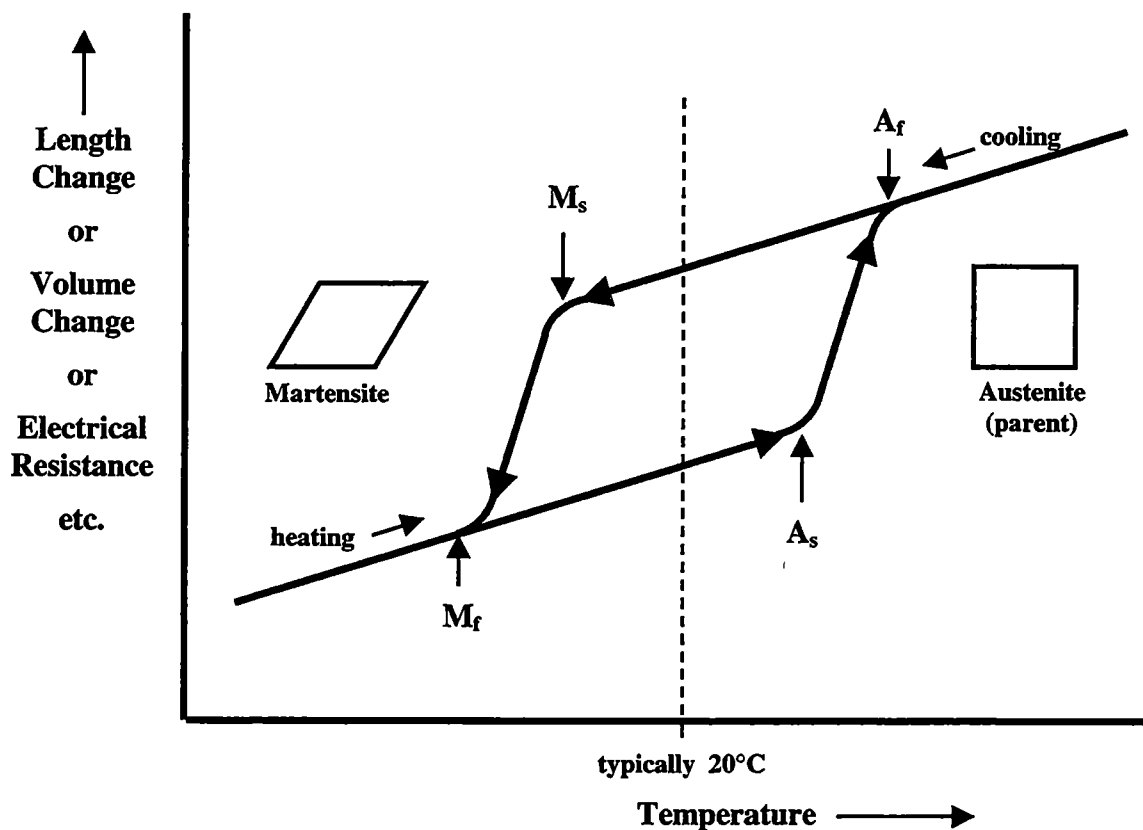
Figure 1 4 1 · The properties of the NiTi SMA phase transformation behavior as a function of temperature Note the hysteresis loop (Wayman[1])

No macroscopic shape change takes place during this process although on a microscopic level, there is crystallographic deformation. When the specimen is deformed below the M_f temperature, it remains deformed until being heated. Upon reheating, it follows the M_f A_s A_f curve, where A_s is the austenitic starting temperature, reverting to the austenite in the process. As the SMA reverts to the austenitic, a face-centered-cubic crystal structure is formed, and the original macroscopic shape is recovered. There is no subsequent shape change if the SMA is again cooled below the M_s temperature, except under certain conditions of applied stresses. This topic will be considered in more detail later, (see *Stress-Induced Martensite*). Deformation in the martensite phase must be repeated to utilize the shape-memory effect again. Note that there is approximately a 20°C difference between M_f and A_f in NiTi, and that between these two temperatures, there exists a hysteresis loop (Figure 1.4.1).

Figure 1.4.2 [1] shows the three-dimensional, stress-strain-temperature diagram and the shape-memory behavior of NiTi deformed at various temperatures. In the figure, the temperature drops from the austenitic in the foreground to the martensitic in the background. The graph in the foreground presents the behavior in the austenitic phase, while the graph in the background indicates the behavior in the martensitic phase. Note that the martensitic has a lower yield strength than the austenitic, and that the yield strength slowly drops over the transition range.
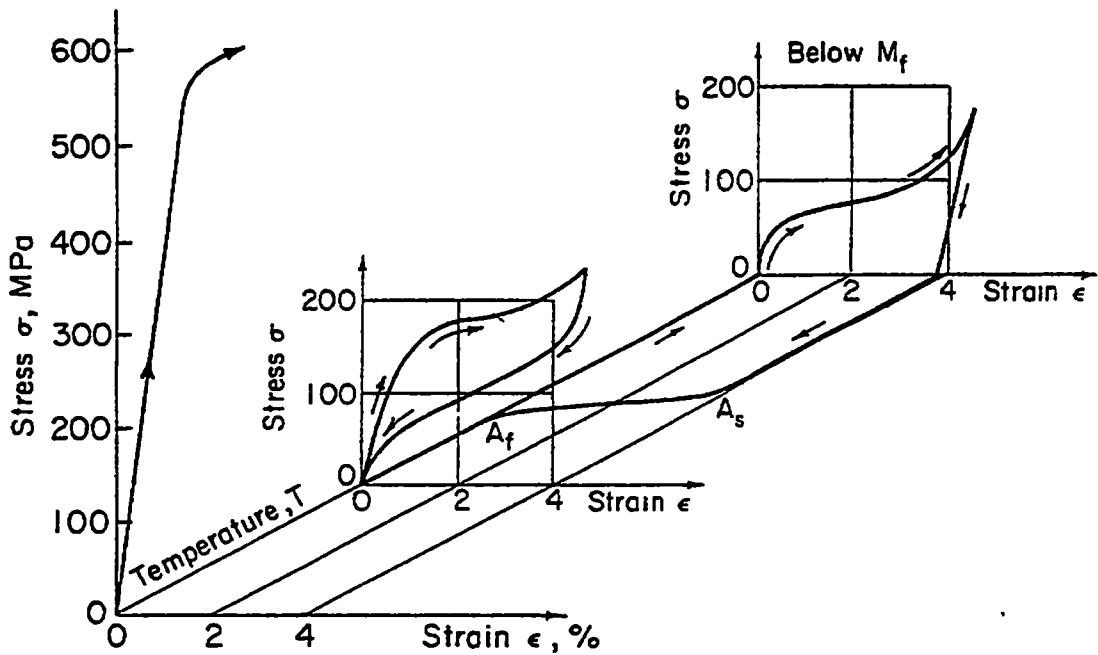
Figure 1.4 2 The three-dimensional, stress-strain-temperature diagram and the shape-memory behavior of NiTi deformed at various temperatures. (Wayman[1])

In summary, shape-memory alloys exhibit the shape-memory behavior as a result of a thermally or stress-induced, reversible martensitic transformation. It is interesting to note that the material is totally elastic (with less than 8 to 10% gross deformation). Some alloy compositions exhibit a reversible transformation, depending on certain conditions and some do not. Again, the composition of a SMA is crucial in determining the transformation temperature.

Stress Induced Martensite

The application of a stress on a shape-memory alloy may result in an interesting phenomenon in its behavior, during the shape-recoverable phase transformation. These stresses may restrain the phase transformation, and cause martensite to remain in the

14

particle, thus relieving the surrounding stress fields. This behavior is termed *stress-induced martensite* (SIM), and is a phenomenon which may be quite possible in the work described.

Wayman[1] describes this type of the shape-memory effect that is independent of temperature. Instead of a transformation induced by a thermal change, martensite is induced in a shape-memory alloy by the application of a stress. If martensite is formed in a shape-memory alloy above the transformation temperature, by the application of a stress, it is termed *stress-induced martensite*. Furthermore, as the temperature is raised farther and farther above the martensitic transformation temperature, there is a greater amount of stress required to induce the transformation. When the stress is released, while at the higher temperature, the specimen reverts to the austenitic phase, regaining its original macroscopic shape in the process. Also, for certain compositions of shape-memory alloys, if a constant stress is applied during the phase transformation, while heating above the A_f temperature, a two-way shape-memory behavior may be observed in alloy. This means that the specimen may return to its deformed state, if cooled under the transformation temperature again. Under these conditions, the shape-memory effect provides *superelastic* properties. This behavior is further explained by Otsuka;[2]

> *...deformation resulting from an applied stress occurs by detwinning of transformation twins (i.e., twin boundary movement) in martensites produced on cooling, and/or by transformation of retained austenite to martensite. On the reverse transformation, the detwinned regions revert to the original orientation of the parent lattice because of the internal stress stored in the martensite. Similarly, deformation-induced martensites also revert to the original orientation of the parent*

15

lattice. (Furthermore) ...any irreversible deformation mode, such as slip, should not occur in such a reversible phenomenon. For easy detwinning of transformation twins, a small lattice deformation and easy mobility of transformation dislocations may be necessitated. In addition, a superlattice structure in the parent phase may also promote the shape-memory effect, because the superlattice structure would be destroyed by deformation and so the energy would be increased, if the reverse transformation were not performed by shear processes that are perfectly inverse to those involved in the initial martensitic transformation and subsequent deformation. Thus, it is understood why an ordered Fe₃Pt alloy undergoes a thermoelastic martensite transformation and exhibits the shape-memory effect, whereas the disordered alloy does not.

The stress-strain-temperature relationship, demonstrated in Figure 1.4.2, is consistent with the Clausius-Clapeyron equation,[1,13] which is:

$$\frac{dP}{dT} = \frac{\Delta H}{T \Delta V}$$

(Eq. 1.4.1)

where P is the pressure, T is the temperature, H is the enthalpy, and V is the volume. Concerning the appropriate substitutions according to metallurgical interests, pressure is equivalent to stress, dT is the change in the M_s temperature, and the change in volume represents the strain resulting from the shape-memory effect. Equation 1.4.1 then becomes:

$$\frac{d\sigma_a}{dM_s} = -\frac{\Delta H}{T \varepsilon_o}$$

(Eq. 1.4.2)

where σ_a is the applied stress, M_s the starting temperature of the martensitic transformation, and ε_o is the transformation strain. Experimental results[1] have closely adhered to this equation.

Tobushi and others[14] have also found an interesting phenomenon concerning the modulus of elasticity in NiTi alloys which exhibit stress-induced martensite (SIM). Apparently, the modulus of the SMA will decrease in proportion to the maximum strain experienced. This may be due to the fact that there exist both the martensitic phase and the parent phase within the material after a strain has been experienced. The difference in the modulus can be accounted for by the variation in the moduli of the parent phase and the martensitic phase. This may be explained by the following relationship, where the strain increment is

$$\Delta\varepsilon = \frac{X\Delta\sigma}{E_M} + \frac{(1-X)\Delta\sigma}{E_A} \qquad \text{(Eq. 1.4.3)}$$

X is the fraction of the martensitic phase produced from the SIM transformation, and hence, the fraction of the parent phase (austenite), is 1 - X. $\Delta\sigma$ is the stress increment, and E_M and E_A are the moduli of the martensitic and austenitic phases, respectively. From Equation 1.4.3, the overall modulus of the material is

$$E = \frac{\Delta\sigma}{\Delta\varepsilon} = \frac{E_A E_M}{X E_A + (1-X)E_M} \qquad \text{(Eq. 1.4.4)}$$

Notice that when X = 0, then E = E_A, and when X = 1, E = E_M. If the fraction of the martensitic phase, X, is assumed to be proportional to the induced strain in the SIM transformation strain range, $\Delta\varepsilon_M = \varepsilon_{Mf} - \varepsilon_{Ms}$, then the fraction of martensite present at the maximum strain, ε_{max}, is

$$X = \frac{\varepsilon_{max} - \varepsilon_{Ms}}{\varepsilon_{Mf} - \varepsilon_{Ms}}$$

(Eq. 1.4.5)

Therefore, the mechanical properties of the material depend partially upon the fraction of martensite present. If stress-induced martensite is present, then these differences in the properties may be noted, and the fraction of martensite present might be deduced from the applied strain, or from the observed differences in the moduli.

1.5 Composite Materials

Composite materials offer an attractive combination of several properties, such as strength, stiffness, dampening capacity, and low density, among others, not to mention any number of preferences in manufacturing techniques, and can be designed to maximize the performance of any one or two properties in particular. This is the main reason that composite materials have attained a secure and steadily-growing place in today's technology. In order to successfully create a composite material, there are a few guidelines that must be observed. This section briefly describes the theory behind composite strengthening (for particulate reinforcements), and the qualities and qualifications that are necessary in order to combine two materials together to create a composite material. Although the NiTi reinforcement offers great potential for a composite strengthener by itself, the present study is especially interested in the added benefits which might be obtained through the activation of the shape-memory effect in the NiTi particles embedded in the matrix.

Strengthening Theory [15]

During deformation, as a dislocation approaches a reinforcement particle, its strain field interacts with that produced in the matrix by the particle. In a composite material, the strain field around the particle is usually produced by contrasting coefficients of thermal expansion between the particle and matrix, which produces internal strains during cooling from the manufacturing temperatures. However, in the

19

case of the NiTi shape-memory alloy as a reinforcement, theoretically, there should also be an additional strain in the matrix caused by the stress, $\overline{F}$, from the shape-memory effect.

$$\overline{F} = -[\tau_{zy}b_y + \tau_{zx}b_x]\overline{j} + [\sigma_{yy}b_y + \tau_{yx}b_x]\overline{k} \qquad \text{(Eq. 1.5.1)}$$

The Peach-Koehler equation (Eq. 1.5.1) describes the retarding force, $\overline{F}$, which is experienced by the dislocation. τ is the shear stress, b is the edge dislocation vector, and σ is the tensile stress. $\overline{j}$ and $\overline{k}$ are the y and z vectors, respectively. The contribution to $\Delta\tau$ from this mechanism is known to be[16]

$$\Delta\tau = \left[\frac{27.4E^3\varepsilon^3b}{\pi T(1+v)^3}\right]^{\frac{1}{2}} f^{\frac{5}{6}}r^{\frac{1}{2}} \qquad \text{(Eq. 1.5.2)}$$

where E is Young's modulus, T is the line tension, v is Poisson's ratio, f is the volume fraction of spherical particles with a radius r, and ε is a function of the disregistry, δ. The disregistry is the concentration of dislocations along a semi-coherent boundary, and is given in Equation 1.5.3.

$$\delta = \frac{a_\alpha - a_\beta}{a_\alpha} \qquad \text{(Eq. 1.5.3)}$$

where a_α and a_β are the lattice parameters of the two constituent materials, ($a_\alpha > a_\beta$).

Even after a dislocation overcomes the strain field barrier, it must still cut through the particle (assuming debonding does not occur). For this reason, composite materials

20

have less elongation and greater resistivity to crack propagation than the matrix material alone.

Reinforcements [17,18]

Composite material strengthening is the use of a second material, called a reinforcement, which is embedded within a matrix. Composites have different categories determined by the shapes of their reinforcement. Reinforcement can take the shape of fibers, wires, filaments, whiskers, flakes, or particles. The strength and stiffness of the composite are provided by the reinforcement, while the role of the matrix is to bind the reinforcement together, hold its shape, protect it from corrosion and abrasion, and distribute the stress evenly. Therefore, the matrix material generally has a lower elastic modulus than the reinforcement. The modulus of NiTi in the austenitic phase is, indeed, higher than that of the aluminum, which meets this requirement. But the modulus of NiTi in the martensitic phase is lower than the aluminum, thus allowing the cold working of the entire composite at that temperature.

The Young's modulus of a metal matrix composite can be described by the following equation,[19] where E_m and V_m are the elastic modulus and the volume fraction, respectively, of the (aluminum) matrix, and E_r and V_r are the elastic modulus and the volume fraction, respectively, of the (NiTi) reinforcement material. The solution of Equation 1.4.4 (in the section covering Stress-Induced Martensite), may be used as the value for E_r.

$$E_{comp} = \frac{E_m V_m + E_r V_r}{V_m + V_r}$$ (Eq. 1.5.4)

A more quantitative solution may involve the variational principles in the linear theory of elasticity. Hashin and Shtrikman[20] have derived the bulk modulus, K, and the shear modulus, G, of a composite material, using the elastic polarization tensor.

$$K = K_m + \frac{f}{\dfrac{1}{K_p - K_m} + \dfrac{3(1-f)}{3K_m + 4G_m}}$$ (Eq. 1.5.5)

$$G = G_m + \frac{f}{\dfrac{1}{G_p - G_m} + \dfrac{6(K_m + 2G_m)(1-f)}{5G_m(3K_m + 4G_m)}}$$ (Eq. 1.5.6)

where

K_m = bulk modulus of the matrix alloy
K_p = bulk modulus of the reinforcement particulate
G_m = shear modulus of the matrix alloy
G_p = shear modulus of the reinforcement particulate, and
f = volume percentage of the reinforcement particulate.

The Young's modulus of the composite, E, may be calculated from the following equation, once K and G are known.

$$E = \frac{9K}{1 + \dfrac{3K}{G}}$$ (Eq. 1.5.7)

It is important to select matrix and reinforcement materials that are compatible. That is, they do not react chemically, have similar coefficients of expansion, and have good adhesion between them. Therefore, much of the present research involves the

development of a treatment technique for the NiTi powders that would limit chemical reactions and promote a substantial interfacial bond between the NiTi and aluminum matrix.

Fabrication Processes [18]

Composite materials are sometimes classified according to their process of manufacturing. There are several processes available, but the three main methods of fabricating metal matrix composites (MMCs) are:

1. Liquid processes,
2. Deposition processes, and
3. Diffusion processes.

Liquid processes basically involve the liquid casting of the matrix material around the solid reinforcement. Alloys are commonly used as a matrix material, because the wider temperature region between the solidus and liquidus can be utilized to provide a "slushy" material which has a greater ease in casting. Powder-metallurgy (P/M) techniques are included in this category, because the powder mixture is usually heated above the solidus temperature during compaction. The main disadvantage of this method is the high temperature involved, and the liquid metal being in contact with the reinforcement material. In this state, chemical reactions can become commonplace, and can be a very detrimental characteristic of manufacturing composites by this technique (as will be seen later in our example.)

In the deposition process, the reinforcement material is arranged, as desired, and the matrix is deposited on it by any number of methods. These techniques commonly include electroplating, electrodeposition, plasma spraying, and vacuum deposition.

Diffusion processes are based on pressure and heating. Often times, this process is used in combination with a deposition process. For example, a reinforcement material coated with a metal by a deposition process will then be heated and pressed together to increase density and coercive bonding through diffusion. Sintering may also be employed, which does not heat the metal to its melting point, but does reach a temperature that allows recrystallization to take place, further combining the constituents into a single, solid mass.

1.6 Shape-Memory Alloy Reinforced Aluminum Composites

Literature Review

The idea of using a shape-memory alloy for the purpose of reinforcing an aluminum composite is not new. Several attempts have been made with moderate success. However, research has focused mainly on the use of SMA *fibers*.[5,21,22] Articles describing some previous work done in the manufacturing and testing of aluminum/NiTi SMA metal matrix composites have been reviewed, and some of the major findings have been summarized.[3,5,6,21-23] Only one reference, written by Wei et. al.,[6] could be found on any work done using a SMA in the form of a *powder* in a matrix, and their research was limited to the basic manufacturing of a material with the shape-memory effect intact. The phase transformations of their composites were characterized by Differential Scanning Calorimetry (DSC). Unfortunately, Wei et. al. did not conduct mechanical property characterization tests, beyond the observation of the dampening properties.

Concerning the work done with NiTi *fibers*, Furuya, Sasaki, and Taya[21] were able to incorporate NiTi fibers which were 200 μm in diameter into an aluminum casting to produce a SMA composite material. They "set" the shape-memory effect by heat-treating the composite at 500°C (930°F) for 30 minutes (which is above the A_s temperature) to anneal the fibers, and relieve any previous shape-memory effects. This step was followed by quenching the composite in ice water to induce martensite, then subjecting the specimen to a constant tensile prestrain, while heating to 100°C (212°F) to

return to austenite, thus utilizing the thermoelastic effect. This produced a composite with a tensile stress in the fiber and a compressive residual stress in the matrix. Upon testing, a 9 fiber vol. % composite with a 4% prestrain, proved to double the area under the stress/strain curve. Furuya also found that it had a high damping capacity. An electron dispersive spectrometry (EDS) analysis showed that there was limited diffusion on the NiTi/Al interface. Aluminum diffused as far as 6 μm into the NiTi, and Ni or Ti diffused as far as 2.5 μm into the aluminum. Reaction products were scarcely observed. Moreover, the Young's modulus, yield stress, and work-hardening rate increased with the volume fraction of NiTi fibers and the amount of prestrain. Furuya, Sasaki and Taya's results are an accurate precedent to the present work. The same amounts of diffusion and changes in mechanical properties also characterize the NiTi/Al composite made by P/M processing techniques in the present work.

Research Objectives

The purpose of the present study was to create a NiTi/aluminum metal matrix composite material which would have mechanical properties superior to those of the aluminum matrix. The goal was to fabricate this composite material using isostatic or hot-pressing, powder-metallurgy processing techniques. The author and his collaborators desired to obtain a material with a satisfactory density (> 97% of theoretical density), and, if possible, utilize the shape-memory effect of the NiTi to introduce residual stresses into the matrix in order to improve both the strength and fatigue resistance.

The theoretical foundation for this strengthening mechanism is portrayed in Figure 1.6.1. The NiTi shape-memory alloy, in the form of a powder, is dispersed throughout an aluminum matrix to create the composite material. The composite is chilled below the M_s temperature to produce martensite in the NiTi particles, and is then cold rolled to produce ten percent deformation. Since the martensitic phase of the NiTi has a lower modulus than the aluminum matrix, these particles may also be deformed during the cold-rolling process of the gross body. Upon reheating above the A_s temperature, a phase transformation is generated, and the shape-memory effect is exhibited by the NiTi particles.

1. Dispersion of a shape-memory alloy in a metal matrix
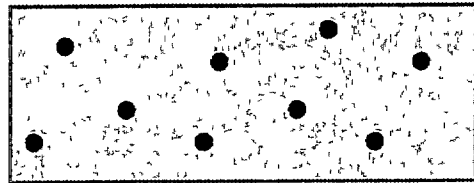
2. Deformation below the transition temperature
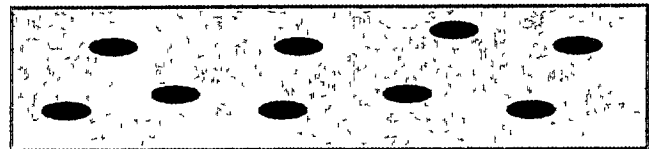
3. Raising the temperature, enacting the shape-memory effect, and inducing internal stresses
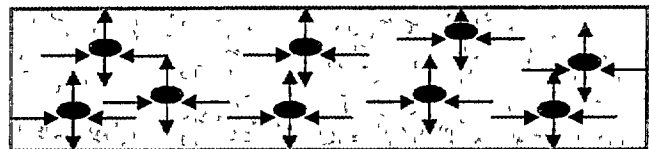
Figure 1.6 1. A schematic diagram of the behavior of the shape-memory alloy particles and their theoretical effect on the matrix

Besides the stresses produced from the NiTi particles as a consequence of the shape-memory effect, there is an additional influence on these stress fields resulting from the differing coefficients of thermal expansion in the constituents of the composite material. These coefficients are listed in Table 1.6.1. Since the coefficient for aluminum (23.6 μm/°C) is much greater than that of NiTi (11.0 μm/°C), it can be expected that the NiTi particles will undergo compression during the cooling of the composite from manufacture. This effect is enhanced when the M_s temperature is reached, as the martensitic phase of the NiTi has a still lesser coefficient of thermal expansion (6.6 μm/°C) than the austenitic phase. Because of the presence of the compressive stress, it is expected that an additional amount of strengthening may be achieved from the combination of these properties.

Moreover, the shape change of the NiTi particles resulting from the shape-memory effect, and the residual stresses resulting from differing coefficients of thermal expansion, both contribute to produce stress fields surrounding the particles, which are tensile in the longitudinal and transverse directions, and compressive in the through-thickness direction. These stress fields are expected to disrupt the homogenous plastic flow of the material during the deformation of the composite, and interfere with the propagation of a crack at its tip, causing deflection and branching. Thus, the yield and ultimate strength, as well as the fatigue life of the composite, will be increased in comparison to the unreinforced matrix material.

Table 1 6 1 A comparison of the coefficients of thermal expansion for aluminum
and two phases of nickel-titanium that are related to the shape-memory effect

Material	Coefficient of Thermal Expansion $(10^{-6}m/°C)$
Aluminum	23.6
Austenitic NiTi	11 0
Martensitic NiTi	6 6

PART II.

FABRICATION PROCEDURES OF THE COMPOSITE MATERIAL

2.1 Introduction

Powder metallurgy was chosen as the method of fabrication in the present work for several reasons. Primarily, a quality composite can be fabricated at temperatures well below the melting temperature of the matrix. This allows the composition of the constituent materials to be preserved, thus leaving the shape-memory effect intact. Powder-metallurgy processing also yields a material that contains relatively fine grains, which enhance the physical properties. The sizes of these grains are in proportion to the powder size. Usually, one powder particle will become one single grain. Thus, finer powders will produce a finer grained P/M product. During manufacture, the use of pressure aids in the densification of the composite, in comparison to a casting or deposition process. Also, powder-metallurgy processing is less laborious and more cost-effective than many other methods for producing such a composite of the same quality.

In the present work, aluminum possesses a major volume content of the composite (90 vol. %). It was chosen as a matrix material because of its high commercial use, low density, and thus, marketability. The main goal was to increase the yield strength and fatigue resistance of the aluminum by combining it with the NiTi shape-memory alloy in the form of a metal matrix composite. Before the fabrication of such a composite material could be done successfully, the mechanics, kinetics, and thermodynamics which were involved had to be carefully resolved. Early in the research, many problems were discovered, that hindered the development of the desired product. These problems included, but were not limited to, (1) insufficient product densities which led to extensive

31

fracturing during deformation, (2) poor NiTi particle to Al matrix bonds which became sources of crack initiation, (3) brittle intermetallic compounds due to diffusion, and (4) the inability to utilize the shape-memory effect after fabrication.

The problem of diffusion was extensive and most troublesome. Several possible solutions were investigated. One such possibility was the enhancement of the interface with a thin coating. Several experiments were conducted using the oxidation or nitridation of the NiTi powder under various conditions to create a diffusion-barrier coating. One such oxidation procedure, in which the NiTi powder was baked in air at 450°C (840°F) for 30 minutes, worked extremely well at preventing the diffusion of aluminum into the SMA particle during hot pressing.[24] However, during this procedure, the oxygen diffused into the particles and upset the shape-memory effect.

Another possible solution was investigated, which minimized the length of time at which the sample was exposed to high temperatures. This step was accomplished using cold, isostatic pressing followed by a short period of sintering at a higher temperature. However, isostatic pressing proved to be a failure, because a good density (usually considered greater than 97% of theoretical density) could not be obtained. The cold rolling of the sample became unsuccessful because of cracking, which was aggravated by insufficient densities and poor particle-to-matrix bonding.

2.2 General Procedure for Composite Material Fabrication

Most composites that have an aluminum matrix are not made with pure aluminum, but with aluminum alloys. However, after producing several specimens which were ruined because of extensive diffusion that created intermetallics, the author adopted pure aluminum as a matrix material, in an effort to avoid complications arising from the reaction of NiTi with aluminum alloying elements, such as copper. Simplifying the composition of the entire composite to three elements eliminates the problem of identifying phases and constituent elements for the initial work.

The basic fabrication procedure was as follows. The NiTi powder was mechanically-milled for six hours to reduce the powder size and to produce coarse surfaces on powders. The powders were then heat-treated at 800°C (1470°F) which restored the shape-memory effect, that was lost during milling, and also produced a light oxide coating on the surfaces which protects the NiTi phase from diffusion while hot-pressing. After processing, the NiTi powders were combined with aluminum powders in a ten volume percent proportion, and were mixed in a blender for four hours. The powder was removed from the blender, and weighed into appropriate sized charges of about 110 g for pressing. A steel die was used for pressing, with inner surfaces lined with a carbon foil. The die was then filled with the charge of powders and placed in the press. The pressure inside the press was reduced to 10^{-5} torr. A degassing technique[25-27] may or may not be employed at this stage. In degassing, the sample is brought to an elevated

33

temperature, usually between 200°C and 400°C (390-750°F), and held for an extended amount of time, usually around two hours. This allows surface oxides and gas particles to escape from the powders. The sample was then brought up to the desired pressing temperature, and pressed for ten minutes using a hydraulic ram. After pressing, the heating elements were turned off, and the chamber was allowed to cool. An inert flushing gas, such as nitrogen, argon, or helium, may have been used to induce a greater heat flow away from the sample in cooling. After the temperature dropped below 300°C (570°F), the atmospheric pressure was equalized, and the chamber opened. Note that above 300°C, the carbon heating elements may combust if exposed to an oxygen environment. The die was then removed, and the sample was pressed out of it using a Carver™ hydraulic press. Samples were then sliced into pieces, 1.4 mm (0.055 inches) thick. These samples were cold-rolled, some at room temperature, and some at the sub-zero, martensitic temperature to enact the shape-memory effect, with ten percent deformation, resulting in pieces, 1.27 mm (0.050 inches) thick. These pieces were stamped into tensile test coupons, and experiments were conducted on these coupons. Samples made with an age-hardenable aluminum alloy as the matrix material were kept in freezer storage until age-hardening was to be commenced.

2.3 Description of Powders

Several powders were considered for the fabrication procedure. Table 2.3.1 illustrates the differing properties of each in a convenient comparison. The NiTi alloys of two different compositions are comparable in the density and melting temperature. Note that the table includes some NiTi powders that have undergone a milling procedure. This is because better compaction can be achieved during hot pressing, due to the differing particle sizes resulting from the milling of the NiTi powder. The milled particle properties are also included. Note that the Al 1050 (99.5% pure) and Al 1090 (99.9% pure) aluminum materials have a melting point of 660°C (1220°F), while Al 2124 (4.5 weight % copper) has a melting range of 570-650°C (1060-1200°F). Those particle sizes marked with an asterisk are those indicated on the shipping documentation. However, a scanning electron microscope (SEM) study revealed that the actual particle sizes vary from those indicated for some materials. If the documented particle size of a material is different from the actual particle size, then the actual particle size is also given.

Figure 2.3.1 is a SEM photomicrograph of the NiTi powder, as received from the manufacturer. Average particle sizes range from 10 to 40 μm. Even though these powders are large in comparison with most commercially-produced powders, this is still the smallest size of NiTi powders available. Figure 2.3.2 depicts the Al 1050 aluminum powder (JM 11067, 99.5% pure aluminum), as received from the manufacturer, Johnson and Matthey. Particle sizes are less than 5 μm.

Table 2.3.1: The Physical Properties of Powders.[7,12]

* Sizes according to shipping identification information
† Actual sizes measured through Scanning Electron Microscopy

Powder	Particle Size	Density	Melting Temperature
NiTi ($A_s = -20°C$) as received After Milling	-325 mesh* or 40 µm† 5-10 µm†	6.45-6.50 g/cm^3	1310°C
NiTi ($A_s = +40°C$) as received After Milling	-325 mesh* or 40 µm† 5-10 µm†	6.45-6.50 g/cm^3	1310°C
Al 1050	-325 mesh* or 5 µm†	2.713 g/cm^3	660°C
Al 1090	20 µm*	2.705 g/cm^3	660°C
Al 2124	-325 mesh* or 40 µm†	2.796 g/cm^3	570-650°C

36
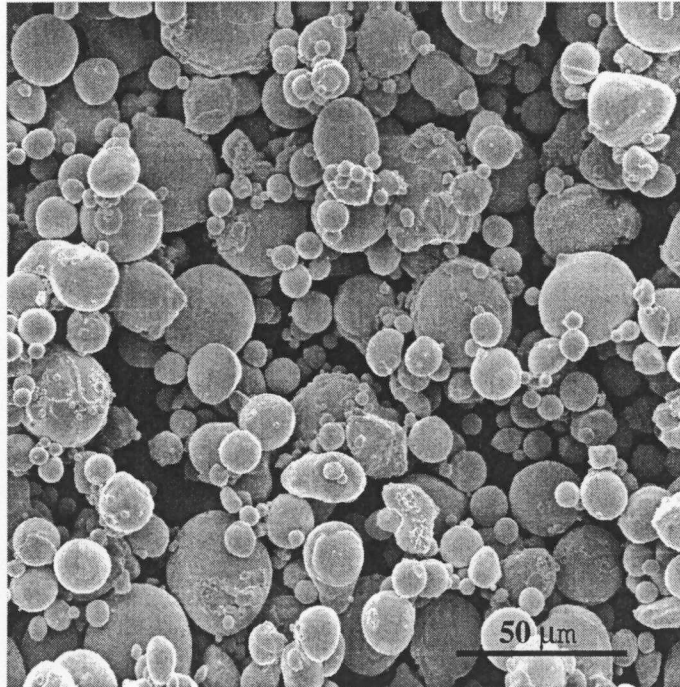
Figure 2.3.1: NiTi powders, as received from the manufacturer, U-Di-Met. This is the smallest size of NiTi powders available. Average particle sizes range from 10 to 40 μm. (File: ez16652)
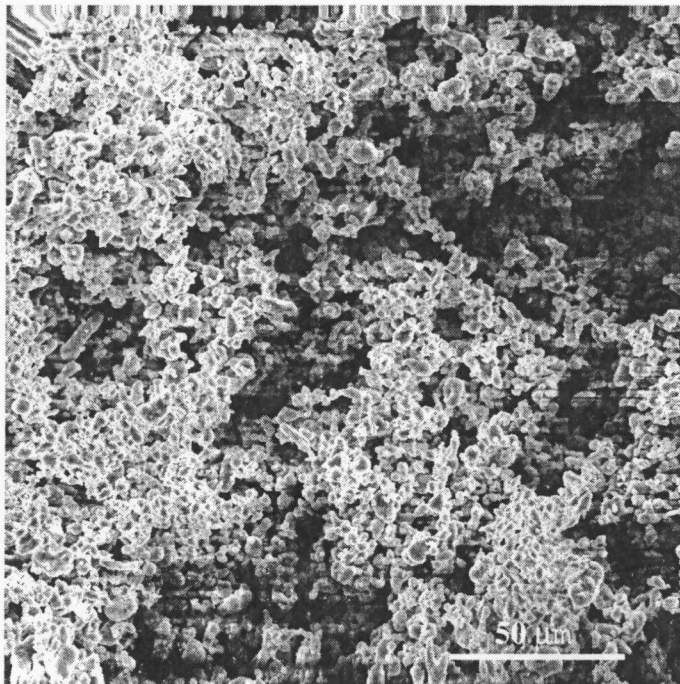
Figure 2.3.2: Al 1050 aluminum powder (99.5% pure), as received from the manufacturer, Johnson and Matthey. Particle sizes are less than 5 μm. (File: ez16826)

37

2.4 Mechanical Milling

NiTi shape-memory alloy powders are produced by gas-atomization,[28] which results in relatively large particle sizes as far as the industry concerns. Since the powders are used mainly for powder processing of materials, these large, spherically-shaped, powder particles may be undesirable for any number of reasons. Since a sphere has the maximum volume per surface area for any kind of shape, this shape minimizes the amount of the surface area available for interfacial bonding. Better compaction during hot pressing may be achieved from the differing particle sizes resulting from the subjection of the NiTi powder to a mechanical-milling process.[29-31] The present chapter entails the study which determines if the NiTi powder may be reduced in size, randomized in shape, and roughened in the surface texture, in order to enhance bonding, and overall composite deformation characteristics.

Initial work showed that the NiTi/Al interface in the composite matrix became the source of crack initiation during mechanical deformation (see Figure 2.4.1). It was thought that the NiTi/Al interface was weak, because the NiTi particles are relatively large and spherical in shape. The NiTi powder, which was previously used in the as-received condition, was nearly spherical in shape and 40 μm in size (see Figure 2.3.2). When the composite material was cold-rolled, micro-cracking occurred along the interfaces which were normal to the direction of rolling, as indicated in the figure. This problem led the authors to conclude that the size and shape of the NiTi particles needed to be altered. Subsequently, the milling technique, known as mechanical alloying, has been employed. The name is misleading in this case, because no actual alloying is done.

NiTi Particle

Aluminum Matrix
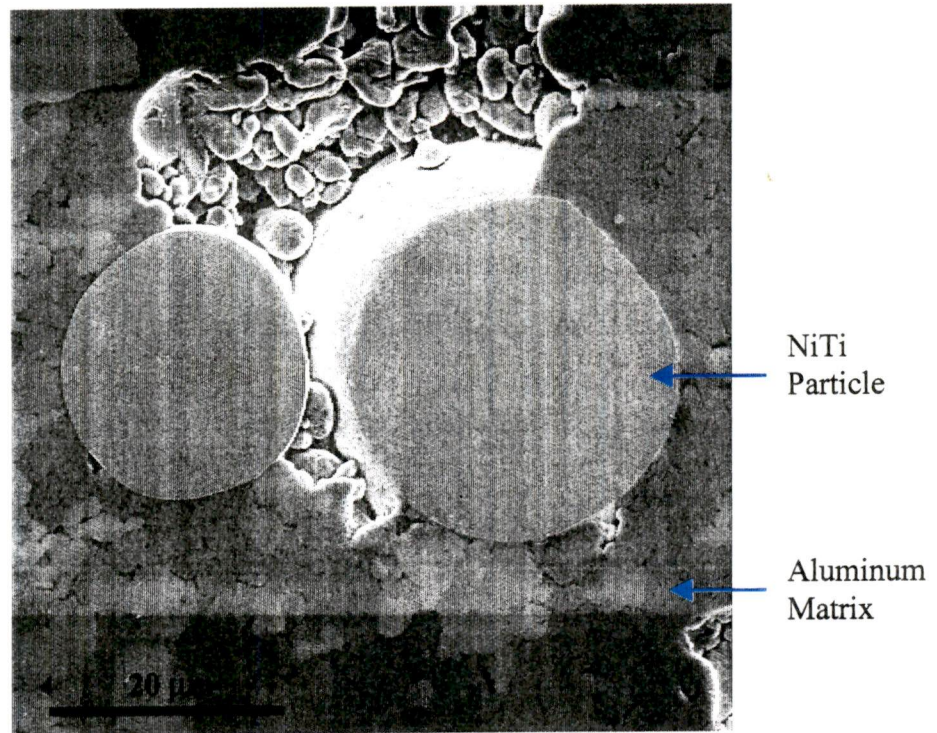
Figure 2.4.1: Poor NiTi to Al bonding. (File: ez17972)

However, other benefits are achieved from this process besides alloying, namely, the reduction of particle size. Mechanical milling of the NiTi powder before mixing with the aluminum powder proved to reduce the SMA particle size and increase the surface area.

According to German,[29] powder production and refinement can be achieved through mechanical impaction (or milling). In this process, the material is subjected to rapid, successive blows. As the process continues, the material reaches its ultimate strength, fractures, and breaks into smaller particles. The particle size is further refined through the continuation of the process. Most materials do not have an immediate response to mechanical milling, because of their ductility and cold welding. However, as the process continues, these materials become hard and brittle due to strain hardening.

Powder production, thereby, becomes more efficient after this initial stage. As German[29] states,

> *Powder fabrication techniques based on high strain rate impacts are useful for brittle materials. Compressive crushing can be applied to weak materials to bring the particle size down to 1 mm or so. High-velocity impact mills using tungsten carbide blades can further reduce the particle size. The production rate is slow, with the particle size controlled through milling time.*

Also, the optimal efficiency of milling is achieved in a container, when the total volume of contents, which includes all powders plus any milling media, is about half of the volume of the milling container.

In the present work, a polyethylene container is filled with 10 grams of NiTi powders and 40 grams of 3 mm diameter ZrO_2 milling media. The container is then put into a Spex™ milling machine, which rapidly shakes and turns the container. The powder is milled on an electronically-controlled schedule of five minutes of milling followed by ten minutes of rest to allow for cooling. This milling schedule is employed for eighteen continuous hours, which provides six hours of total milling time. After milling is completed, the container is removed, and its contents are separated with a sieve. The ZrO_2 media may be reused several times, although after about six uses, the media develops a thin layer of the powder on the surface, which reduces its hardness and effectiveness.

This procedure has reliably provided NiTi powders which have undergone a sufficient reduction of the particle size due to work hardening. After the milling

procedure, the particle size is reduced to an average diameter between 6 and 10 μm. Figures 2.4.2 and 2.4.3 show the NiTi powder after the mechanical milling procedure. 82.5 grams of NiTi powders are needed to produce one batch of composite powders which yields two, 110 gram samples of a NiTi/Al composite material, with a NiTi volume content of 10%. The overall production of powders is indeed a slow one, since only ten grams of powders may be milled in a single day.
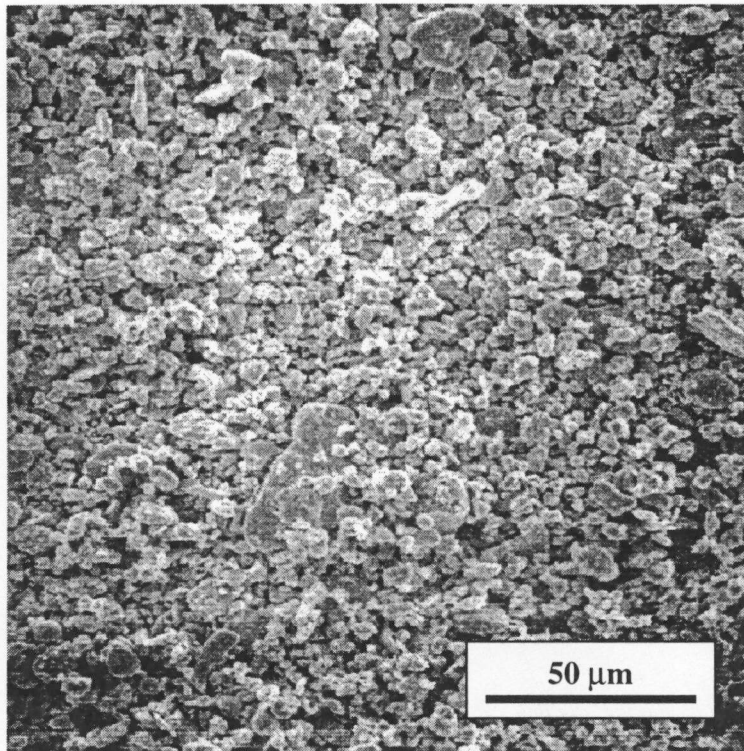
Figure 2.4.2: NiTi powder after the mechanical milling procedure.
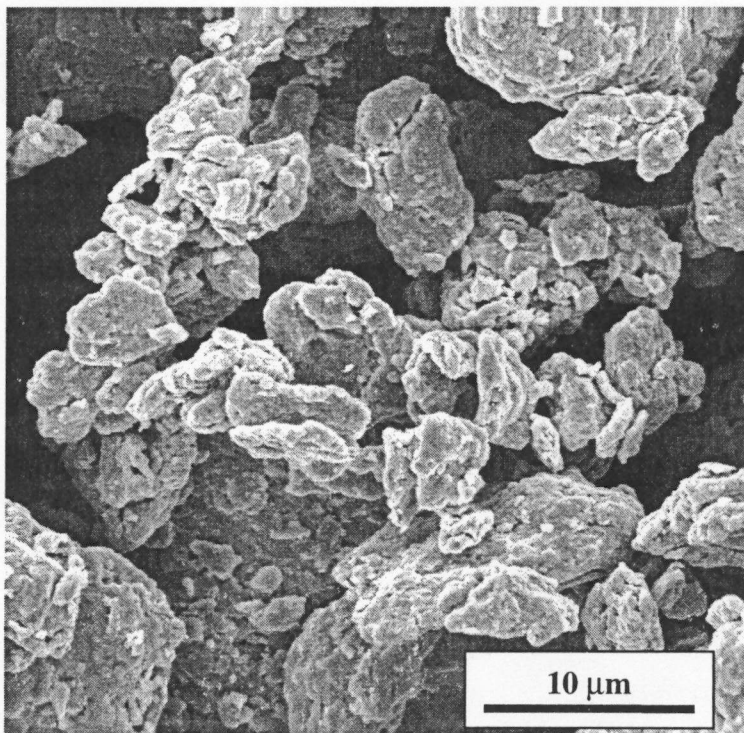
Figure 2.4.3: NiTi powder after the mechanical milling procedure. The average particle size is between 6-10 μm. (File: ez17622)

2.5 Recrystallization of Powders

The milling process, which was previously discussed, is necessary to reduce the NiTi particle sizes. However, this process produces an amorphous, high free-energy crystal structure, which introduces two main difficulties,

1. The loss of the shape-memory effect;

2. The extreme reactivity of the NiTi powders in the presence of other compounds, such as oxygen or aluminum.

The first difficulty is that the equiatomic NiTi work-hardens readily during the six hour milling process, and a high amount of free energy is imparted to the alloy. NiTi is a metallic glass in this state, with an amorphous crystal structure. Metallic glasses are characterized by a lack of long range order. Slip becomes difficult, and hardness is enhanced, which enables fracture during the mechanical milling process. However, the introduction of high dislocation densities interferes with the twinning deformation of the martensite. As a result, the crystallographic reversibility is lost, due to the lack of long range order, and the shape-memory effect is ruined.[2,31]

The second obstacle is that the NiTi particle becomes extremely reactive when combined with the aluminum during hot pressing, if the NiTi phase is not first returned to a lower free-energy, austenitic crystal lattice,. This reaction has been known to induce the complete obliteration of the NiTi phase from the matrix. Figure 2.5.1 illustrates the extensive reactions that can derive from the high free-energy, amorphous powder being hot-pressed with aluminum, resulting in the presence of intermetallic phases.
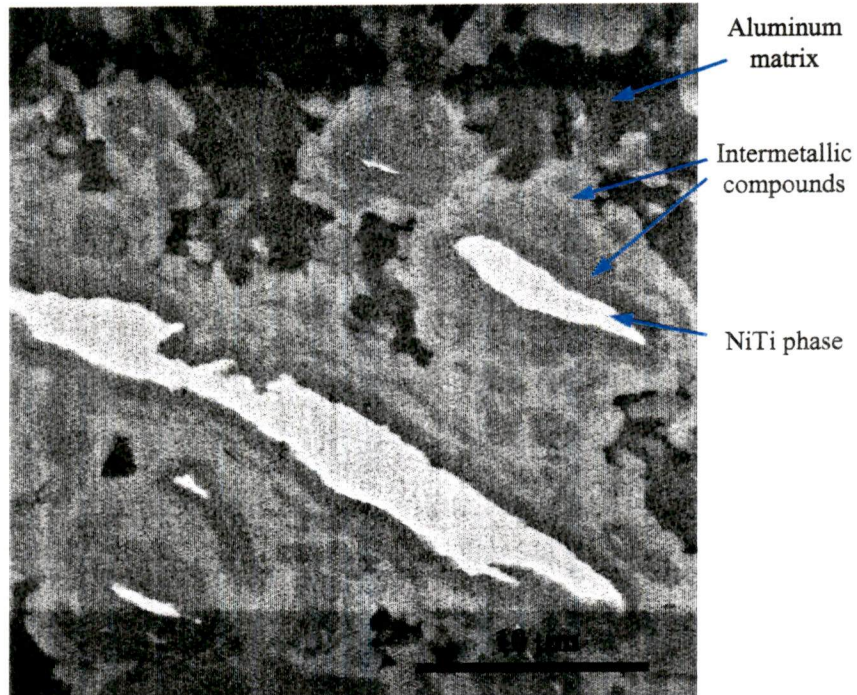
Figure 2.5.1: The presence of intermetallic compounds due to extensive diffusion from NiTi particles which have been mechanically milled, but not annealed. These intermetallic phases are composed of Ni, Ti, and Al, although their exact ratio is undefined. (File: ez17759)

To correct these difficulties, the powder must subsequently undergo a heat-treatment procedure, in order to recrystallize the material, lower the free energy to prevent unneccesary reactions, provide long-range order, and restore the associated shape-memory behavior. During this heat-treatment, the crystal structure of the amorphized NiTi shape-memory alloy powders, the recovery processes begin at temperatures as low as 275°C (525°F). The solvus temperature is about 550°C (1020°F). Partial annealing does not recrystallize the material, but it does bring about the onset of recovery processes. The aging of unstable (nickel-rich) compositions begins at 250°C (480°F), causing the precipitation of a complex sequence of Ni-rich precipitates. As these products leach nickel from the alloy, their general effect is to raise the M_s temperature. A fully-annealed condition is needed to recrystallize the matrix and restore

44

the shape-memory effect. Recrystallization begins between 500°C and 800°C (930-1470°F), depending on the alloy composition and the degree of cold working. For the extreme degree of cold working that has been introduced to the powder through mechanical milling, an 800°C annealing temperature is necessary to fully restore the original crystal structure (see Figure 3.4.1, the NiTi phase diagram).

The heat treatment and annealing of the NiTi has proved to be a tenacious process. With a higher free energy, the powder is very reactive when placed in contact with air or the aluminum matrix, especially at elevated temperatures, such as the hot-pressing temperatures of the composite (500°C to 550°C). Because the NiTi powders are so reactive in the amorphous state after milling, this heat treatment must be done in a high vacuum ($< 10^{-5}$ torr). The powder will rapidly oxidize (and under certain conditions will combust), with the slightest amount of oxygen present at the recrystallization temperature. Most metals will spontaneously oxidize during heating in the presence of oxygen, according to the following reaction,[13,31]

$$x\mathrm{M}_{(s)} + \tfrac{1}{2}\,\mathrm{O}_{2\,(g)} \rightarrow \mathrm{M}_x\,\mathrm{O}_{(s)} \qquad\qquad \text{(Eq. 2.5.1)}$$

which occurs with a release of free energy. The heats of formation, ΔH_f, of NiO and TiO_2 oxides, in relation to this work, are found to be,[13,32]

$$\mathrm{Ni}_{(s)} + \tfrac{1}{2}\mathrm{O}_{2\,(g)} \rightarrow \mathrm{NiO}_{(s)} \qquad \Delta H_f = -241 \text{ kJ/mol} \qquad \text{(Eq. 2.5.2)}$$

$$\mathrm{Ti}_{(s)} + \mathrm{O}_{2\,(g)} \rightarrow \mathrm{TiO}_{2\,(s)} \qquad \Delta H_f = -956 \text{ kJ/mol} \qquad \text{(Eq. 2.5.3)}$$
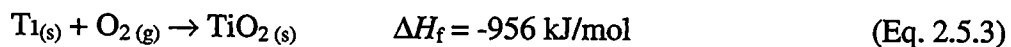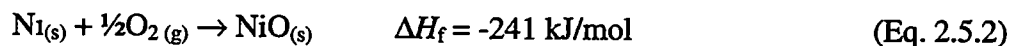
The large difference between these values, with TiO_2 releasing almost four times the enthalpy of NiO formation, predicts a dominance of TiO_2 in the oxide coating on the surfaces of the NiTi particles. Since the oxidation reaction thermodynamically prefers to produce TiO_2, this trend draws Ti out of the matrix and effectively lowers the M_s temperature. Oxygen can also diffuse into the NiTi and destroy the shape-memory effect. (See *The Role of Composition and the Effects of Diffusion*, under the Physical Characterization Section.)

An interesting corollary to this process is that an oxide coating on the NiTi particles will inhibit the diffusion of aluminum into the particles during hot pressing. In fact, a large fraction of the research focused on developing a heat-treatment procedure which would yield a suitable surface coating intended for this purpose. Several heat treatment and surface-coating studies have been investigated, including possibilities of nitridation, instead of oxidation. One such method was to treat the powders at 450°C (840°F) for fifteen minutes to recrystallize the crystal structure, followed by increasing the temperature to 700-800°C (1,290-1,470°F), and the release of nitrogen gas into the chamber to produce a nitride surface coating. Other studies used the same recrystallization procedure, but were followed by furnace treatments in air or submergence in water to produce an oxide coating. None of these procedures proved to be successful due to the severe damage inflicted on the composition as a result of the reactivity of the high free-energy powder.

After several experiments, a successful method was found. Heat-treating the milled NiTi powders in a high vacuum (10^{-5} torr) at 800°C (1,470°F) has proved to be successful in producing a restoration of the original crystal lattice, exhibiting the shape-memory effect, and the lowering of the free-energy. Milled NiTi powders were spread into alumina trays and placed inside a furnace. The pressure was lowered below 10^{-5} torr, and then, the temperature is raised to 800°C (1,470°F) for ten minutes. This process fully recrystallized the NiTi powders. Fortunately, even with the high vacuum in the chamber, there still remains enough oxygen present to deposit a thin oxidation layer on the surfaces of the powders. This layer provides the needed diffusion barrier during hot pressing, and also promotes better bonding to the matrix. In fact, the limitation of diffusion and the matrix bonding were so good for the heat-treated powders, that this heat-treatment was also used on the unmilled NiTi powders as well. Not only does this standardize the surface condition of all NiTi powders used, but it also improves the quality of the composite material.

2.6 Mixing Powders[29]

Most powder mixing has been done using rotating containers. There are several properties that influence the rate and efficiency of mixing. The shape of the interior of the container is very influential. Figure 2.6.1 presents some of the more common geometries, including a cylindrical, rotating cube, double cone, and twin shell. An oblique blender (not pictured) is like one half of a twin shell configuration. Often times, baffles, intensifiers (turning blades), or free tumbling mixing media are used to ensure timely and adequate mixing.

A quart-sized plastic container was filled to 25-30% of its volume with powders. (about 220 g) Several alumina mixing media, approximately 1.25 cm. (0.5 inch), in diameter, were added. The container was then filled with argon gas and put into an oblique blender, which turns at a rate of 12 rpm, and is pictured in Figure 2.6.2. The powders were then mixed for four hours. Afterwards, the container is removed from the blender and kept in storage until hot pressing.

As can be seen from the optical observation of the finished composite materials, this procedure has proved to mix powders adequately, providing a homogenous distribution of NiTi particles throughout the aluminum powders. The apparatus used for mixing has also been used to separate clumps of NiTi powders after the annealing procedure. The mixing media breaks up the clumps and pulverizes the remaining particles into the respective powder after approximately two hours of tumbling.
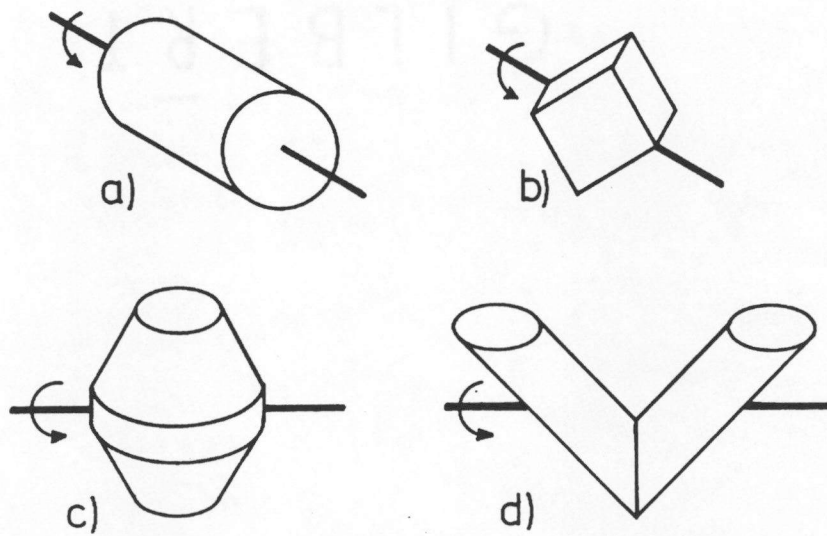
Figure 2.6.1: Four common mixer configurations: a) cylindrical, b) rotating cube, c) double cone, and d) twin shell. An oblique blender (not pictured) is like one half of a twin shell configuration.

Mixer.jpg

Figure 2.6.2: The oblique blender used at the Metals and Ceramics Division of the Oak Ridge National Laboratory.

2.7 Hot Pressing

At first, cold-isostatic pressing (CIP) was chosen because the exposure of the specimen to high temperatures is undesireable. It aids the process of diffusion, thus upsetting the delicate nature of the composite. CIP proved to be ineffective in producing samples of a sufficient density. Hot pressing was then chosen as a method of manufacturing because of its effectiveness in producing high-density P/M samples. It is known that producing a sample at a higher hot-pressing pressure will increase the density on a logarithmic scale. Much of the research concerned the determination of the pressing conditions that would yield a full density with the pressures achievable with the dies and hot press used. A 7.62 cm (3 inch) inside diameter, carbon die cannot withstand pressures above 30 MPa (4.35 ksi). Consequently, a steel die was chosen, which enabled the authors to press 5.715 cm. (2.25 inch) diameter samples at 69 MPa (10 ksi), yielding samples of a higher density. The use of a higher pressure allows high-density samples to be manufactured without the extensive use of heat or excessive degassing times at elevated temperatures, all of which contribute to diffusion, leading to the eradication of the shape-memory effect. Also, it is possible to raise the temperature to pressing conditions, press the sample, and then cool the assembly in a very short period of time. This concept is beneficial because there is little time for diffusion to occur at higher temperatures.

The hot-pressing procedure was conducted at ORNL where a Brew™ hot press was available. This hot press has a vacuum capability of 10^{-5} torr, a pressing capability of

about 10.35 GPa (1,500 ksi), and a carbon heating element capable of producing temperatures up to 1,500°C (2,730°F). Metal dies were specially-machined with a 1.6 mm (0.0625 inch) diameter hole through the center of the end cap. This hole accommodated a thermocouple, which extended through the die and barely protruded into the die cavity, which was filled with powders during pressing, to aid in temperature-measurement accuracy. A graphite sheeting, called Grafoil™, was used to cover and protect cylinder walls and punch faces. A boron-nitride aerosol spray was used to coat any cracks in the Grafoil™. Prepared powders were measured by weight and placed into the die using a paper funnel. The punch was inserted loosely, and the die assembly was placed into the hot press. The chamber was then put under vacuum. After the desired vacuum had been reached, usually about 7 x 10^{-5} torr, heating elements were used to bring the die up to the degassing temperature, which is usually between 200 and 400°C (390-750°F). Degassing is a technique in which the powders are held in a vacuum at an elevated temperature for an extended period of time. This allows moisture and other volatiles to dessicate from the surface, and also reduces certain surface oxides. It has been found that degassing can improve the density of a sample by up to 2% of theoretical density.[25,26] However, the present study has shown that the extended time at an elevated temperature allowed diffusion to occur and intermetallic compounds to form, thus destroying the shape-memory effect. If a particular sample doesn't employ the degassing technique, the die is brought directly up to the pressing temperature after a vacuum has been obtained.

When the pressing temperature had been reached, the hydraulic pressure was increased until the desired pressure on the die had been obtained. An equation is needed to convert the hydraulic pressure to the actual force on the punch area. This equation is,

$$P_{hyd} = \frac{P_{punch} \cdot A_{punch}}{A_{cyl}}$$
(Eq. 2.7.1)

where P_{hyd} is the hydraulic pressure applied to the ram, P_{punch} is the desired pressure on the die punch, A_{punch} is the area of the die punch, and A_{cyl} is the area of the ram cylinder. The diameter of ram cylinder is 15.24 cm (6 inches). The pressure and temperature were held constant until the pressing was completed, about 10 minutes, then the heating elements were turned off. The hydraulic pressure remained on the die, while the temperature dropped due to a water-cooling jacket around the chamber. Argon gas may have been released into the chamber to aid heat transfer and increase the cooling rate. When the temperature dropped below 300°C (570°F), air was released into the chamber to equilibrate the atmospheric pressure in order to open the chamber. Above 300°C, the oxygen in air may cause the combustion of the carbon heating elements.

After the thermocouple was unplugged, and the die assembly was removed with the aid of high-temperature mittens, the end cap was removed, and the sample was pressed out of the die using a Carver™ Press. The sample may or may not have been quenched in water. The pressed sample was cleaned, filed smooth, marked with identification and tested for density using the Archimedes immersion technique.

The described hot-pressing procedure produced samples of composite materials with the dimensions shown in Figure 2.7.1. A sample of this size provided enough material to cut approximately 20 tensile test coupons (see Figure 2.8.1). Although initial tests produced samples with densities lower than 80%, the development of the hot-pressing procedure described earlier eventually yielded samples with densities in excess of 99%. This certainly provided a sufficiently dense sample for further fabrication of the composite material and the mechanical testing coupons. Densities of the samples and the Archimedes immersion technique are discussed in further detail under the Density section in the Physical Characterization Chapter.

Simple though it may seem, the production of the composite material has been heavy-laden with misfortunate discoveries. First of all, the aluminum oxide which coats the surfaces of the aluminum powders presented a slight difficulty in obtaining good bonding in the matrix. Figure 2.7.2 is a SEM micrograph exhibiting the fracture surface of Al 1050 aluminum powders pressed into a green pellet and sintered at 800°C (1470°F). The melting temperature of the metal is 660°C (1220°F). Note that an oxide film is stretched across the granules of powders. During hot pressing, this film must be penetrated and dispersed for good intra-matrix bonding to occur.

Another one of the foremost hindrances to the development was the diffusion of aluminum into the shape-memory alloy. This process created difficulty for several reasons discussed already, but one main reason is the change of the SMA composition and a resulting loss of the shape-memory effect. It was important to consider what
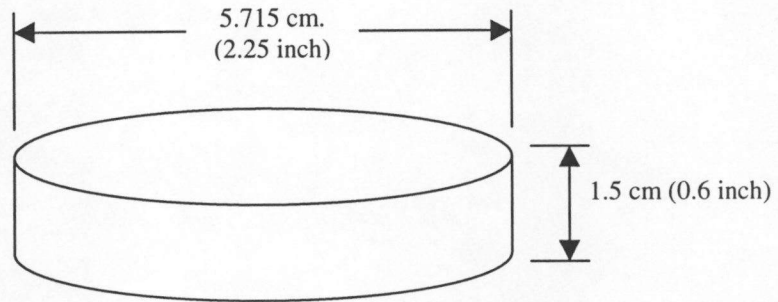
Figure 2.7.1: Schematic diagram of the pressed sample dimensions.

A thin film of Al_2O_3 on the surface of, and stretched between particles
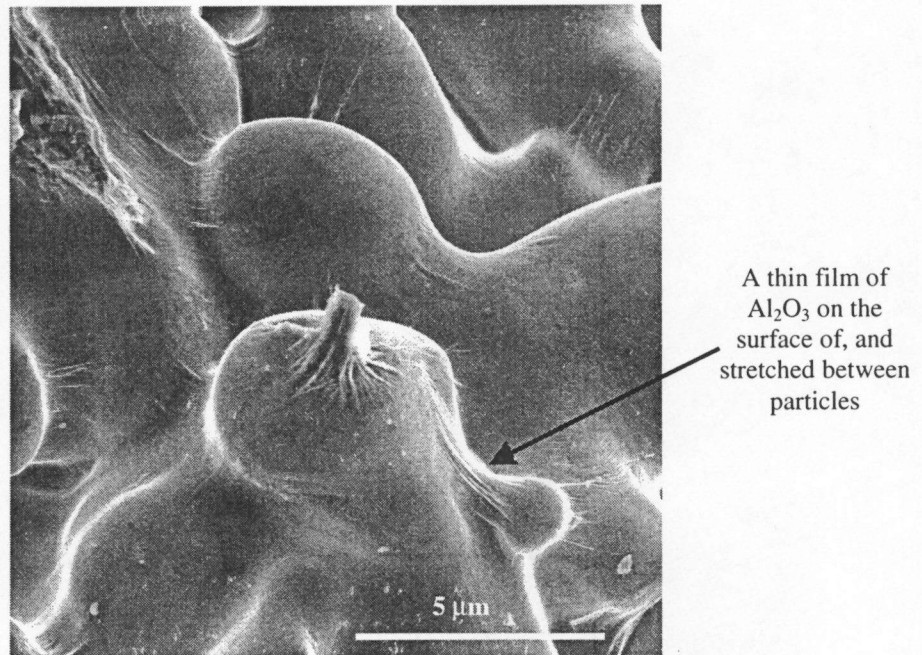
Figure 2.7.2: Fracture surface of Al 1050 (JM11067) aluminum powders pressed into a green pellet and sintered at 800°C. Note that the surface is covered with a thin film of oxide. (File: ez18171)

possible phase changes or reactions would take place as a result of the NiTi being in proximity to aluminum under high temperature and pressure conditions like those encountered during hot pressing. The following phase diagrams[33] are important in this consideration.

Figure 2.7.3 depicts the Al-Ni phase diagram which suggests a number of Al-Ni compounds that may form due to diffusion in the matrix. Although there is diffusion of nickel as well as titanium, the lower free energy of the titanium causes it to bond preferentially over nickel to the aluminum, creating intermetallics (see Figure 2.5.1).

Figure 2.7.4 is the Al-Ti phase diagram. It is difficult to surmise through analysis, but it is assumed that the great extent of the intermetallic compounds which formed between the NiTi particles and the aluminum matrix are of an Al-Ti composition. This is unfortunate, because this family of compounds tends to be very brittle, thus debilitating ductile deformation characteristics.

In Figure 2.7.5, there are two NiTi/Al ternary diagrams, one at 600°C (1,110°F), and another at 800°C (1,470°F). From this, we can see that the NiTi phase can contain a small amount of aluminum in a certain ratio and still maintain the shape-memory properties. However, since the diffusion cannot be controlled to the extent of being able to maintain this ratio, this is not very beneficial in producing composite materials.
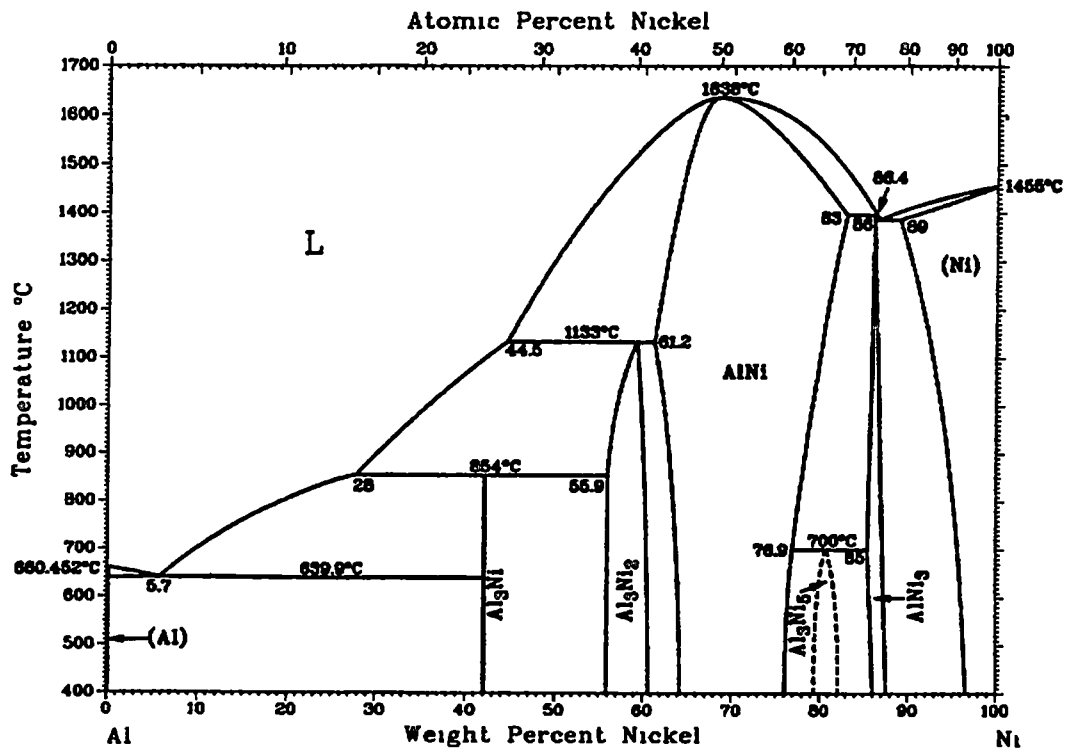
Figure 2 7 3 [33] The Al-Ni phase diagram
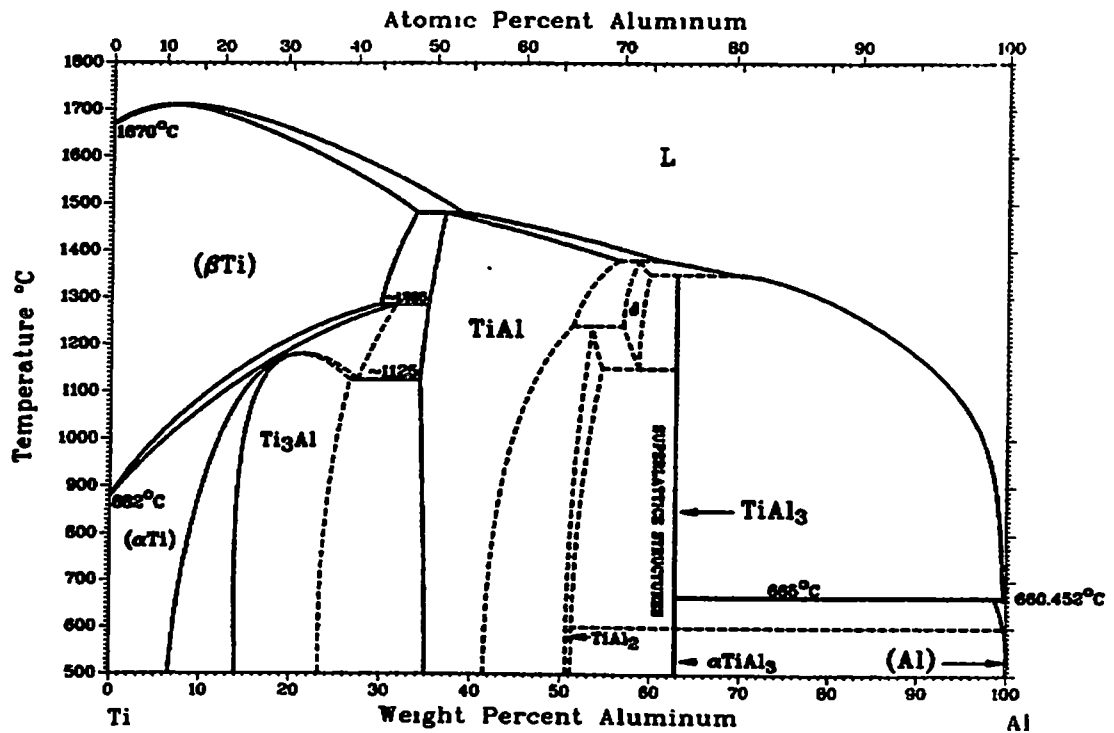
Figure 2 7 4 [33] The Al-Ti phase diagram
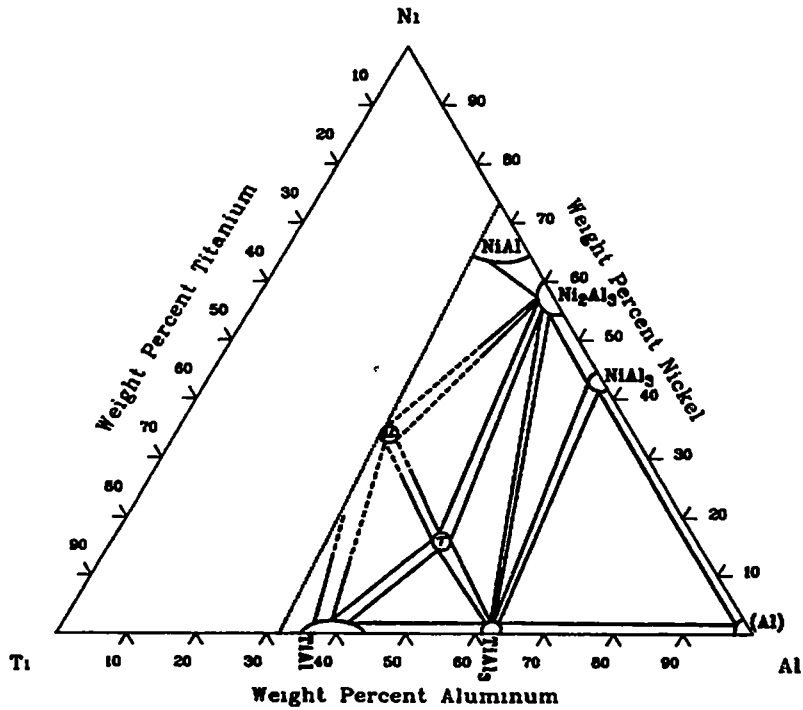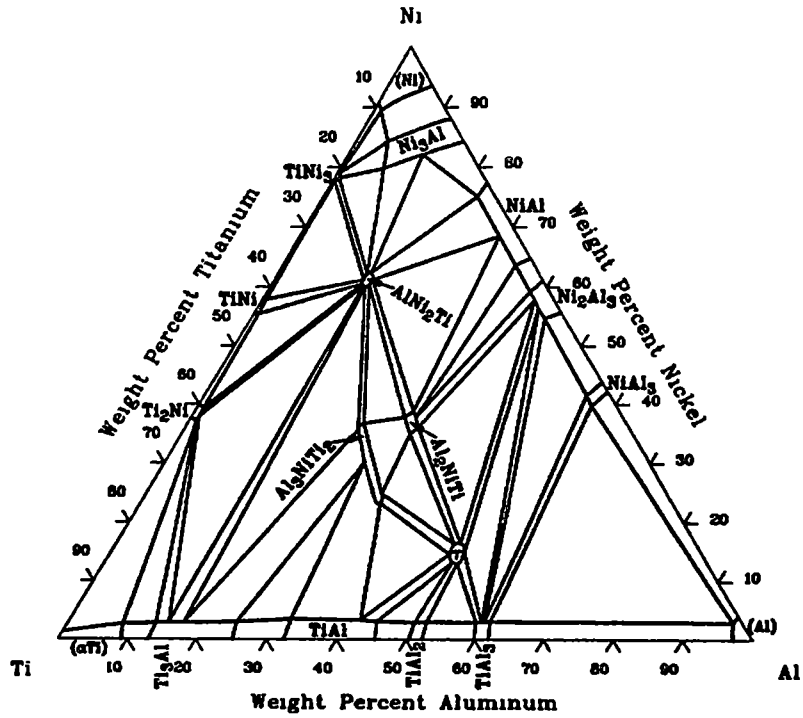
Figure 2 7 5 [33]   Two Al-Ni-Ti ternary diagrams   The top figure is the isothermal section at 800°C. The NiTi phase is indicated on the middle-left side of this figure   The lower figure is the isothermal section at 600°C

x

57

2.8 Sample Cutting

After pressing, the samples needed to be cut into appropriately sized pieces for cold rolling and die stamping. Each sample was mounted on a steel base-plate using a thermo-setting glue. The sample/base-plate was then magnetically mounted in a programmable Harig™ saw, and slices were cut from the sample according to Figure 2.8.1. The blade of this saw is a 17.78 cm. (7 inch) diameter disc of a copper-based alloy, which has a diamond grit embedded into the surface of the edge. Due to the precise nature of the saw/mill, samples could be cut into slabs within a 0.025 mm (0.001 inch) tolerance. Thicknesses of samples were cut at 0.84 mm (0.033 inch) and 1.40 mm (0.055 inch), to allow 0.76 mm (0.030 inch) and 1.27 mm (0.050 inch) thick specimens to be made with 10% deformation, from those samples, respectively. After cutting, samples were washed, deburred with a file, bagged, and labeled.
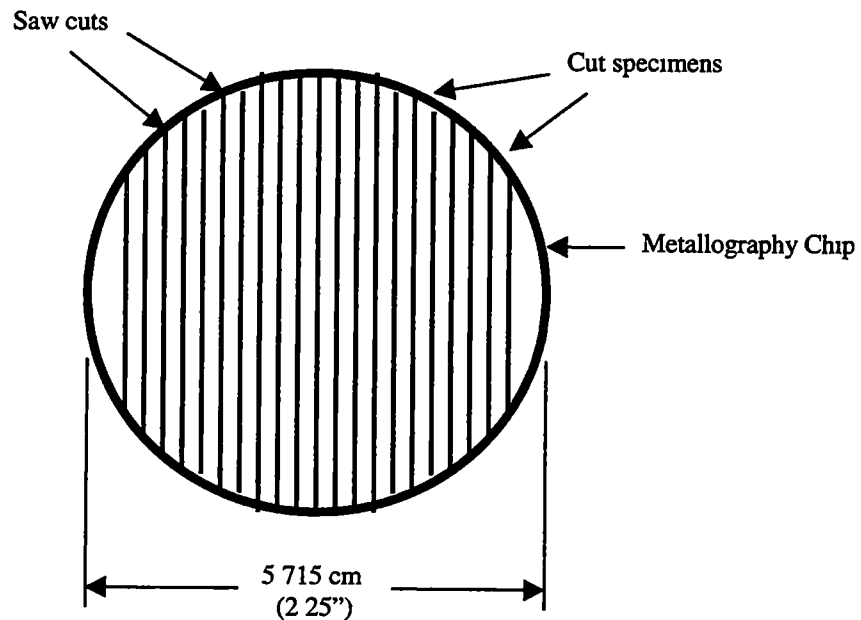
Figure 2.8 1 Schematic figure of a hot-pressed sample which is cut into specimens

2.9 Cold Working[34-36]

The main purpose of cold-working the composite material was to deform the NiTi particles so as to enact the shape-memory effect. Theoretically, when the particle is embedded within the aluminum matrix and deformed, the deformation and resulting phase change will create residual, internal stresses around the NiTi particle. These will be tensile stresses in the longitudinal and transverse directions, and compressive stresses in the through-thickness direction. In order to accomplish this easily and efficiently, the matrix material must have a greater hardness than the NiTi particles. Surprisingly, when the NiTi particles are in the martensite phase, they are much softer than the aluminum matrix (Figure 2.9.1). Even more astounding is the fact that the hardness of the particles is greater than the matrix after they are returned to the austenite phase. Thus, this unique coincidence allows the deformation of the particles within the matrix, and also supplies a reinforcement with a higher modulus than the matrix material, which is one of the primary requirements for a composite material.

Deformation was obtained by the use of a rolling mill with 5.72 cm (2.25 inch), diameter rolls. Less cracking was obtained, if the total amount of deformation was distributed over a number of passes rather than just a few. No oil was used on the rolling surfaces in order to maintain friction and good surface contact. Two stainless steel shrouds were fabricated to hold dry ice around the mill, which kept its temperature below -20°C (-4°F). Long strips of tantalum foils were folded once around each sample of the composite material to aid in feeding the sample into the mill and to discourage slipping
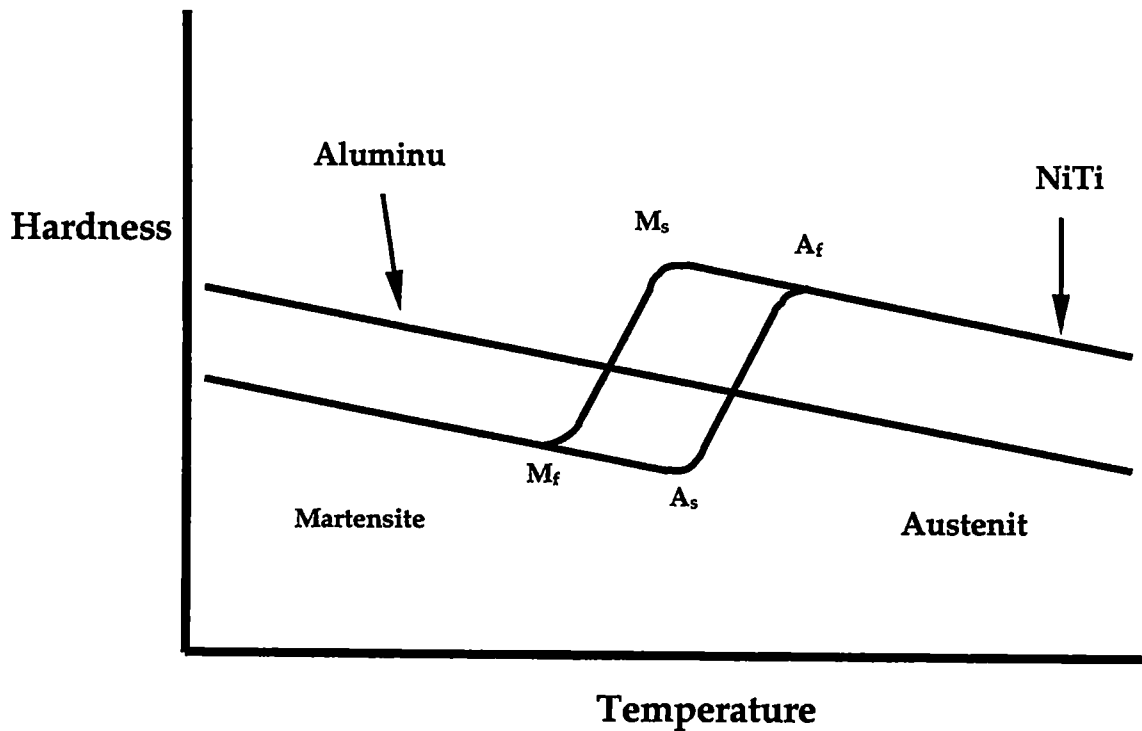
Figure 2 9 1. A schematic comparison of the relationship between hardness and temperature, for the aluminum and the nickel-titanium shape-memory alloy Note that aluminum lies between the NiTi martensite and austenite hardness ranges

and curling during deformation. The tantalum also insulated the aluminum from heat in-between passes. After each pass was made, the specimen was returned to a receptacle filled with crushed dry ice, which maintained its temperature below the M_f temperature. It was kept there until the next pass through the rolling mill. The thicknesses of each specimen was measured with a digital micrometer. A thickness reduction of 10% is used to ensure a deformation of 10%. When the desired amount of deformation had been obtained, the samples were removed from the dry ice and the tantalum casings, and were put into boiling water in order to recover the austenite phase in the particles. (The A_f temperature was around 35° C.)

The cold rolling of the samples at the dry-ice temperature proved to be a very convenient method of enacting the shape-memory effect. Figure 2.9.2 depicts a NiTi/Al composite rolled at the temperature of dry ice (-60°C or -76°F). Cracking around the particles is only on the surface of the specimen. Note that the rolling direction is from the left to right. For comparison, Figure 2.9.3 is a NiTi/Al composite rolled at the temperature of liquid nitrogen (-170°C or -274°F). Cracking is slightly more severe due to the brittleness of the composite. However, cracking still remains only on the surface of the specimen.

It was difficult to determine from a microscopic inspection if the NiTi particles themselves had been deformed, since they were randomly distributed and oddly shaped. However, DSC tests showed that there was indeed a phase change to the martensite, which was softer than the aluminum, and that the composite was deformed at a temperature at which the martensite phase was present. It is, therefore, logical to assume that the particles themselves had undergone a minimum of 10% deformation, while inside the matrix which had endured a 10% reduction in thickness in the cold-rolling process. These findings are discussed later in more detail.

NiTi
particle

Aluminum
matrix

Cracking

50 µm
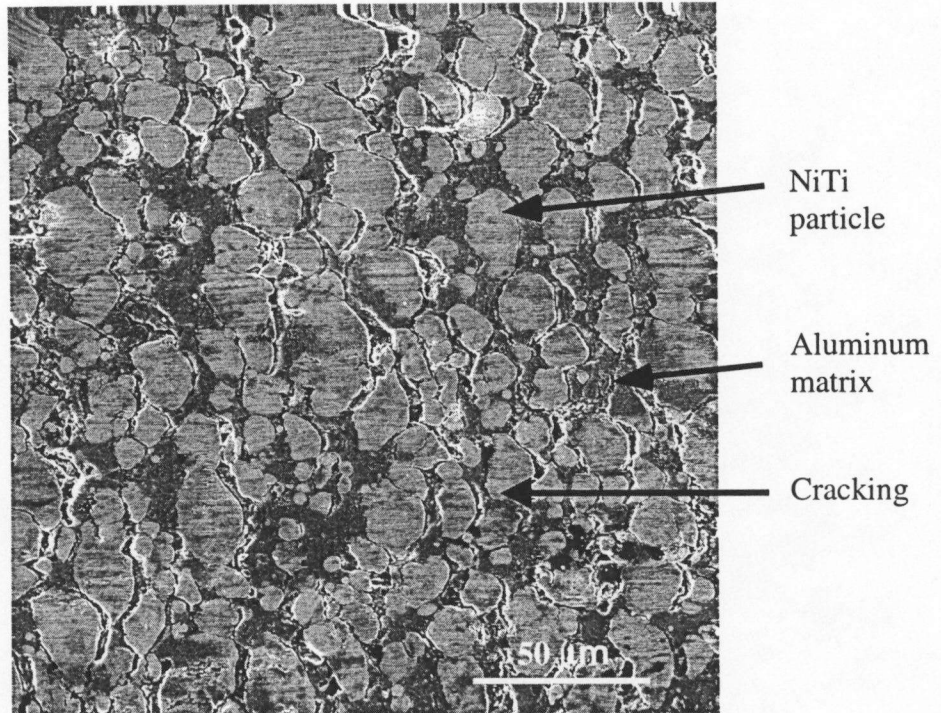
Figure 2.9.2: NiTi/Al composite rolled at the dry-ice temperature (-60°C).
Note that the rolling direction is from the left to right. (File: ez16297)

Aluminum
matrix

Cracking

NiTi
particle

80 µm
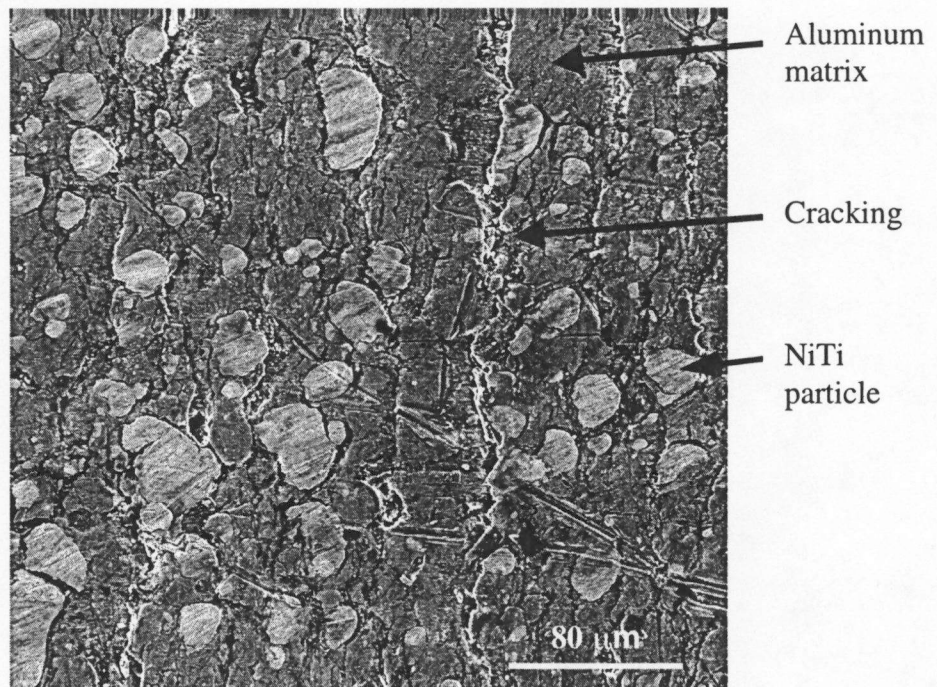
Figure 2.9.3: NiTi/Al composite rolled at the liquid nitrogen temperature
(-170°C). Note that the rolling direction is from the left to right. (File:
ez16222)

PART III.

PHYSICAL CHARACTERIZATION

3.1 Microstructural Characterization

An examination of the composite microstructure is necessary to determine or verify physical characteristics, such as the NiTi volume percent, the presence or absence of diffusion or intermetallic reactions, particle-bonding characteristics, grain structure and size, porosity, the locations of pores, and the sources of crack initiation. The optical microscope and scanning electron microscope have been used extensively as a guide towards the production and examination of the NiTi/Al composite material.

A scanning electron microscope was needed to determine the extent of diffusion between the NiTi particles and the aluminum matrix. Electron Dispersive Spectroscopy (EDS) was necessary to detect the degree of diffusion that has taken place during the fabrication of the composite. This is because only a small amount of diffusion is necessary to destroy the shape-memory effect, an amount much less than that needed to create a separate phase which would become obviously visible in any microscope.

The following figures (Figures 3.1.1 to 3.1.4) were chosen from several of the materials, as a representative sample of each material. The first two photos exhibit one kind of specimen, WX-11, which is a composite made with a 20 μm diameter, Al 1090 aluminum powder in the matrix, and a mechanically-milled 5 μm NiTi powder as the reinforcement. The last two photos exhibit another type of material, WX-12, which is a composite made with a 20 μm diameter, Al 1090 aluminum powder in the matrix, and NiTi powder, used in the as-received 40 μm size, and otherwise unchanged except for the
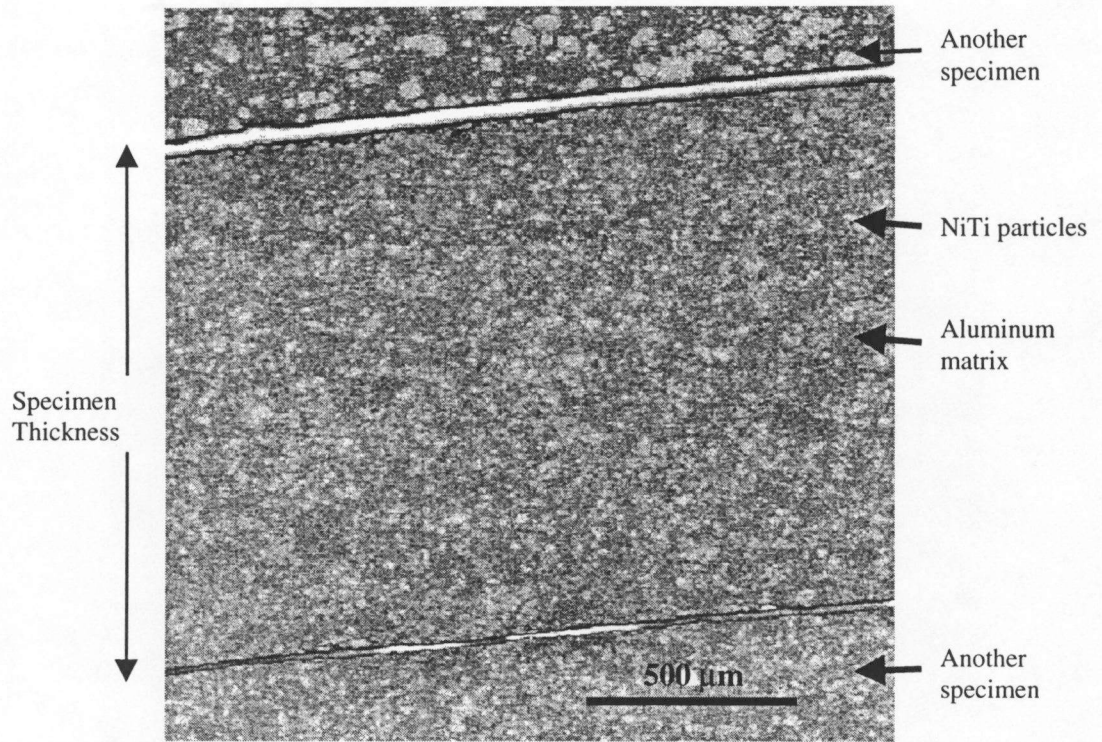
Figure 3.1.1: NiTi/Al metal matrix composite (WX-11). NiTi particle sizes are approximately 5 μm in diameter. Specimen thickness is 0.127 cm (0.050 inch).
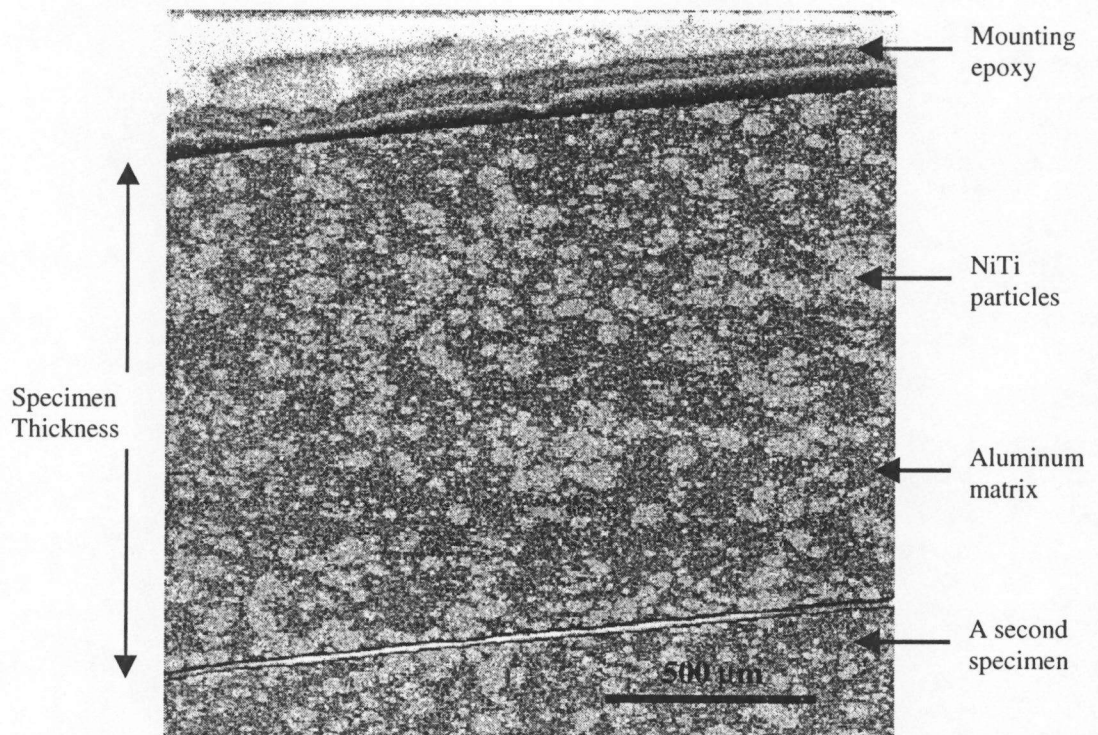
Figure 3.1.2: NiTi/Al metal matrix composite (WX-11). NiTi particle sizes are approximately 5 μm in diameter.
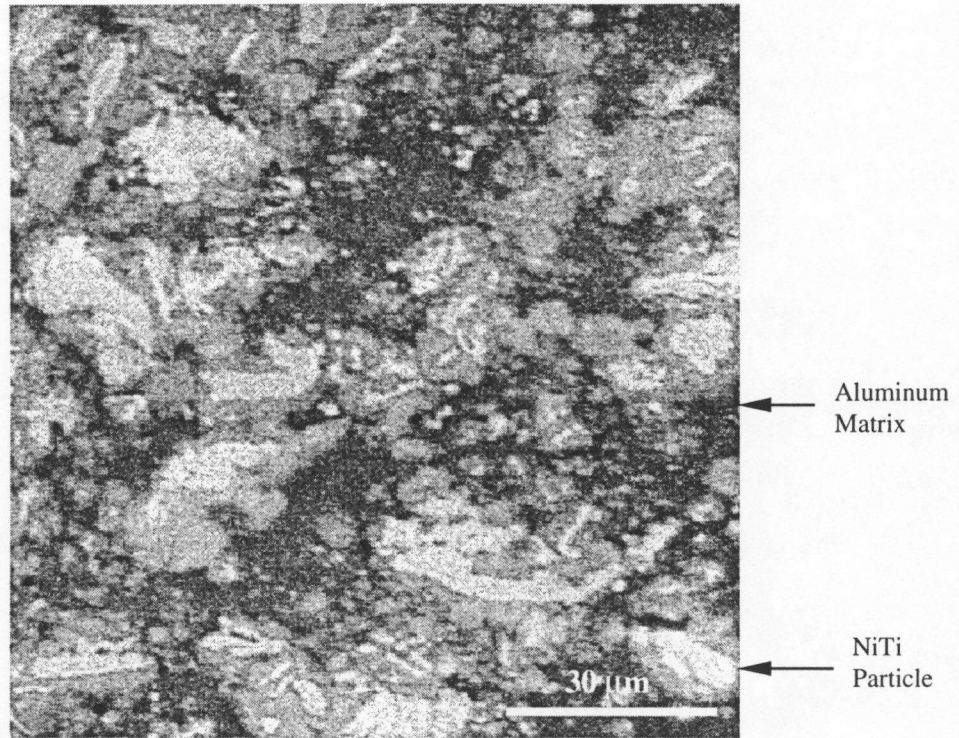
Figure 3.1.3: NiTi/Al metal matrix composite (WX-12). NiTi particle sizes are approximately 40 μm in diameter. Specimen thickness is 0.127 cm (0.050 inch).
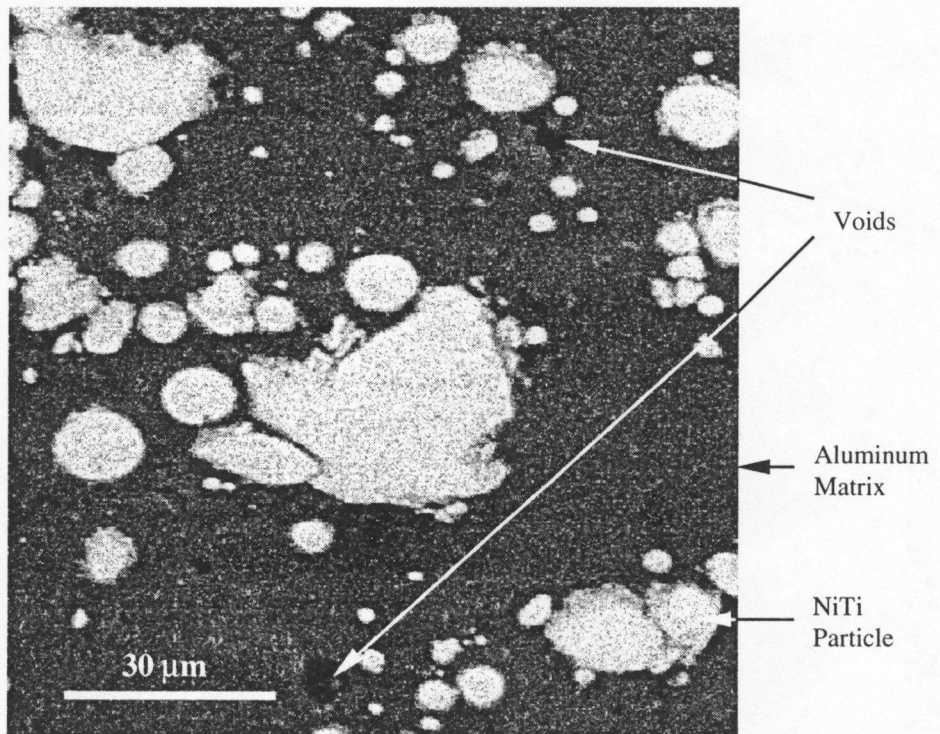
Figure 3.1.4: NiTi/Al metal matrix composite (WX-12). NiTi particle sizes are approximately 40 μm in diameter.

66

800°C heat treatment. Note that the NiTi particles are generally, evenly distributed throughout the matrix, although there are streaks and spots of areas that are sparsely concentrated. The following chapter concerning the Mechanical Characterization will conclude that these lightly-covered areas are weaknesses in the material, and will basically become paths for crack growth. The physical and mechanical characteristics of these samples will be discussed in greater detail in the following chapters.

The following two figures display the mechanically-milled 5 μm NiTi powder in an Al 1090 aluminum matrix material. Figure 3.1.1 is a macroscopic cross-sectional view of the finished specimen, cut from a tension coupon blank. Figure 3.1.2 reveals the microstructure of the material in a greater detail. It can be seen that the particles are fairly well distributed, but there is also quite a bit of diffusion, creating a second phase around the particles. Fortunately, even though the sizes of the NiTi particles have been reduced, the shape-memory effect still remains, although it is not nearly as pronounced as it is in some of the other compositions.

Figures 3.1.3 and 3.1.4 are similar views of a different material. This material has 40 μm NiTi powders in a pure aluminum matrix. It is much easier to ascertain the distribution of the particles in this material, due to their large size and the fact that there is much less diffusion. However, this material also shows more porosity, and therefore, a diminutive composite density in comparison to some of the other specimens made with the same 20 μm diameter aluminum powder used as the matrix material.

3.2 Product Density

Since the presence of voids in the composite can produce stress concentrations and thus, sites for crack initiation, the product density must be known in order to accurately predict material behavior. The Archimedes immersion technique has been used for measuring density. This method measures the weight of the sample, while suspended in ethanol, and compares that weight with the dry weight of the sample. The density of the ethanol, which is sensitive to temperature, can be used to find the density of the sample. The density of the sample is defined by the following equation,

$$Density = \frac{(m_{dry})(\rho_{ethanol})}{m_{wet} + m_{app} - m_{sus}}$$
(Eq. 3.2.1)

where m_{dry} is the mass of the dry sample, m_{wet} is the mass of the sample completely soaked in ethanol, m_{app} is the mass of the appliances used to suspend the specimen in the ethanol solution, and m_{sus} is the mass of the specimen measured while suspended in the ethanol solution. $\rho_{ethanol}$ is the density of the ethanol, at the temperature of the ethanol that the sample is measured in. The percentage of theoretical density was calculated by taking the ratio of the sample density to the commonly-accepted scientific value of the density, which can be found in any catalog of physical constants,[32] or calculated from these values using the proportions of the constituent elements involved. The densities of samples have been used in the comparison of the mechanical behaviors of samples made with different powders and pressing conditions.

Table 3.2.1 summarizes a few combinations of the various particle sizes used to produce different samples of materials, their pressing temperatures, and the resulting densities. There are different combinations of 5 μm and 40 μm NiTi powders with 5 μm Al 1050, and 20 μm, Al 1090 aluminum powders. There are two (WX-6 and WX-10), that have no NiTi powders at all. The pressing temperatures ranged from 520°C to 550°C (970°F to 1020°F), and the densities ranged from 97.3% to 99.94%. Of course, the higher temperature pressing conditions produced a greater density, but it is interesting to note that the materials using the 20 μm aluminum powders in the matrix yielded a higher density than the materials using the 5 μm powders. It can generally be said that the materials made without the NiTi particles have higher densities than those made with the NiTi, and in some cases, as with WX-10 and WX-12, the differing powder sizes have a greater influence on the density than the pressing temperature does.

Table 3 2 1   A companson of the densities of several materials, formed by hot-pressing powders of differing sizes at different temperatures   All samples were produced using 69 MPa (10 ksi) pressure on a 5 715 cm (2 25 inch) steel die

Name	NiTi Powder Size (μm)	Aluminum Powder Size (μm)	Pressing Temperature (°C)	Theoretical Density (%)
WX-6	~	5	550	98.5
WX-8	5	5	520	97.3
WX-9	5	5	540	97 8
WX-10	~	20	540	99 61
WX-11	5	20	550	99 94
WX-12	40	20	550	99 49

Density as a Function of Particle Size

It has been found that the use of differently sized and shaped NiTi and aluminum powders affects the product density. It can be seen that the larger, 20 μm-diameter-sized Al 1090 aluminum powders provide a significantly higher composite density to the material than the 5 μm diameter sized Al 1050 aluminum powders. This trend seems to contradict the findings of German,[29] who theorized that finer powders permit greater densification. However, finer particles also require greater pressures in order to achieve this densification. Since all samples have been pressed at the same pressure, it is conceivable how the finer particle mixtures may yield composite samples with lower densities. Also, consider that each aluminum particle has a surface oxide coating. From simple geometry, it is known that the surface area of a spherical particle is $4\pi r^2$, and the volume is $4/3\pi r^3$. Therefore, as the diameter is enlarged, the surface area to volume ratio decreases. In the present case, the surface area represents the amount of Al_2O_3 that is on the surface of each particle, and the volume represents the body of the particle, composed of aluminum. As a result, it naturally follows that there would be a much lesser amount of Al_2O_3 incorporated into the matrix when using the larger particles. This results in the material being more ductile and more easily compacted during hot-pressing, yielding higher densities.

German[29] also states that materials are more easily densified when combining particles of differing sizes, as opposed to using particles that all have the same size. Conveniently, the mechanical-milling procedure produces a large assortment of particles

with different sizes, with the average size being around 5 μm. In accordance with Germans' predictions, the samples made with the mechanically milled NiTi particles (WX-8, WX-9, WX-11), do show a higher density than other samples using the 40 μm diameter NiTi particles (WX-12), or no NiTi particles (WX-6, WX-10), considering the differences in pressing temperatures.

In conclusion, the 20 μm Al 1090 aluminum will produce a composite sample of greater density than the 5 μm Al 1050 aluminum powder, and the 5 μm mechanically milled NiTi powder will produce a composite sample of greater density than the unmilled, 40 μm NiTi powder, provided that temperature and pressure are held constant, among other variables.

Density as a Function of Pressure for Green Pellets

A pellet, pressed without the use of heat (e.g., at room temperature), is called a "green" pellet. The density of a green pellet is termed the green density. Green density is especially important when manufacturing a P/M sample by cold isostatic pressing, but can also lend qualitative knowledge about the densification characteristics of a powder during hot pressing. An experiment was done in which several green pellets were made at different pressures. One series with one punch mobile and another fixed (Table 3.2.2), and another series done with both punches mobile (Table 3.2.3). A Carver™ metal die with an inner diameter of 2.858 cm (1.125 inch) was used (Catalogue #: 2090-0, Wabash, IN, USA). 30.0 grams of Alcoa 201 powders were employed for each run in this

Table 3.2.2: Green density measurements in relation to the applied pressure, using two punches, one fixed and another mobile.

Pressure (MPa)	(ksi)	Theoretical Density (%)	Density (g/cc)	Reading (mm)	(in)
Tapped	Tapped	46.2	1 2283	67.28	2.6490
10 3	1.5	52.8	1.4716	133.39	5 2515
13.8	2 0	53.9	1 5028	132 73	5 2255
17 2	2.5	55 7	1.5529	131 72	5 1860
20 7	3 0	57 0	1 5897	131.03	5 1585
24 1	3.5	58 4	1 6290	130 31	5.1305
27.6	4 0	59 6	1.6630	129 73	5 1075
31 0	4 5	60 7	1 6935	129.22	5.0875
34.5	5.0	61 2	1.7077	128.99	5 0785
41 4	6.0	63.5	1 7717	128.00	5 0395
48.3	7 0	65.5	1 8270	127 20	5 0080
55.2	8 0	66.7	1 8613	126.73	4.9895
62 1	9 0	68.0	1.8957	126 28	4.9715
69.0	10 0	70 5	1 9677	125.37	4 9360

Table 3.2.3: Green density measurements in relation to the applied pressure, with both punches mobile.

Pressure (MPa)	(ksi)	Theoretical Density (%)	Density (g/cc)	Reading (mm)	(in)
Tapped	Tapped	43.2	1 2057	140 40	5 5275
6 9	1 0	50 3	1.4038	134 92	5 3120
10 3	1 5	52 8	1 4716	133 39	5.2515
13.8	2.0	53.9	1.5028	132.73	5 2255
17 2	2 5	55 7	1.5529	131 72	5 1860
20.7	3.0	57.0	1 5897	131 03	5.1585
24 1	3 5	58 4	1 6290	130.31	5 1305
27.6	4.0	59.6	1 6630	129 73	5.1075
31.0	4 5	60 7	1.6935	129.22	5 0875
34.5	5.0	61.2	1.7077	128 99	5.0785
41 4	6.0	63.5	1.7717	128 00	5 0395
48 3	7 0	65.5	1 8270	127.20	5 0080
55.2	8 0	66 7	1.8613	126.73	4 9895
62 1	9.0	68.0	1 8957	126 28	4 9715
69.0	10 0	70.5	1.9677	125 37	4.9360

experiment. The theoretical density is calculated using a fully-dense specimen as a standard, based on the density, ρ = 2.79 g/cm^3. The column labeled "reading" is the length between the two ends of the upper and lower punches. Note that the densities are equal, regardless of the punch configuration.

Pressure-Density Relationships Involving Hot Pressing

Another preliminary experiment was conducted to determine the overall effect of the pressure on the densities of the samples during hot pressing. The authors theorized that the low volume percent and the relatively high melting point of NiTi would cause the aluminum powders to be primarily responsible for product densification during pressing. Therefore, since the aluminum matrix would play the main role in particle bonding, pure aluminum powders (JM11067, Al 99.5% pure, 5 μm particle size) were used without any NiTi powders in this procedure. The data resulting from this experiment, shown in Table 3.2.4, was then fit to a regression analysis in order to establish a linear relationship of density versus pressure (Figure 3.2.1). The density may be calculated from the following equation,

$$\rho = 60.52 + 30.196 \log\left(\frac{P}{6,896,000}\right) \qquad \text{(Eq. 3.2.2)}$$

where ρ is the percentage of theoretical density of the P/M composite material, and P is the hot pressing pressure in Pascals. It should be noted, however, that the actual temperature of the powder during pressing for all data in this experiment was only

73

approximately 275°C (530°F), due to temperature gradients inside the steel die. But from this data, it is estimated that a 99.5% theoretical density may be achieved with 69 MPa (10 ksi) at a temperature of 580°C (1,080°F). A sample was later pressed which offered evidence of validity to the estimation. This sample was pressed at 69 MPa (10 ksi) at a temperature of 550°C (1,020°F) with no degassing, and obtained a theoretical density of 97.2%. In conclusion, the data shown in Table 3.2.4 can be used as a guide in determining the pressure necessary to produce a desired density in a sample. However, there may be inconsistencies due to the fact that this data only concerns the aluminum matrix material. Densification properties may change with the addition of a second, harder, larger-sized powder.
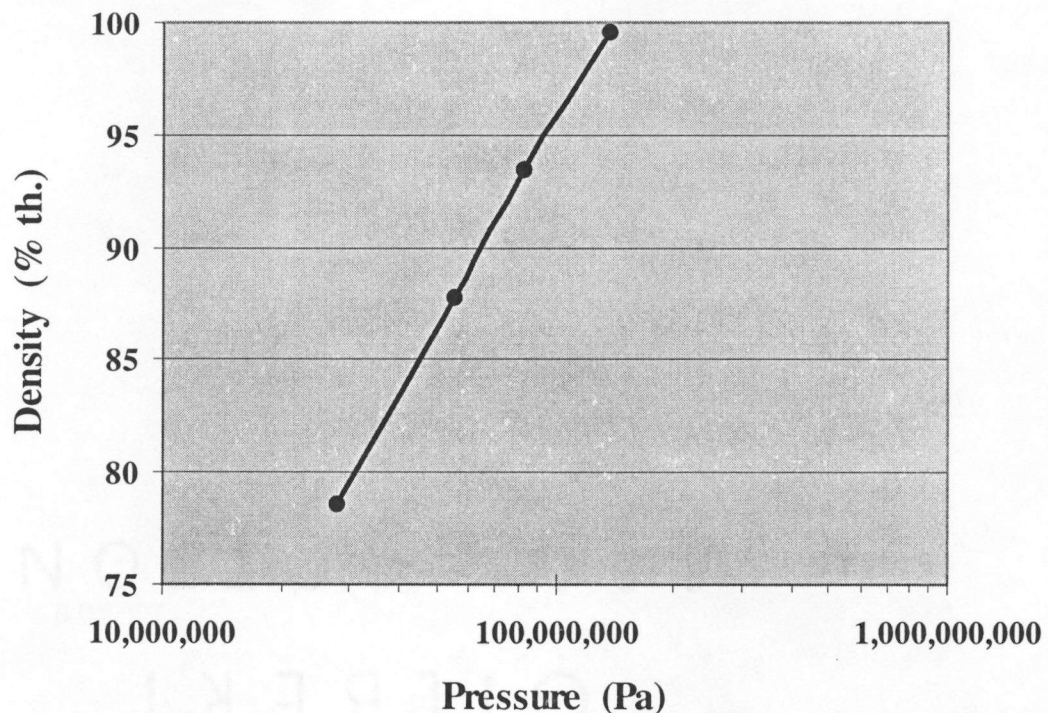
Figure 3.2.1: The relationship between the density and applied pressure of a sample hot-pressed at 275° C.
(1ksi = 6,896,000 Pa)

74

Table 3.2 4: Density measurements of hot pressed samples in relation to the applied pressure

Pressure (MPa)	Pressure (ksi)	Theoretical Density (%)
27 6	4	78.6
55 2	8	87.8
82 8	12	93 4
137 9	20	99.6

3.3 Phase-Transformation Characterization by Differential Scanning Calorimetry

Since the shape-memory effect is a phase transformation within the material, differential scanning calorimetry (DSC) could be used to measure the presence of the shape-memory effect and the specific temperatures associated with it. If phase transformations were detected in the composite material, it revealed whether the shape-memory effect was present, and if its desired effect on the matrix was possible. It is important to consider, not only if the shape-memory effect had been *preserved* through the particle size reduction procedure, but also if the transformation temperatures had been altered or skewed from the original locations as a result of diffusion or oxidation (see the following section, *The Role of Composition and the Effects of Diffusion*). DSC tests were conducted for each different batch of NiTi powders produced by various methods. A second investigation using the DSC was necessary to determine if the phase transformation continued to be preserved in the composite materials through the hot-pressing procedure, and the exact temperatures at which they take place. DSC curves were generated and compared to each other, to consider the effects of differing conditions of production and mechanical behavior of each.

After experimenting with several samples, DSC tests showed that the phase transformation could be retained in the NiTi powders through the milling process by way of the heat-treatment procedure. NiTi powders used for the composite materials in consideration retained their phase transformation throughout the annealing process. The A_s temperature in these NiTi powders dropped approximately 20°C, which suggests that

a small amount of titanium had leached from the particle during the heat-treatment procedure. The shift in the transformation temperature is probably due to the small amount of surface oxidation which was hoped to occur during heat treatment (see the following section, *The Role of Composition and the Effects of Diffusion*). Since the free energy of Ti is much lower than Ni, the formation of TiO_x compounds are thermodynamically preferential over NiO_x.[13,31] This thin titanium oxide layer was expected to act as the necessary barrier to prevent diffusion during hot-pressing. Further tests (discussed in the following section) were necessary to determine if there is a sufficient oxide layer present, and whether that layer was successful in preventing diffusion, thus preserving the shape-memory effect.

An attempt will be made to display a comparison between the phase-change behavior before processing and that of the powder after processing. (See Figures 3.3.1 and 3.3.2.) These results are summarized in Table 3.3.1. Figure 3.3.1 displays the DSC curves for the NiTi powder in the as-received condition. Note that the earmarked A_s temperature is 40°C, with the peak austenitic transformation at 50°C. The A_f temperature is around 57°C. The total transformation extends through a space of about 17°C. The M_s temperature is about 30°C, with the peak martensitic transformation at about 22°C. The M_f temperature is approximately 13°C. The total martensitic transformation also spans a range of about 17°C.

Figure 3.3.2 depicts the DSC curves for the NiTi powder, after being mechanically-milled and recrystallized through the heat-treatment procedure. Note that the A_s
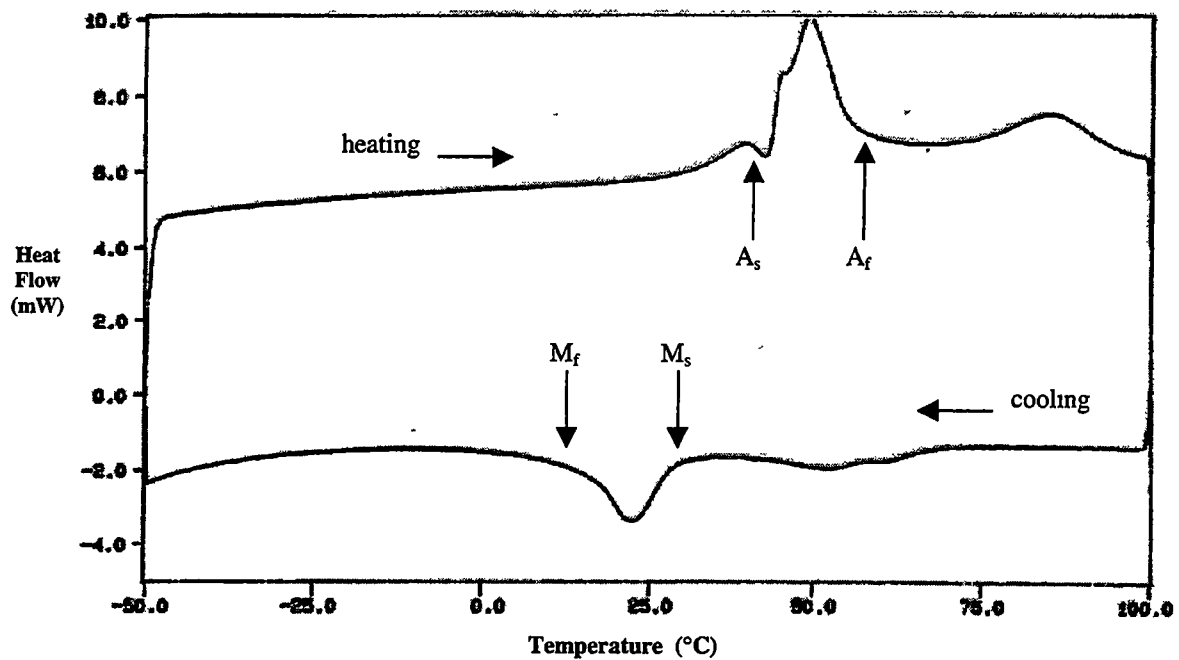
Figure 3 3 1 DSC curves for the NiTi powder, in the as-received condition from the manufacturer
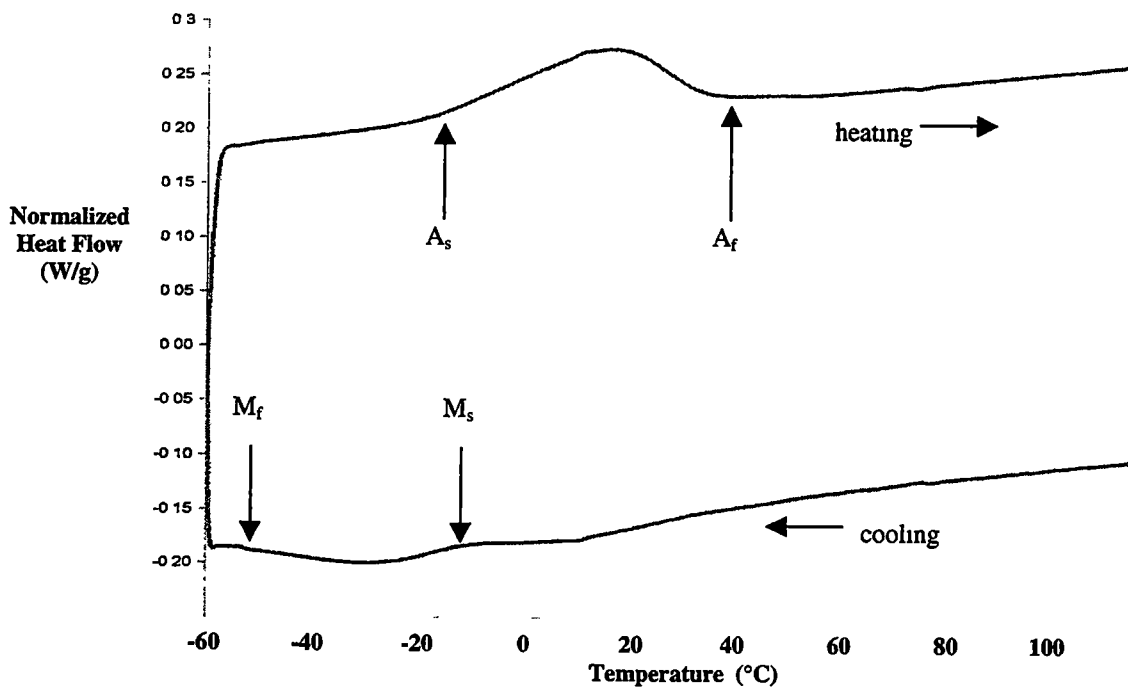
Figure 3 3 2 DSC curves for the NiTi powder, after being mechanically-milled and heat-treated

Table 3 3 1· Temperatures associated with certain critical points of the phase-transformation for the NiTi shape-memory particles ΔT is the corresponding changes in those temperatures.

Transformation Temperature	A_s (°C)	A peak (°C)	A_f (°C)	A span (°C)	M_s (°C)	M peak (°C)	M_f (°C)	M span (°C)
Before milling (as received)	40	50	57	17	30	22	13	17
After milling and heat treatment	-20	15	35	55	-10	-25	-50	40
ΔT	-60	-35	-22	+38	-40	-47	-63	+23

,

temperature is around -20°C, with the peak austenitic transformation at 15°C. The A_f temperature is around 35°C. The total austenitic transformation extends through a space of about 55°C, as opposed to the 17°C of the original powder. The M_s temperature is around -10°C, with the peak martensitic transformation at about -25°C. The M_f temperature is approximately -50°C. The total martensitic transformation extends through a space of about 40°C. Remarkably, the phase-transformation behavior, as indicated by DSC curves, had no appreciable change between that of the annealed powder and the composite material after pressing. This trend indicates that the oxide layer on the particles has demonstrated a sufficient hindrance to diffusion.

3.4 The Role of Composition and the Effects of Diffusion

The composition of a shape-memory alloy is very sensitive, and crucial in determining the temperatures at which the shape-memory behavior is observed. Consequently, the changing of the composition may be used to tailor an alloy's shape-memory performance to a specific temperature range. An accurate control in producing a transformation at a desired temperature is invaluable and adds to the versatility in the commercial use of SMAs.

In the NiTi system, a higher nickel content decreases the temperature at which the martensite begins to form, as shown in Table 3.4.1. However, if the nickel content exceeds 56.0 weight percentage (wt.%) in the solid solution, Ni_3Ti may precipitate and detract from the shape-memory behavior. Figure 3.4.1 illustrates the NiTi phase diagram, with the NiTi phase at the center of the diagram. This region is utilized during the annealing procedure, when the amorphous powder is solution-treated at 800°C in order to allow recrystallization to occur upon cooling (see Chapter 2.6, *Recrystallization of Powders*).

Table 3 4 1 The difference in the transformation temperature in relation to the composition
(from   U-Di-Met Manufacturing Company material data sheets)

Powder	Transformation Temperature	Nickel (wt. %)	Titanium (wt. %)
NiTi	A_s -20°C	55.9%	44.1%
NiTi	A_s +40°C	55.5%	44.5%
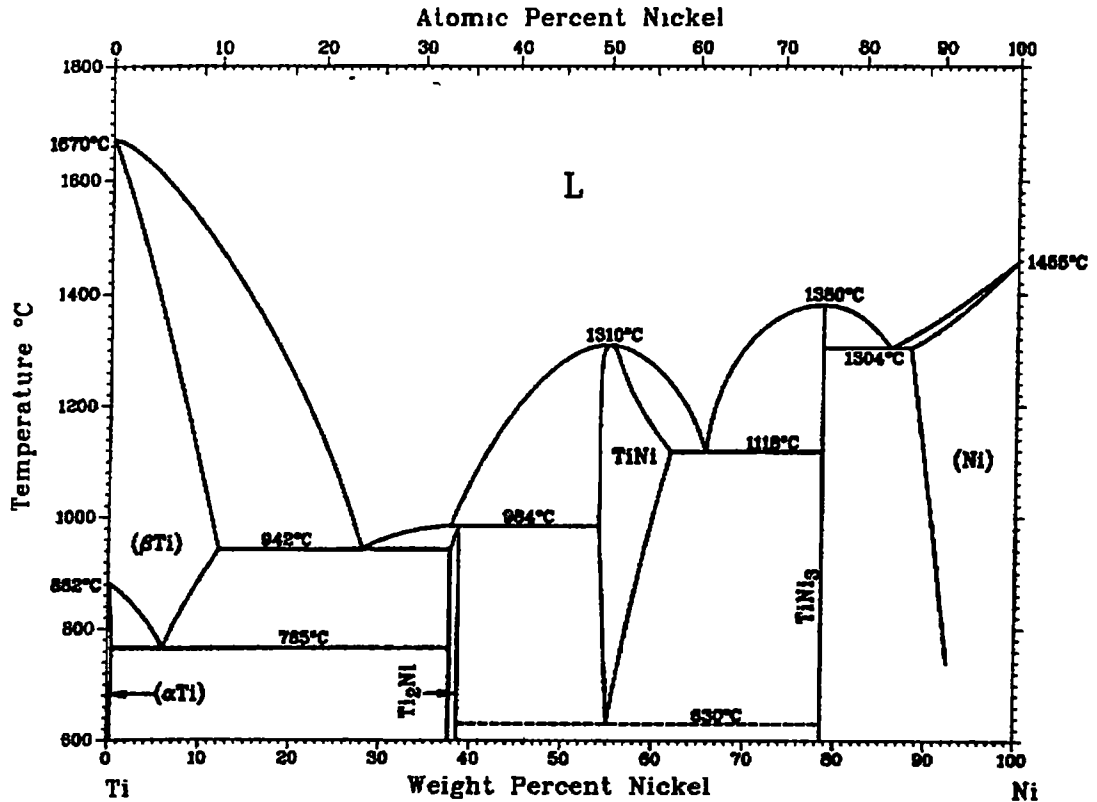
Figure 3 4 1[33] NiTi phase diagram with the NiTi phase at the center of the diagram. The composition is crucial, and the shape-memory effect may be lost entirely, if the composition changes more than 0 5 wt %

However, for the present work, the author is more interested in how diffusion in the NiTi particles may alter the composition, thus changing the shape-memory behavior. The slightest bit of diffusion, while the material is at higher temperatures, will alter the composition and change the transformation temperatures, especially in a very small particle, which can be subjected to a relatively large amount of diffusion quite rapidly. Therefore, the following three sections will consider the effects of surface coatings on the NiTi particles as an attempt to limit the diffusion process, and the effects of hot pressing on diffusion.

The Effects of Annealing on Diffusion

The broadening of the DSC peaks in Figure 3.3.2, which was previously discussed, is probably due to the fact that the NiTi particles have undergone diffusion (see the previous section). The oxidation reaction on the surface, during the annealing process, has caused various elements to migrate into and out of the surfaces of the particles. This process removed titanium from the alloy and has altered the composition. The surfaces of the particles have undergone the greatest amount of diffusion, while the center regions of the particles remained virtually unchanged, depending on the size of each particle and the duration of the heat treatment.

The author theorizes that this alteration of the composition towards the surfaces of the particles has caused a variation in the transformation temperatures in various locations within each particle (see Table 3.4.1 and Figure 3.4.2). For instance, consider a single powder particle, which has undergone the mechanical-milling and heat-treatment procedures. The center of the particle (region A), having undergone a minimal change in the original composition (C_0), has experienced relatively no change in the transformation temperatures. The outer shell of the particle is a thin layer of TiO_x, having its own composition of C_{oxide}. The region between A and C, is the area of titanium diffusion, which has undergone a significant change in the composition, and has also experienced great decreases in the transformation temperatures. These decreases in the transformation temperature are greater at point C than the area in proximity to region A. For example, in region A, the composition is 44.5 wt.% titanium. At this composition, the NiTi begins
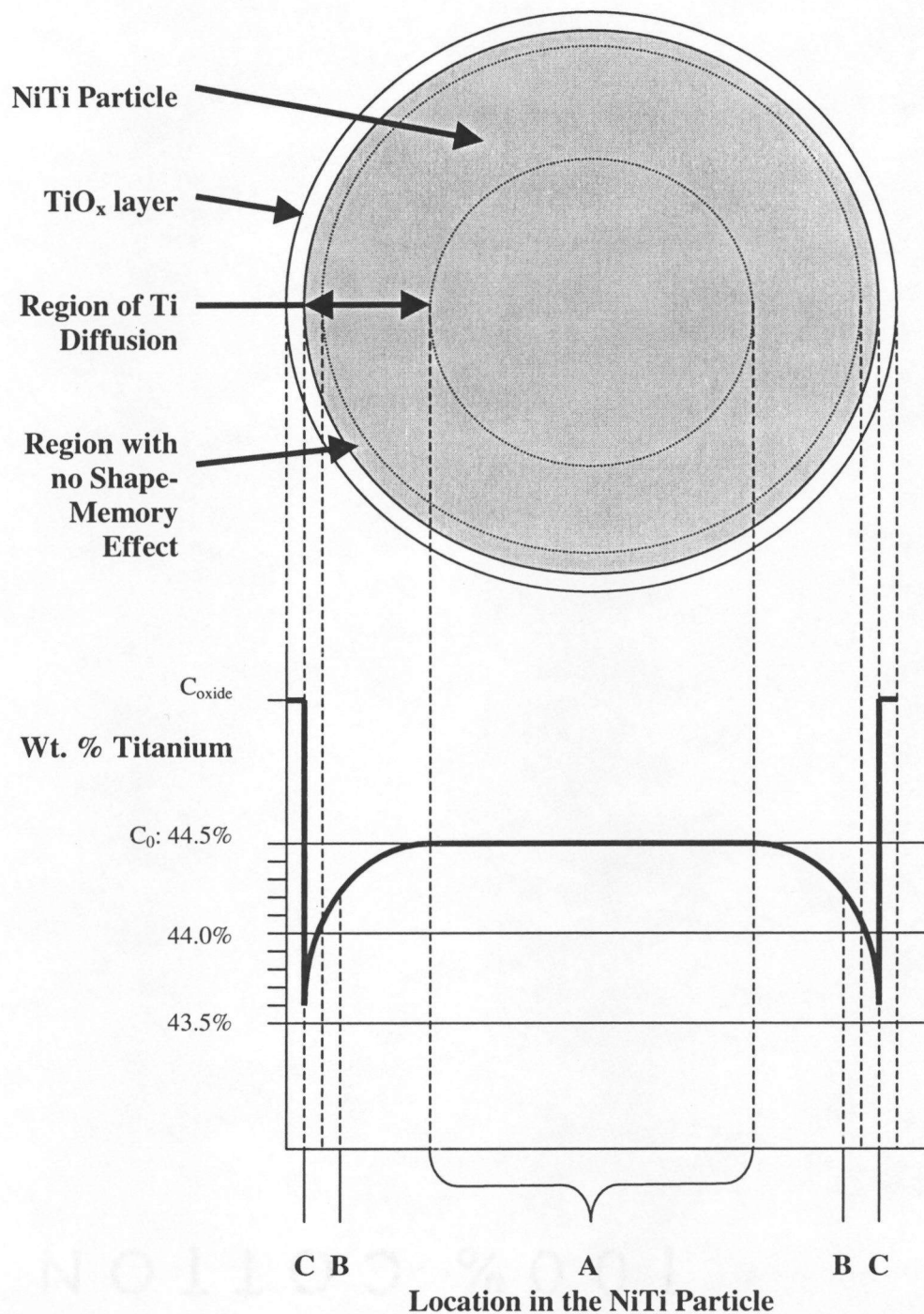
Figure 3.4.2: A schematic diagram of the titanium compositional gradient in the NiTi particle due to the diffusion and formation of the titanium oxide layer during annealing.

the transformation to the austenitic phase, at the temperature of 40°C. At point B, the composition of titanium has dropped to 44.1 wt.% titanium, producing a related phase-transformation to the austenitic at the temperature of -20°C. At point C, the composition has dropped below 44.0 wt.% titanium, thus producing a second phase of Ni_3Ti in the microstructure, which inhibits the shape-memory effect. Since different regions of the particle exhibit various phase-transformation temperatures, the particle as a whole, and thus, the entire composite will show a wider range of phase-transformation temperatures. This behavior produces the smearing effect on the DSC curves of the entire powder, with the effect of broadening the curves, as well as lowering the overall transformation temperature.

The Effects of Surface Coatings on Diffusion

It was very difficult to hold pressing conditions, such as temperature and pressure, constant from sample to sample. Only when these variables were held constant, could a fair comparison be made of trial surface coatings and their effects on the diffusion process. In order to overcome this potential source of deviation, several NiTi powders with experimental surface coatings were put into a single die and pressed simultaneously in one hot-pressing operation. This step ensured that all the powders contained within endured the same manufacturing conditions, and thus, any differences found in the various consitituents were solely because of different powder treatments and surface coatings. In order to find the effects of hot pressing on the rates of diffusion and the formation of intermetallic compounds for different composite materials made with NiTi

powders of differing surface coatings and heat treatments, this experiment was conducted as follows.

Several NiTi powders with differing experimental heat treatments and surface coatings were fabricated, and combined with aluminum powders in the appropriate ratio, to form several charges of powders of differing respective composite materials. Twelve small green pellets [0.3175 cm (0.125 inches) in diameter] of these composite powders with differing NiTi treatments were pressed, and arranged in a single 3.175 cm (1.25 inch) die. Aluminum powders were carefully packed around the green pellets in the die, and the entire assembly was pressed at 550°C (1020°F) and 69 MPa (10 ksi). The result was a single aluminum specimen containing twelve circular regions of different composite materials. This procedure ensured that all the composite powders endured the same pressure and heat treatment throughout hot-pressing, and were basically of equal densities. After pressing, the 3.175 cm (1.25 inch) sample was polished with a standard metallographic technique, using corundum discs for the rough polishing and diamond pastes for the final polishing. The microstructure of each region was examined using a SEM and EDS methods.

The purpose of this study was to test the effects of different NiTi processing methods in relation to hot-pressing and their effectiveness in preventing diffusion. It was found that a couple of the NiTi surface coating treatments worked extremely well at preventing diffusion. These two surface coating treatments were an oxide layer and a nitride layer. Of these two, the oxide layer was chosen to be used for the NiTi powder

employed in the fabrication of the composite material, because of the simplicity of the process and the fact that the nitride coatings were very brittle.

The M_s and A_s temperatures of the composite material after pressing remained unchanged from that of the milled and annealed powders. However, DSC tests for some samples pressed at higher temperatures (around 580°C or 1080°F) showed only broad, very shallow peaks (however, similar to Figure 3.3.2), indicating that an additional 60°C in pressing allowed enough aluminum to diffuse into the NiTi phase to effectively destroy the shape-memory effect. Evidently, there was very little diffusion of Ni or Ti out of the particles during pressing, otherwise, there would be a change in the M_s and A_s temperatures, which was not present. Much of this behavior is inherently linked to the diffusional barrier provided by the oxide surface coating.

The Effects of Hot Pressing on Diffusion

The extended period of time that the samples have spent at elevated temperatures during degassing and hot-pressing has permitted extensive diffusion of aluminum into the NiTi particles. This occurrence has changed the composition of the shape-memory alloy and may have caused the loss of the shape-memory effect. Figure 3.4.3 shows an apparently functional NiTi particle in a pure aluminum matrix, exhibiting good bonding and no visible second phases.

However, an EDS investigation, as exemplified in Figure 3.4.4, has revealed that that Al has diffused 6 µm into the surface of the particle   Several EDS measurements
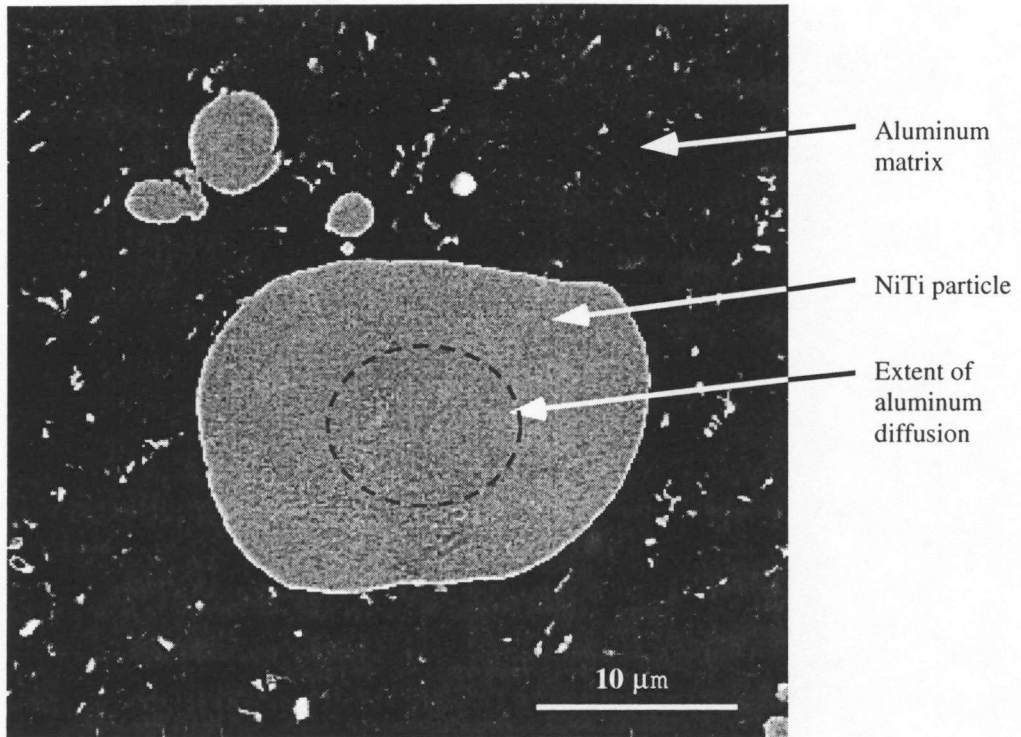
Figure 3.4.3: An apparently functional NiTi particle in an aluminum matrix (JM11067) showing good bonding and no visible second phases. However, aluminum has diffused into the NiTi particle in the form of a solution, altering the composition and destroying the shape-memory effect. (File: ez16082)
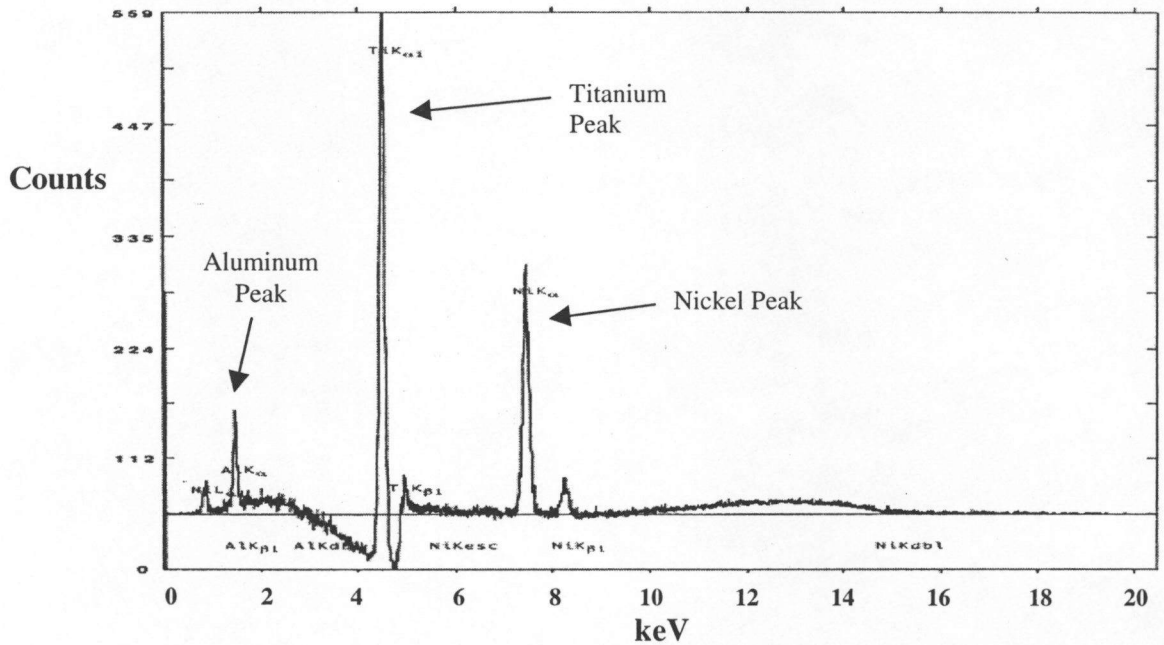
Figure 3.4.4: An EDS analysis of the NiTi particle 6 μm from the particle/matrix interface.

were taken in a linear array from the surface of the particle going toward the center. The last EDS probe that showed the presence of aluminum was 6 µm from the surface. The present result is similar to what Furuya has found in his work on NiTi *fibers* in an aluminum matrix.[21] Unfortunately, EDS will not reveal the quantity of constituent elements that are depicted in the diffraction measurements, but Fick's law of diffusion[37] declares that the concentration of one element diffusing into another is governed by the following equation,

$$\frac{\partial C}{\partial t} = D \frac{\partial^2 C}{\partial x^2} \qquad \text{(Eq. 3.4.1)}$$

where C is the concentration of the diffusing element, D is called the diffusion coefficient, which is expressed in square meters per second, t is the time, and x is the distance from the interface. The solution to this second-order differential equation will reveal the concentration of the diffusing element as a function of distance. Since we know that the concentration of aluminum at x = 0 is 100%, and the concentration at x = 6 µm is 0%, we can fix the endpoint constants and deduce the aluminum concentration profile depicted in Figure 3.4.5.

This leads to the conclusion that Al has diffused from the matrix into the NiTi particles and exists in the solution of NiTi, enveloping between 40 and 100% of the volume of each particle and effectively destroying any shape-memory effect in the particles. A DSC analysis, discussed in Chapter 3.3, confirms this speculation.
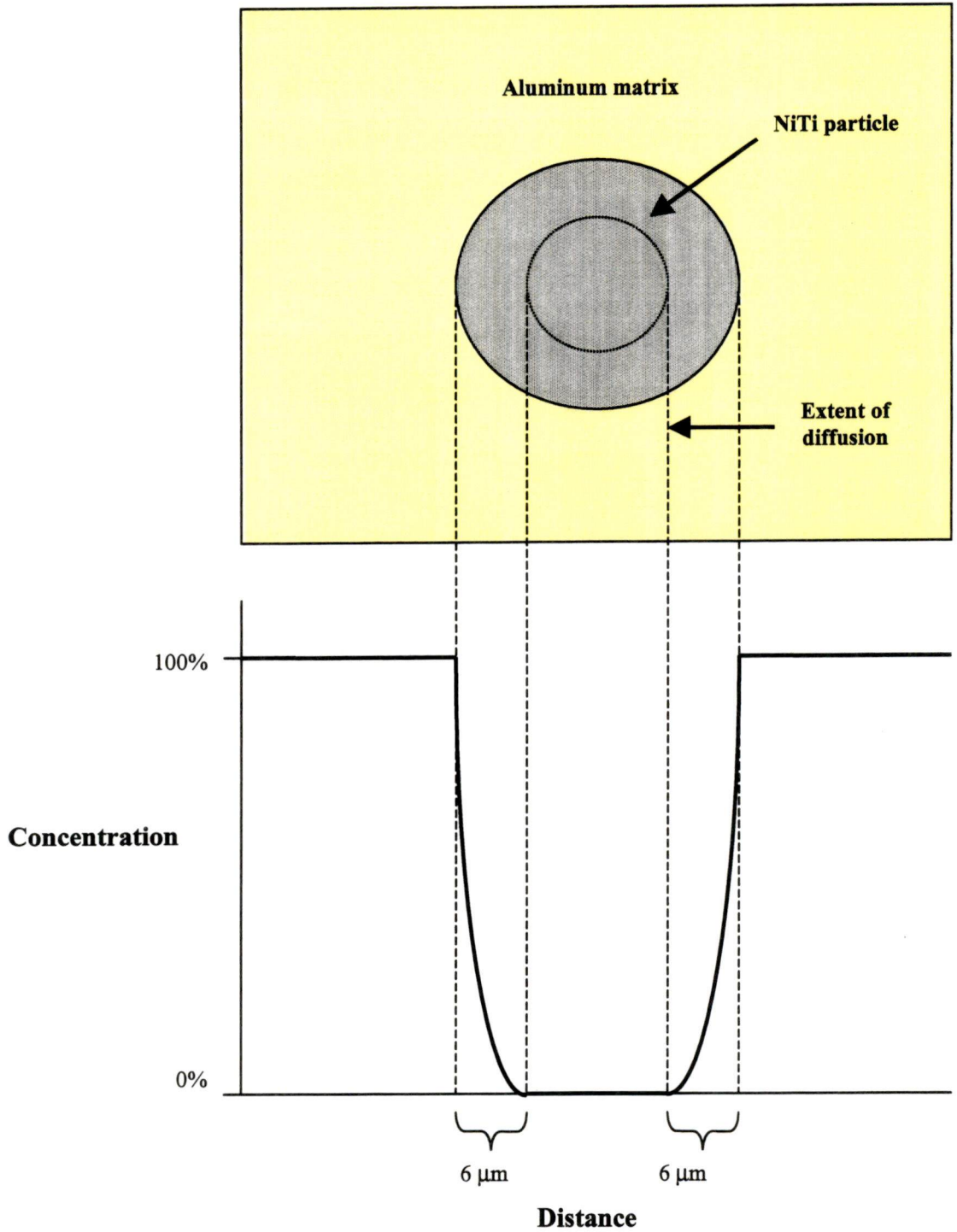
Figure 3.4.5: A two-dimensional schematic diagram of the aluminum concentration profile in an uncoated NiTi particle within the matrix. Note the greatly diminished size of the area of the unchanged composition, which is a volume in the real material, since the actual composite is three-dimensional.

Difficulties, such as the diffusion of aluminum into the NiTi particles, became commonplace. There were brittle intermetallic phases, such as TiAl, that formed and caused premature edge cracking during the cold rolling of the composite. The relative thicknesses of these intermetallic layers also dwarfed the volume of the NiTi particles, thus reducing the shape-memory effect on the matrix. Curiously, the DSC curves show little change between those of the annealed powder and the hot-pressed composite material. This trend indicates that the extent of the diffusion of aluminum into the surface of the particle during hot-pressing is of an equal or lesser degree than the extent of the diffusion of titanium out of the particle during the annealing procedure. In the end, approximately the same material near the surface of the particle has had the composition disrupted adequately to alter the phase-change behavior, either by the loss of titanium or the gain of aluminum.

PART IV.

MECHANICAL CHARACTERIZATION

4.1 Compression Tests

In order to identify the optimal temperature for cold deformation, a compression test was conducted. This is a convenient experiment, which only requires samples of the material to be a small cube with dimensions of 2.54 mm (0.100 inch) on each side. Four samples, cut from a hot pressed pellet (#146) composed of Al 2124 aluminum alloy with 20 vol.% NiTi, were each subjected to compression tests at different temperatures. Figure 4.1.1 shows the results of those tests. The specimen compressed at 120°C has approximately 150 MPa (20 ksi) greater yield strength at 7% deformation than the specimen compressed at 0°C. Samples must be deformed below 0°C in order to enact the shape-memory effect. From this behavior, it can be seen that a maximum cold-working benefit can be obtained at around 7%. This is a noteworthy discovery, since only 8-9% deformation can be recovered through the shape-memory effect. It is a convenient coincidence that the maximum cold working strain is roughly equal to the maximum recoverable strain through the shape-memory effect. However, since the compression tests were conducted before a phase transformation had been preserved in the development of the material, the results only give reliable information about the work-hardening behavior of the composite. It does not reveal any possible influence on the matrix from the shape-memory effect of the NiTi.
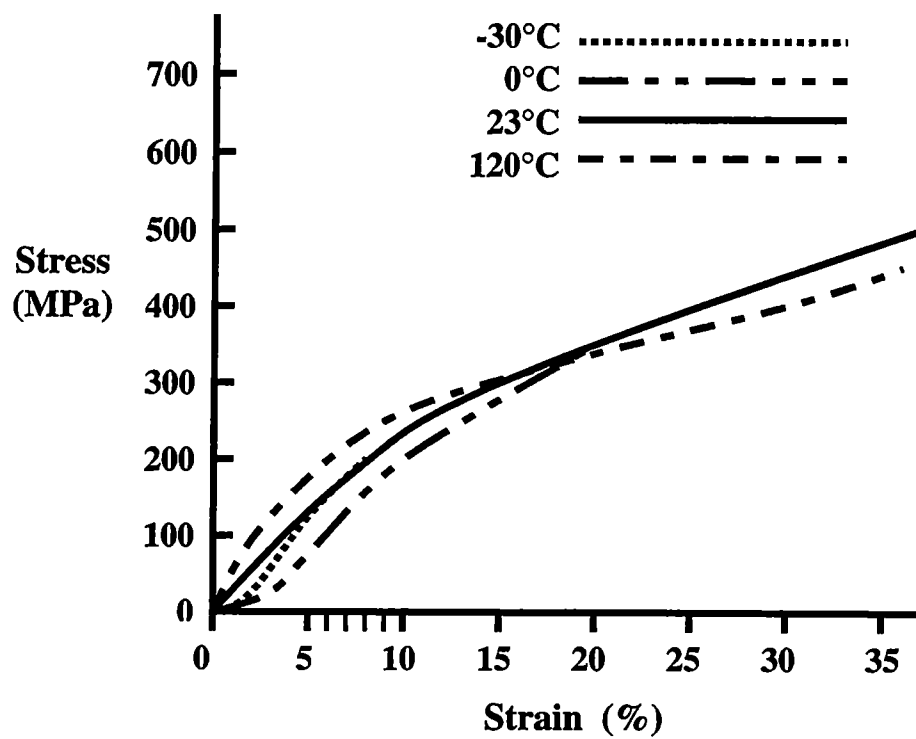
Figure 4 1 1   Schematic results of compression tests on the nickel-titanium shape-memory alloy reinforced aluminum composite

4.2 Static Tension Loading

Mechanical testing is necessary to determine if the NiTi/Al composite materials have any improved characteristics over the bulk matrix material. Static tension tests reveal the general mechanical behavior of the material. The yield strength, the ultimate strength, the Young's modulus, and the maximum elongation are among the most important properties found with this test, and this experiment is usually the standard method of defining these properties. Stress-strain curves were generated and compared to those of other compositions of the same NiTi/Al MMC made under different conditions (refer to Table 3.2.1 on page 63). The testing of these materials was conducted at the Materials Testing Laboratory at the University of Tennessee, Knoxville, under the supervision of Dr. Peter K. Liaw.

In the present study, a servohydraulic Material Test System™ (MTS™) test frame, with a load capability of 100 kN (22 kip), was used to conduct static tension loading tests for several different compositions of NiTi powders in an aluminum matrix material. Rolled samples were cut into pieces slightly over 38 mm (1.5 inch) in length. Tensile test coupons were then punched from these samples with appropriate tooling in a hydraulic press. These tensile test coupons were in accordance to the American Society of Testing and Materials (ASTM) standard E8M-91,[38] and were of the dimensions depicted in Figure 4.2.1. Selected samples were mounted in a shoulder-seating pair of specimen grips, and secured with setscrews. The specimen/grip assembly was then clamped into the electrohydraulic grip system of the MTS™ machine. The upper grip

94

was clamped first, and then, with the specimen/grip assembly hanging freely, the lower one was followed. The load reading was set to zero, and the necessary load settings for the test program were entered into the testing software. The tension test was then conducted at a strain rate of 4.1 mm/sec. (0.16 in/sec.), which is the strain rate typically used for most tension tests. Force, strain, and displacement data were collected and stored on timed intervals. The data were later reconstructed into the stress-strain curves pictured in Figures 4.2.2 through 4.2.5. Figure 4.2.2 exhibits the comparison of the stress-strain curves for the 5 μm powder aluminum matrix materials. Figure 4.2.3 is a detail of the elastic region of Figure 4.2.2. Figure 4.2.4 reveals the comparison of the stress-strain curves for the 20 μm powder aluminum matrix materials. Figure 4.2.5 is an expanded view of the elastic region of Figure 4.2.4. The numerical values for the mechanical properties, which have been mentioned earlier, are listed in Table 4.2.1.
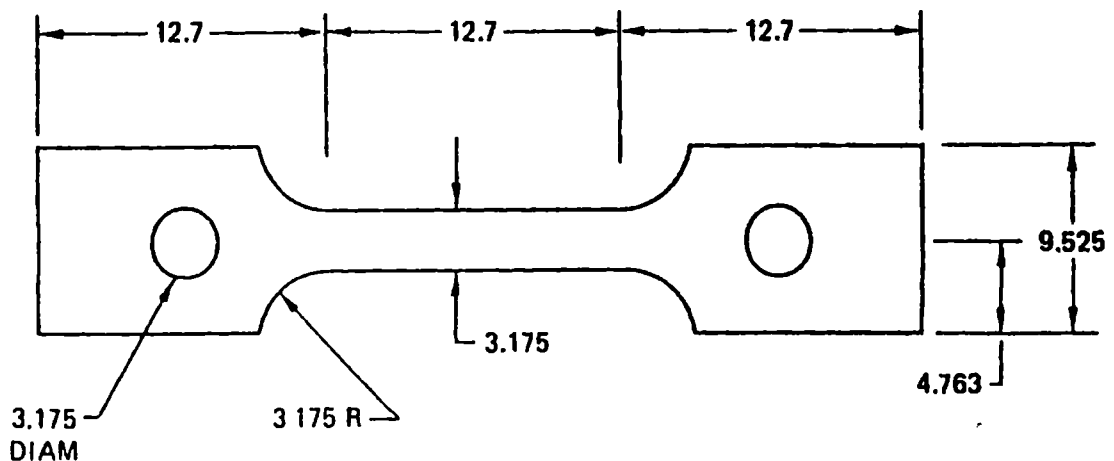
Figure 4.2 1 Dimensions of the tensile test coupons. Dimensions are in mm
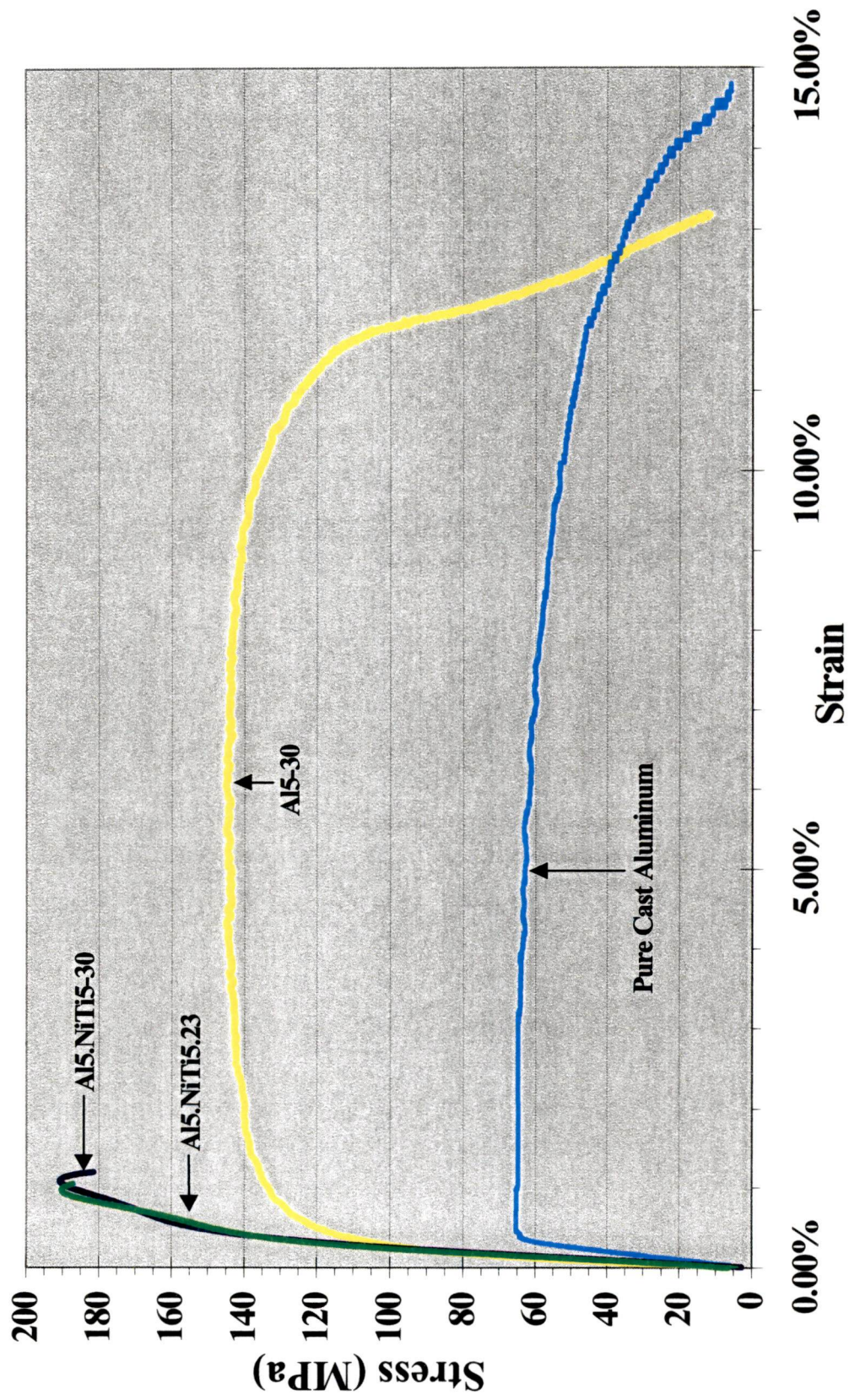
Figure 4.2.2: A comparison of the stress-strain curves for the 5 micron powder aluminum matrix materials.
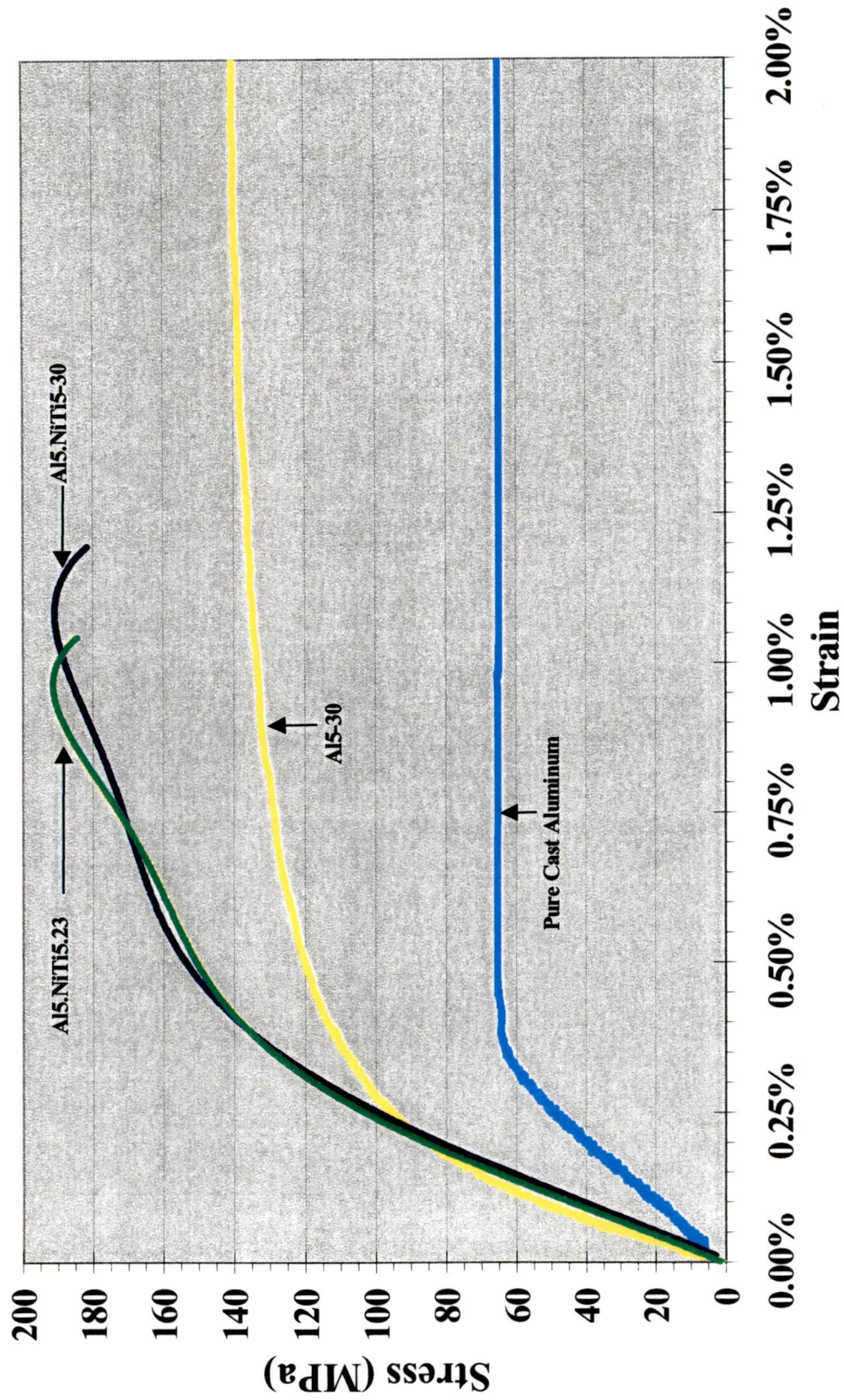
Figure 4.2.3: A comparison of the amplified stress-strain curves for the 5 micron powder aluminum matrix materials.
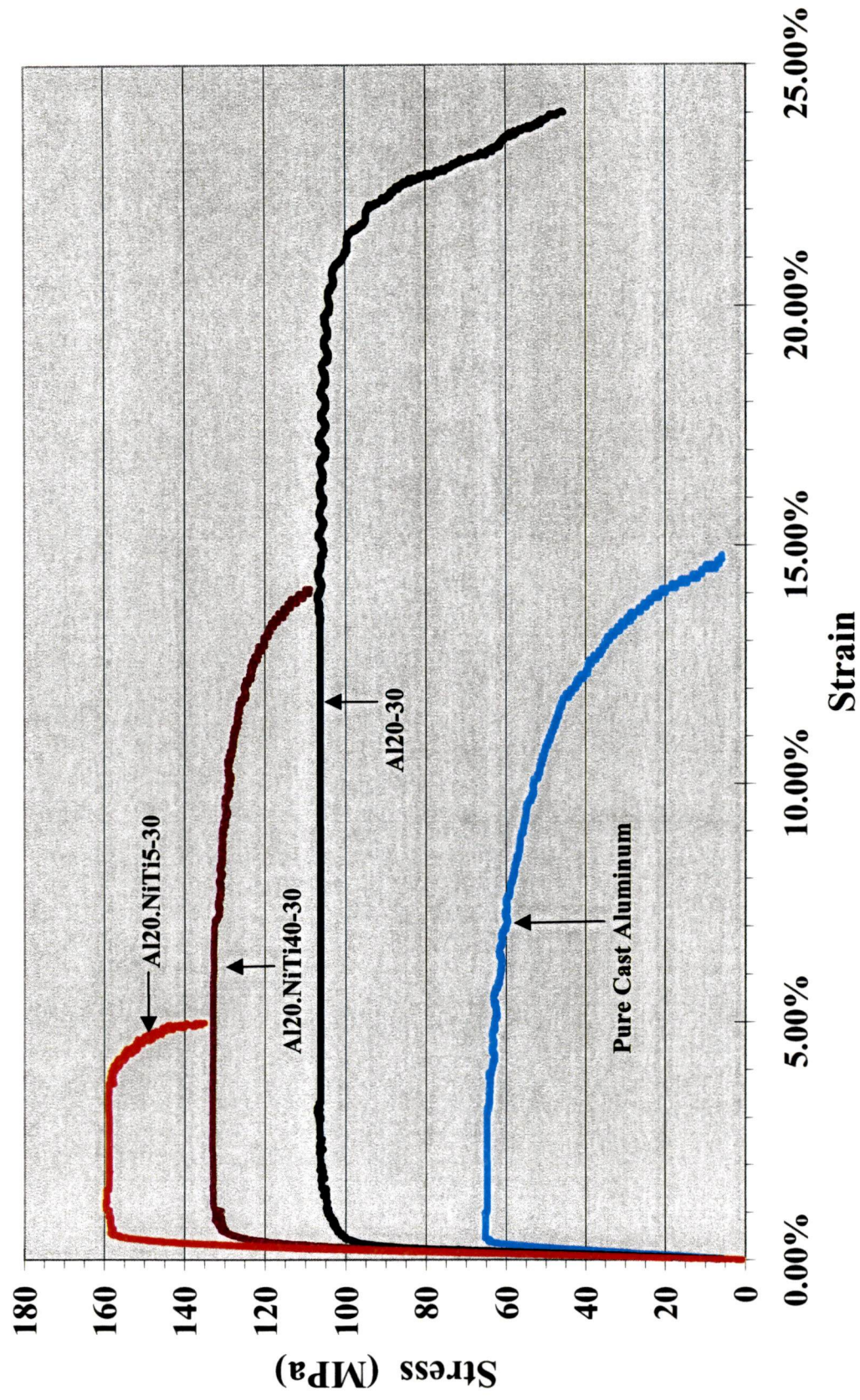
Figure 4.2.4: A comparison of the stress vs. strain curves for the 20 micron aluminum powder matrix materials.
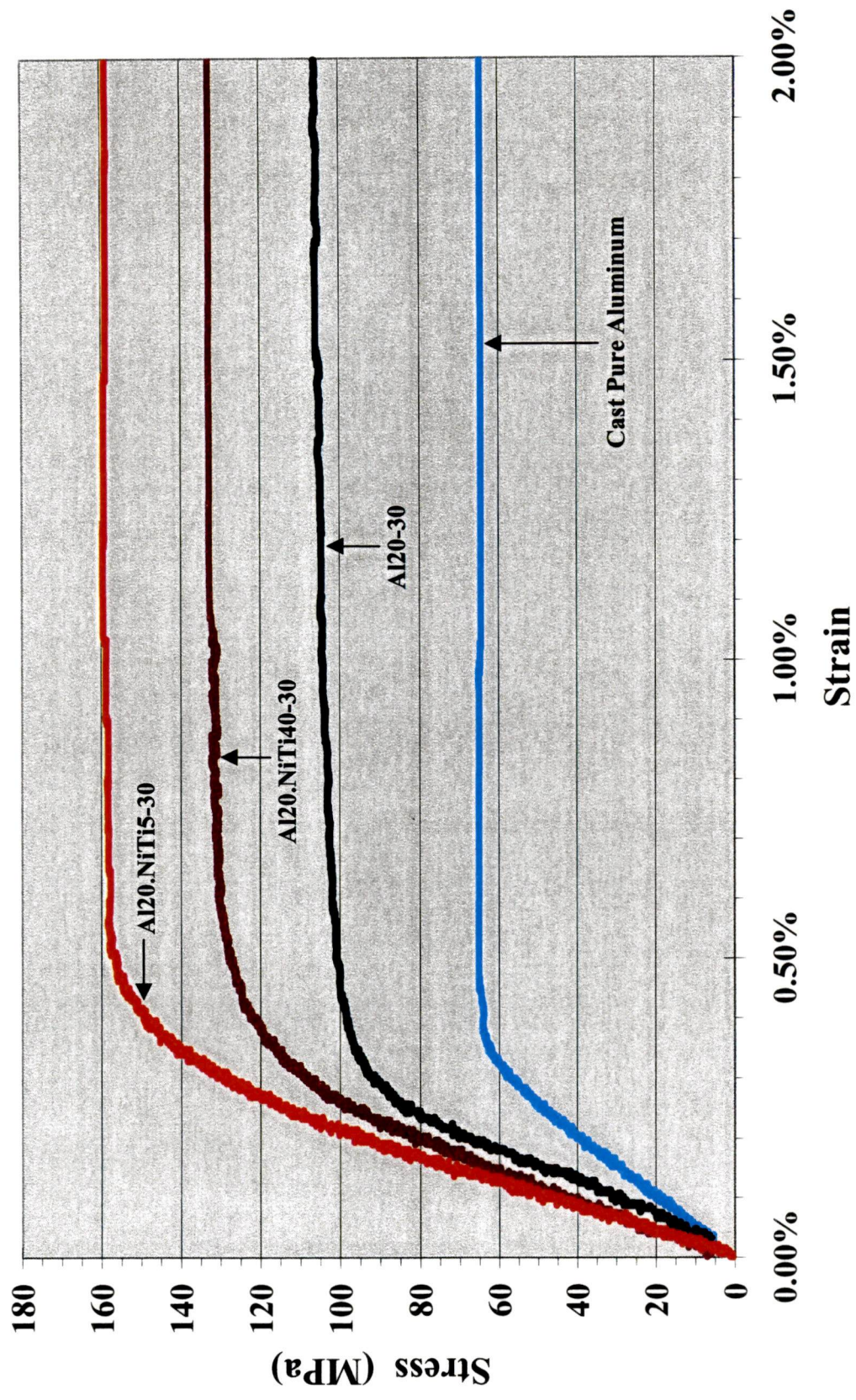
Figure 4.2.5: A comparison of the amplified stress vs. strain curves for the 20 micron aluminum powder matrix materials.

Table 4.2.1: A comparison of the physical and mechanical characteristics of the NiTi SMA reinforced composite materials (WX-9, WX-11 and WX-12), unreinforced matrix materials (WX-7 and WX-10), cast material (WX-13) and wrought material (1100).
* Percentage of the theoretical density.

Name of Sample or Alloy	Al powder size (μm)	NiTi powder size (μm)	Hot-pressing temperature (°C)	Density (% th.)*	Deformation Temperature (°C)	σ_{yield} (MPa)	$\sigma_{ultimate}$ (MPa)	Young's Modulus (MPa)	Elongation (%)
1100	~	~	wrought	100	strain hardened	117	125	69,000	20
WX-7	5	~	585	100	-30	114	146	57,000	13.2
WX-9	5	5	540	97.8	23	156	191	44,000	10
WX-9	5	5	540	97.8	-30	163	192	41,000	12
WX-10	20	~	540	99.61	-30	90	107	35,000	24
WX-11	20	5	550	99.94	-30	128	165	47,000	5
WX-12	20	40	550	99.49	-30	93	134	37,500	14
WX-13	~	~	cast	94.9	23	62	68	18,800	14.8

The following SEM micrographs (4.2.6 and 4.2.7), of the pure cast aluminum samples, indicate the degree of ductility of the unreinforced material, as evidenced by the extreme necking. These photographs also exemplify the growth of porosity as a result of slip movements in the deformation process. Failure mechanisms will be discussed in greater detail in the following discussion.

It is of prime interest to determine the exact causes of the observed tensile properties of the material. There are several factors involved. One is the addition of the second-phase NiTi particles, which stiffen the matrix and affect the modulus and strength. The strengthening theory related to this has been discussed in the chapter on Composite Materials. Another possible influence is the properties of the aluminum matrix. Although an age-hardenable aluminum alloy has not been experimentally investigated, it is theorized that an age-hardenable matrix would play a major role in changing the properties of the composite, especially when concerning the interaction of strain fields around the NiTi particles. The presence of the particles may also influence the hardening and aging rates of the matrix aluminum.

For convenience in the following discussion, the various materials have been given an abbreviated label, indicating the composition, the powder sizes, and the deformation temperature. The first letters signify the matrix material. The next number is the matrix material powder size in microns. The next series of letters represent the reinforcement material (if any). The following number is the reinforcement powder size in microns. The last number is the deformation temperature in degrees Celsius.
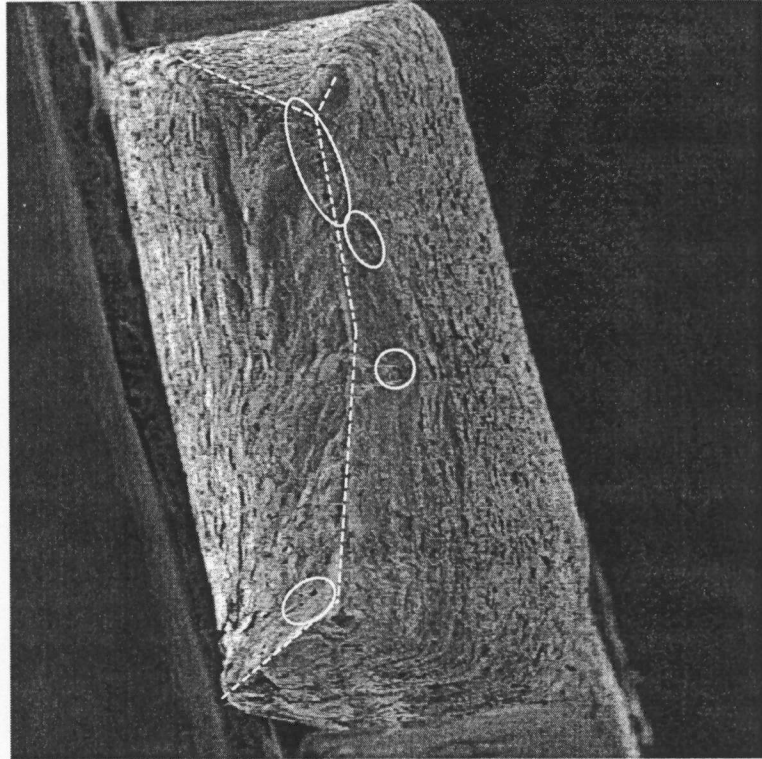
Figure 4.2.6: The fracture surface of a pure cast aluminum tensile test specimen (WX-13). Large pores (circled) and perfect necking (peak indicated by a dotted line) are evident.
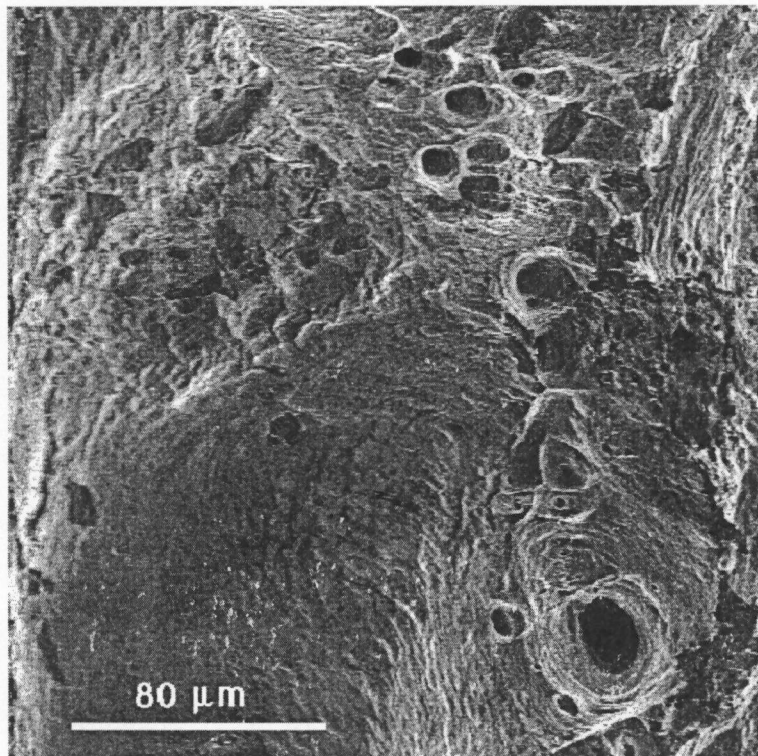
Figure 4.2.7: A magnified view of pores along the peak in the above sample.

102

For example, the composite material designated as "Al20.NiTi5-30," has a mixture of 20 μm aluminum powder and 5 μm NiTi powder, cold-rolled at a temperature of -30°C.

The Influence of the NiTi Reinforcement

Mechanical testing of the preceding research has shown that the NiTi SMA reinforced aluminum composite material has indeed shown a marked increase in yield strength, as it has been improved up to 43%, as compared to the matrix material. These gains are expressed by both the yield strength and the ultimate strength.

In the consideration of the materials made with the 20 μm sized aluminum powders, as depicted in Table 4.2.1, the composite material containing NiTi particles with a 40 μm diameter (Al20.NiTi40-30), provides a 3% benefit in the yield strength over the unreinforced material (Al20-30). The composite material made with the mechanically milled powder (Al20.NiTi5-30), which has a NiTi particle size of about 5 μm, drastically supplements the yield strength 42% over the unreinforced material.

For the composite materials made with the 5 μm sized aluminum powders, the composite material, made with the mechanically-milled powder and deformed at room temperature (Al5.NiTi5.23), provides a 37% gain in the yield strength over the unreinforced material (Al5-30). The material containing the 5 μm sized NiTi particles, and cold-rolled below the M_s temperature (Al5.NiTi5-30), impressively supports the yield strength 43% more than the unreinforced material.

The difference of strengths between the reinforced composite material and the unreinforced aluminum materials will be termed the total amount of strengthening benefit. The author wishes to pinpoint the contributing factors to the strengthening benefit. If the total amount of strengthening benefit is 100% by definition, then each of these contributing factors may be attributed to a certain percentage of the total strengthening. For example, if the yield strength of the material made with the 20 μm sized aluminum particles is 90 MPa, and that of the material made with the 5 μm sized aluminum particles is 114 MPa, then the total amount of strengthening due to the use of the smaller aluminum particle size is (114 – 90) MPa, or 24 MPa. Thus, 24 MPa is the total strengthening benefit from the use of the smaller aluminum particles. As a percentage, the strengthening benefit is [(114 – 90)/90]x100%, or 27%. This method can be used to identify the contribution of each component of material or processing to the total strengthening.

Consider that the addition of the 40 μm sized NiTi particles to the 20 μm sized aluminum particles produces a 3% gain in the yield strength, and the mechanically milled NiTi powders produce a 42% profit in the yield strength of the material with the 20 μm sized aluminum particles. Then the contribution of the NiTi particles to the total amount of strengthening benefit is (3/42)x100%, or 7%. Likewise, the contribution of the mechanical-milling process to the strengthening benefit is [(42 – 3)/42]x100%, or 93% for this particular case.

For the materials made with the 5 μm sized NiTi particles in the 5 μm sized aluminum particles, the addition of the mechanically-milled powders (Al5.NiTi5.23) support the yield strength 37%, and the deformation of the material below the M_s temperature (Al5.NiTi5-30) yields a 43% benefit. In the same manner, the addition of the mechanically-milled NiTi powders produce (37/43)x100%, or 86% of the total strengthening benefit.

Based on these calculations, it is certain that the majority of strengthening benefit achieved in the composite, about 85%, is due to factors, such as the addition of a strengthener, particle sizes, and matrix materials. The remaining 15% of the total strengthening benefit seems to be due to a combination of influences by the shape-memory effect, and the strain hardening due to the cold rolling, as the deformation of the material at sub-zero temperatures introduces dislocations, which result in further hardening of the composite.

The Influence of the Particle Size

As clearly seen in Table 4.2.1, the powder sizes of both the NiTi reinforcement, and the aluminum matrix, play an important role in the physical properties of the materials. In general, under the present manufacturing conditions, the materials made with the 5 μm sized aluminum powders provide a significantly higher strength than the materials made with the 20 μm sized aluminum powders. However, the larger, 20 μm aluminum powders produce higher density composites than the smaller, 5 μm, sized aluminum powders. This behavior may be due to the fact that the particle sizes of the

powders used in fabricating a P/M composite, have a direct influence on the grain size. Generally, one powder particle will generate one grain. As a result, a smaller particle size will yield a composite material with a finer grain. This is reflected in the similarities between the following materials, according to the Hall-Petch relationship. The materials made with the 5 μm diameter sized aluminum powder share a related grain size with the 1100 wrought aluminum material. Note that the moduli for these materials are also on the same order of magnitude. Likewise, the materials made with the 20 μm diameter sized aluminum powder have a much larger grain size than the materials made with the 5 μm diameter sized aluminum powder. The cast aluminum material, as is well known, has a grain size that is extremely large. The moduli for the 20 μm sized aluminum particle materials is about 7,500 MPa lower than the 5 μm sized aluminum particle materials, on the average. However, as previously discussed in the Chapter on Product Density, the smaller aluminum powders contain more surface oxides per unit bulk of material. The presence of these oxides may cause the material to require higher temperatures and pressures during manufacturing, in order to produce an equitable density. As a result, the materials made with these smaller aluminum powders show a slightly diminished density.

It may also be observed from Table 4.2.1 that the NiTi reinforced composite materials exhibit higher strengths than the unreinforced materials, and that the smaller, 5 μm NiTi powder particles provide a greater improvement in the strengths in comparison to the 40 μm sized NiTi particle reinforced composites. This behavior may be because the larger NiTi particles are almost perfectly spherical in shape, lending a minimum of interfacial bonding area and also deferring stress fields around the particles. The smaller,

mechanically alloyed particles have a greater amount of surface area available for matrix bonding. Also, the oxide layer formed on the surfaces of the NiTi particles, and the possible presence of intermetallic compounds which may have formed during hot pressing, contributed towards the enhancement of the interface, and contributed greatly towards the mechanical behavior of the composite material.

The Influence of the Shape-Memory Effect

According to the stress-strain curves in Figure 4.2.3, and the related data, the composite material, deformed at room temperature with no shape-memory effect enacted (Al5.NiTi5.23), showed a 37% increase in the yield strength in comparison with the aluminum matrix. The material, deformed under dry ice with the shape-memory effect enacted (Al5.NiTi5-30), showed a 43% increase in the yield strength over the matrix. Therefore, for this material, we may conclude that there is a (43 – 37)%, or a 6% increase in the yield strength due to the combined influence of the shape-memory effect, and the deformation at a lower temperature.

The Possible Effects of Stress-Induced Martensite on the Modulus of Elasticity

In the composite material made with the 5 µm aluminum powder used in the matrix and deformed at room temperature (Al5.NiTi5.23), it can be seen that the overall modulus of the material decreases with the addition of nickel-titanium powders (in comparison with Al5.23). A further decrease in modulus is attained when the material is deformed, and while the NiTi is in the martensitic state (Al5.NiTi5-30). If we assume

107

that there is good bonding among all the powder particles in the composite, as indicated

by the increase in yield strengths, then it is thought that the decrease in modulus is due to

the *stress-induced-martensite* (SIM) phenomenon. In this case, the shape-memory alloy

will retain a fraction of its martensitic phase due to the presence of stress, despite the fact

that the material may be heated above the A_f temperature. If both the martensitic and

austenitic phases are present in the NiTi particles, then the composite material will

display a combination of the physical qualities of both phases. In effect, the yield

strength and modulus will lie somewhere between those of each phase. If the modified

modulus for the NiTi (Equation 1.4.4), is substituted into the bulk modulus (Equation

1.5.4), the result, given in Equation 4.2.1, will show that this is true.

$$E_{comp} = \frac{E_m V_m + \left(\dfrac{E_A E_M}{X E_A + (1-X) E_M} \right) \cdot V_r}{V_m + V_r} \qquad \text{(Eq. 4.2.1)}$$

Where,

E_{comp} = the bulk modulus of the nickel-titanium reinforced aluminum
composite material,
E_m = the bulk modulus of the aluminum matrix material,
E_A = the modulus of the NiTi SMA in the austenite phase,
E_M = the modulus of the NiTi SMA in the martensite phase,
X = the volume fraction of martensite that is induced by an applied
stress in the NiTi SMA particles,
V_m = the volume fraction of the aluminum matrix material, and
V_r = the volume fraction of the reinforcement material.

Note that $V_m + V_r \neq 1$, if voids are taken into consideration. In such a
case, $V_m + V_r$ = (percentage of theoretical density)/100%

If there is indeed martensite present in the NiTi particles, this will explain why

the modulus of the composite material with the shape-memory effect enacted, has a

lower modulus than either the matrix material, or the composite material without the shape-memory effect enacted.

An issue remains as to whether shape-memory effective NiTi particles exert stresses on the matrix, or if those stresses are absorbed by the *stress-induced martensite* behavior. It would be beneficial to know the magnitude of stress and the degree of strain experienced by a typical NiTi particle within the matrix, and whether the *stress-induced martensite* phenomenon would be displayed by the condition. From this, we would be able to predict the fraction of martensite present, and hence, the general hardness and modulus of the NiTi particles. This information would help develop a working model of the effect the particles have on the matrix, and how they influence the properties of the composite material. But regardless of what mechanism takes place, the author may present a generalized theory about the shape-memory effects of the NiTi particles in the composite material, and any resulting stress-induced martensite behavior. These effects are illustrated in Figure 4.2.8. A single particle/matrix unit is considered for the sake of simplicity. The particle/matrix unit is chilled below the martensitic finishing temperature and deformed. As the temperature of the material is raised above the austenitic starting temperature, the shape-memory associated phase transformation is induced within the NiTi phase, and stresses are generated around the particle. These stresses, in turn, inhibit the formation of austenite due to the *stress-induced martensite* phenomenon, and elevate the temperatures at which the NiTi phase transformations occur. As a result, the material requires higher temperatures to complete the transformation. These stresses may, otherwise, remain in the material and produce a volume fraction of martensite in the

1. Consider a single particle/matrix unit...
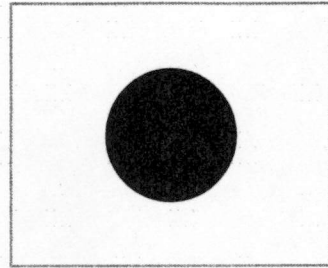
2. Chilled below the martensitic finishing temperature and deformed
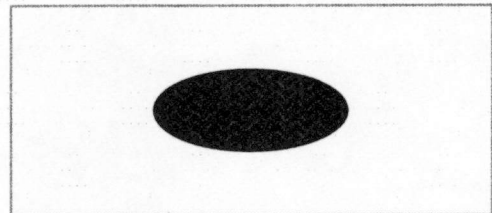
3. As the temperature is raised above the austenitic starting temperature, a phase transformation is induced and stresses are generated.
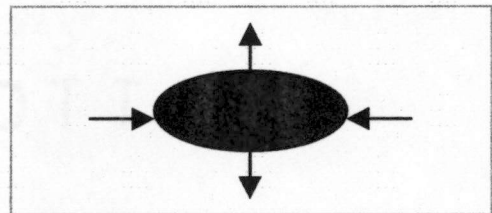
4. These stresses, in turn, elevate the temperatures at which the NiTi phase transformations occur...

5. Requiring higher temperatures to complete the transformation
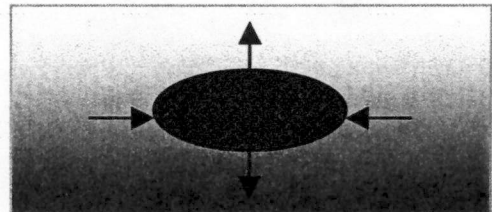
6. ...and possibly resulting in a fraction of the particle volume remaining in the martensite phase.

Since the martensitic phase has a much lower modulus than the parent phase, this may result in a partial decrease in the modulus of the composite as a whole.
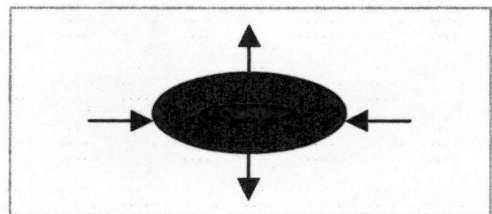
Figure 4.2.8: The possible effects of *stress-induced-martensite* on NiTi particles within the matrix.

particle. Since the martensitic phase has a much lower modulus than the parent phase, this may result in a partial decrease in the modulus of the composite as a whole. With this in mind, it may be understood how the presence of the martensitic phase within the NiTi may contribute toward the decrease of the modulus of the material, since the martensitic phase has a much lower modulus than the austenitic phase. At the present time, nanoindentation tests are being conducted to measure the modulus of point locations in the NiTi particles. Hopefully, experimental evidence of how the modulus changes throughout the particles will help pinpoint locations of differing phases in the particle, further supporting the development of this theory.

4.3 Fatigue Loading

Fatigue loading tests reveal the fatigue behavior of the material. The fatigue properties of a material are important in determining sites of crack initiation and modes of crack propagation. It also gives an indication of the fatigue life of a sample under particular loading conditions.

Fatigue loading tests were conducted at the University of Tennessee for several different compositions of NiTi powders in the matrix material, as well as samples of unreinforced matrix materials. These fatigue tests were performed with a servohydraulic Material Test System™ (MTS™) machine, with a load capability of 100 kN (22 kip). The maximum applied stress versus fatigue life cycle (S-N) curves were developed at a load ratio, R, of 0.2. $R = \sigma_{min} / \sigma_{max}$, where σ_{min} is the minimum stress experienced by the specimen during the cycle, and σ_{max} is the maximum stress experienced during the cycle. These curves are presently compared to the curves of other compositions of the same Al/NiTi MMC. At least ten fatigue tests were conducted for each material over a wide stress range, so that a fairly accurate representation of the data could be displayed in the applied stress vs. the number of cycles until failure (S-N) curves.

Chosen samples were mounted on a shoulder-seating pair of specimen grips, and secured with setscrews. These grips were then clamped into the electrohydraulic grip system of the MTS™ machine. The upper grip was clamped first, and then, with the specimen/grip assembly hanging freely, the lower one was followed. The load reading

112

was set to zero, and the necessary load settings for the test program were entered into the testing software. A peak to peak compensator in the program was used to control the accuracy of the load limits. Fatigue tests were started at a frequency of 1 Hz, to allow the compensator to quickly adjust, and then, the frequency was slowly increased to 50 Hz. This procedure ensured that each cycle experiences accurate values of σ_{min} and σ_{max}, and that the test produced reliable data. For higher stress level (e.g., fatigue life < 500 cycles) tests, the frequency was only increased to 10 Hz, in order to allow more control and accuracy over the short length of the test.

Mechanical testing revealed that a better fatigue life performance had been achieved in the NiTi SMA reinforced aluminum composite materials. The peak stress during the fatigue test was plotted against the number of cycles endured by each sample, producing the following S-N curves. These S-N curves are displayed in Figures 4.3.1, 4.3.2 and 4.3.3. Figure 4.3.1 outlines the S-N curves of the composite materials made with the 5 μm diameter aluminum powders, whereas Figure 4.3.2 represents the S-N curves of the 20 μm diameter aluminum powder matrix composites. Figure 4.3.3 illustrates the S-N curves for all the materials tested. The S-N curve for the pure cast aluminum is given as a reference, and it has the lowest fatigue life of any of the materials. Since most materials have a S-N curve similar to the curve for the pure cast aluminum, which has the concave side facing upwards, it is interesting to find that the S-N curves for the composite materials are either flat, or have the concave side facing downward.
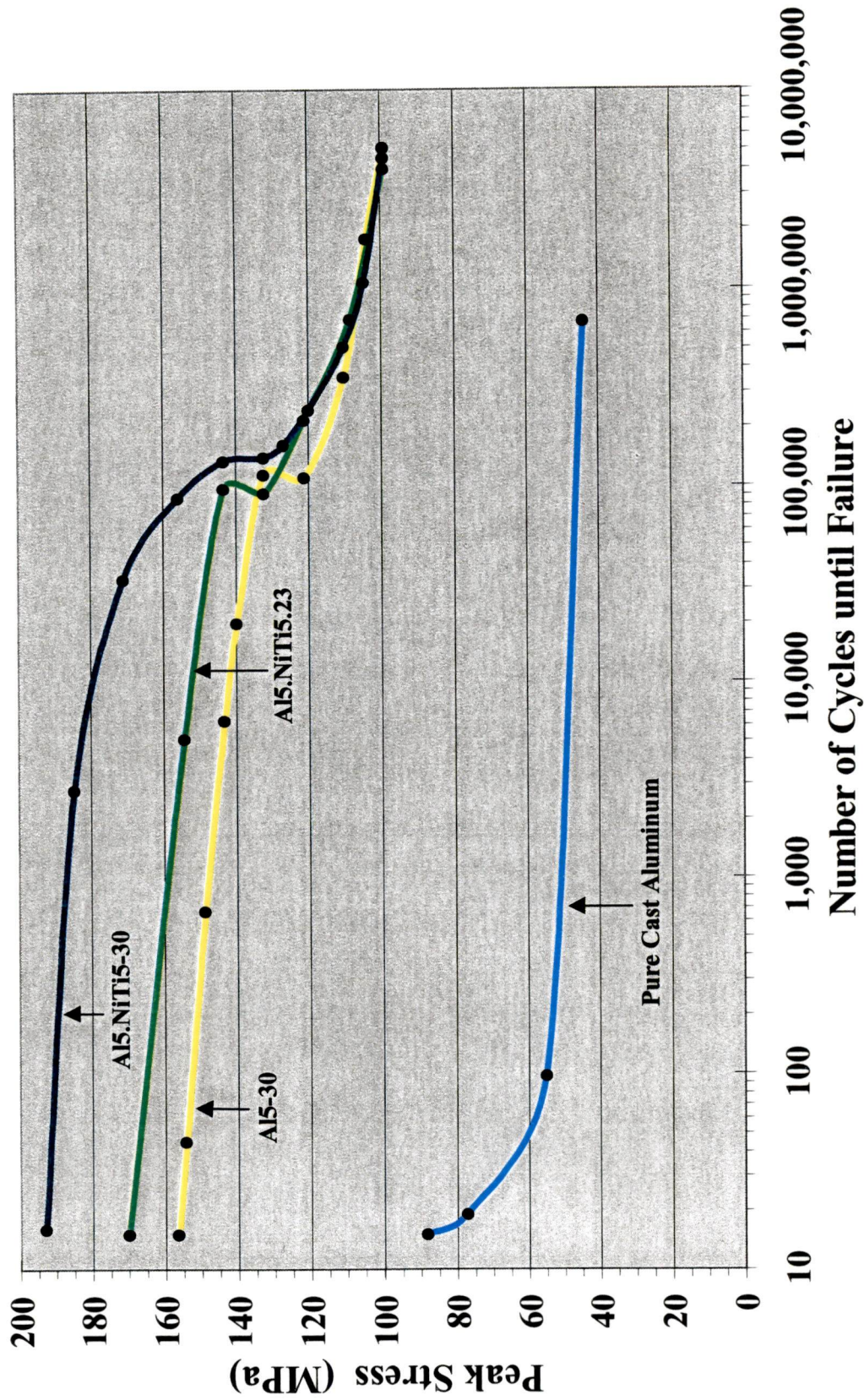
Figure 4.3.1: Peak stress vs. number of cycles until failure for the 5 micron powder aluminum matrix composites.
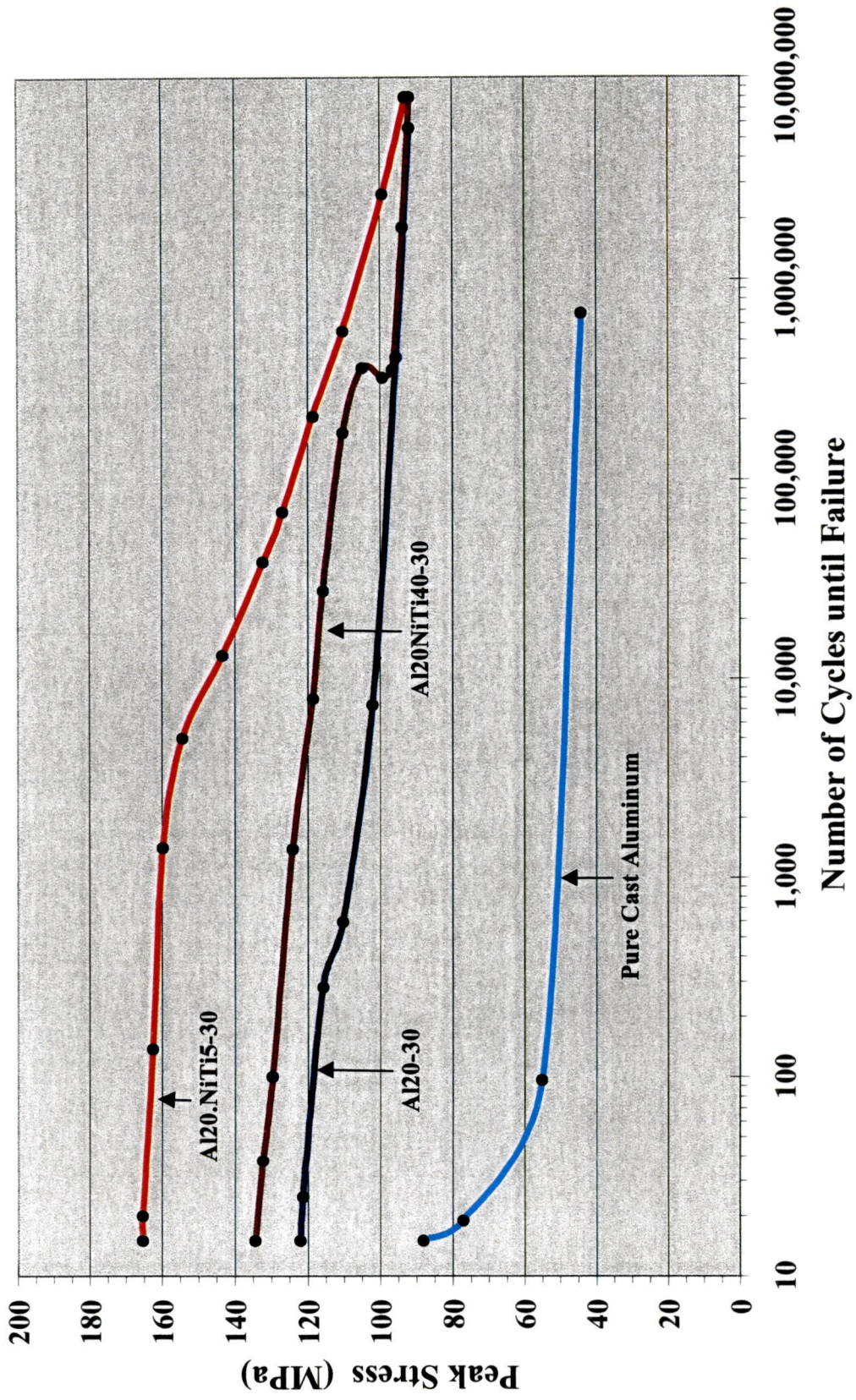
Figure 4.3.2: Peak stress vs. number of cycles until failure for the 20 micron powder aluminum matrix composites.
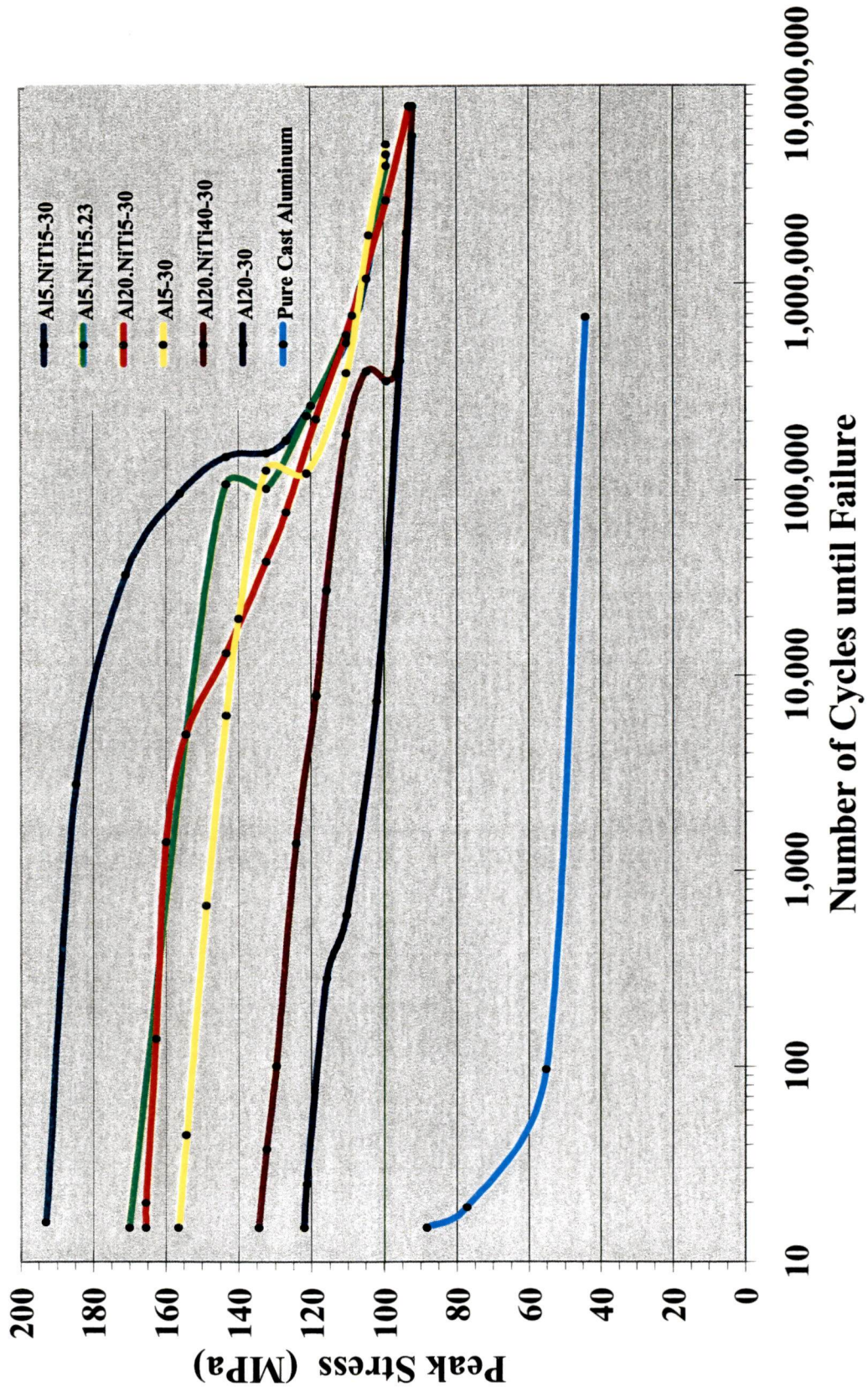
Figure 4.3.3: Peak stress vs. number of cycles until failure, for all materials tested.

116

Another graph may be interpolated from the S-N curves, which may define the differences between materials more clearly, especially the differences such as the yield strengths for each material, the relationships of the yield strengths to the peak-stress levels, and the comprehensive changes in the peak-stresses endured, according to the number of fatigue cycles until failure. These graphs, which categorize the peak-stress corresponding to a given number of fatigue life cycles, according to the yield strength of a material are termed, "peak-stress / life," or, "Porter-Liaw," (P-L) curves, and are shown in Figures 4.3.4 through 4.3.6. Figure 4.3.4 depicts the P-L curves of the pure aluminum materials. Figure 4.3.5 is another graph of the P-L curves, revealing only the nickel-titanium shape-memory alloy reinforced aluminum composite materials. Figure 4.3.6 is a combination of Figures 4.3.4 and 4.3.5, showing all the materials tested. Note the "axis of stress-symmetry," which will reveal the approximate number of life cycles that can be endured by a specimen, before failure occurs at peak-stresses below the yield strength. Those data points, which lie above the axis of stress-symmetry line, have failed at peak-stress levels, which are above the yield strength. Those data points, which lie below the axis of stress-symmetry line, have failed at peak-stress levels, which are below the yield strength. The P-L curves reveal the strong trend that at higher stress levels, (i.e. shorter life conditions), the maximum stress that the sample is capable of enduring, increases proportionately to the yield strength. But at lower stress levels, (i.e. longer life conditions, such as those greater than 150,000 cycles), the peak-stress endurance is constant, as shown by the horizontal lines in the P-L curves.
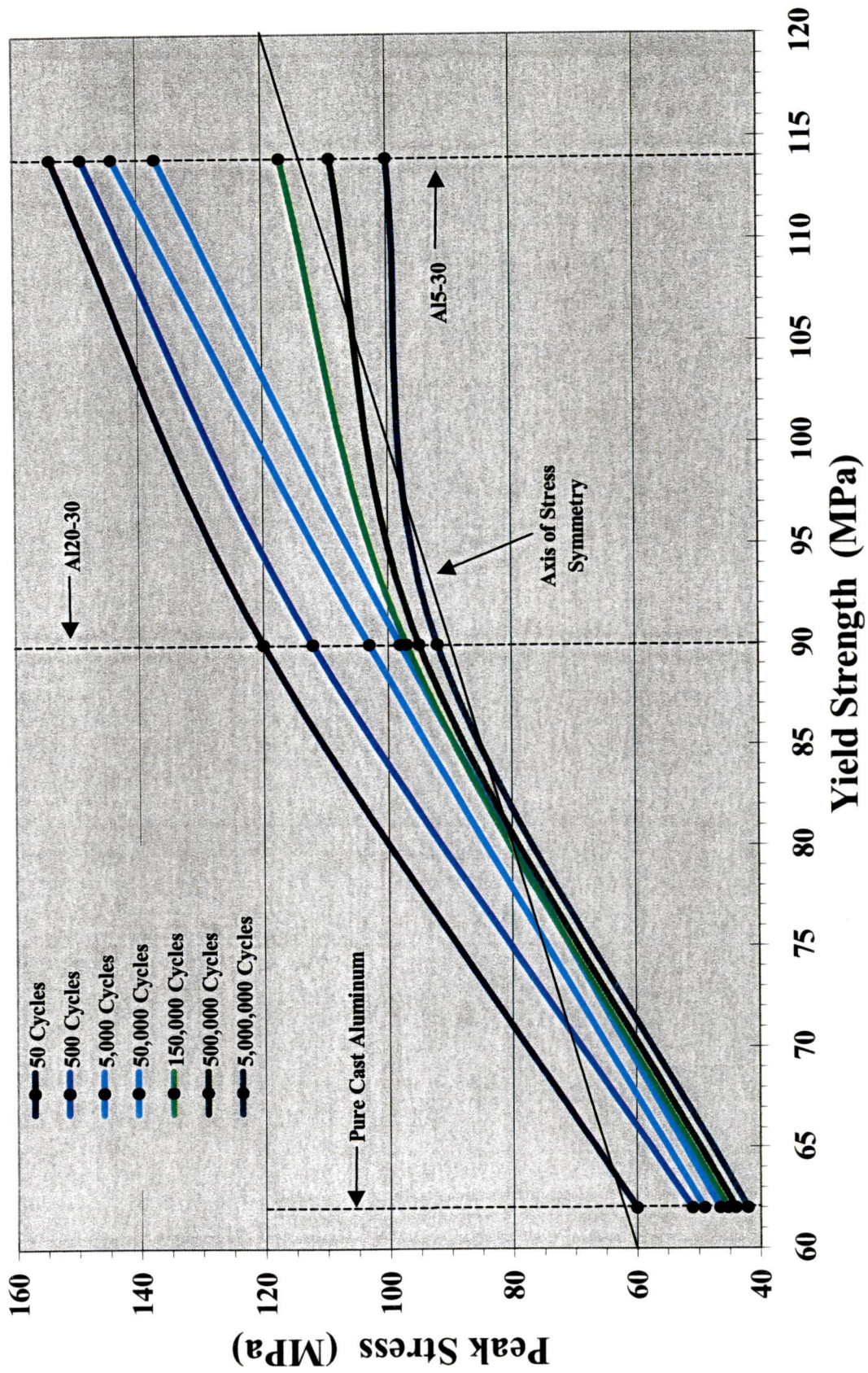
Figure 4.3.4: Peak stress corresponding to a given number of fatigue life cycle vs. yield strength, for the pure aluminum matrix materials. (Some data points have been extrapolated.)
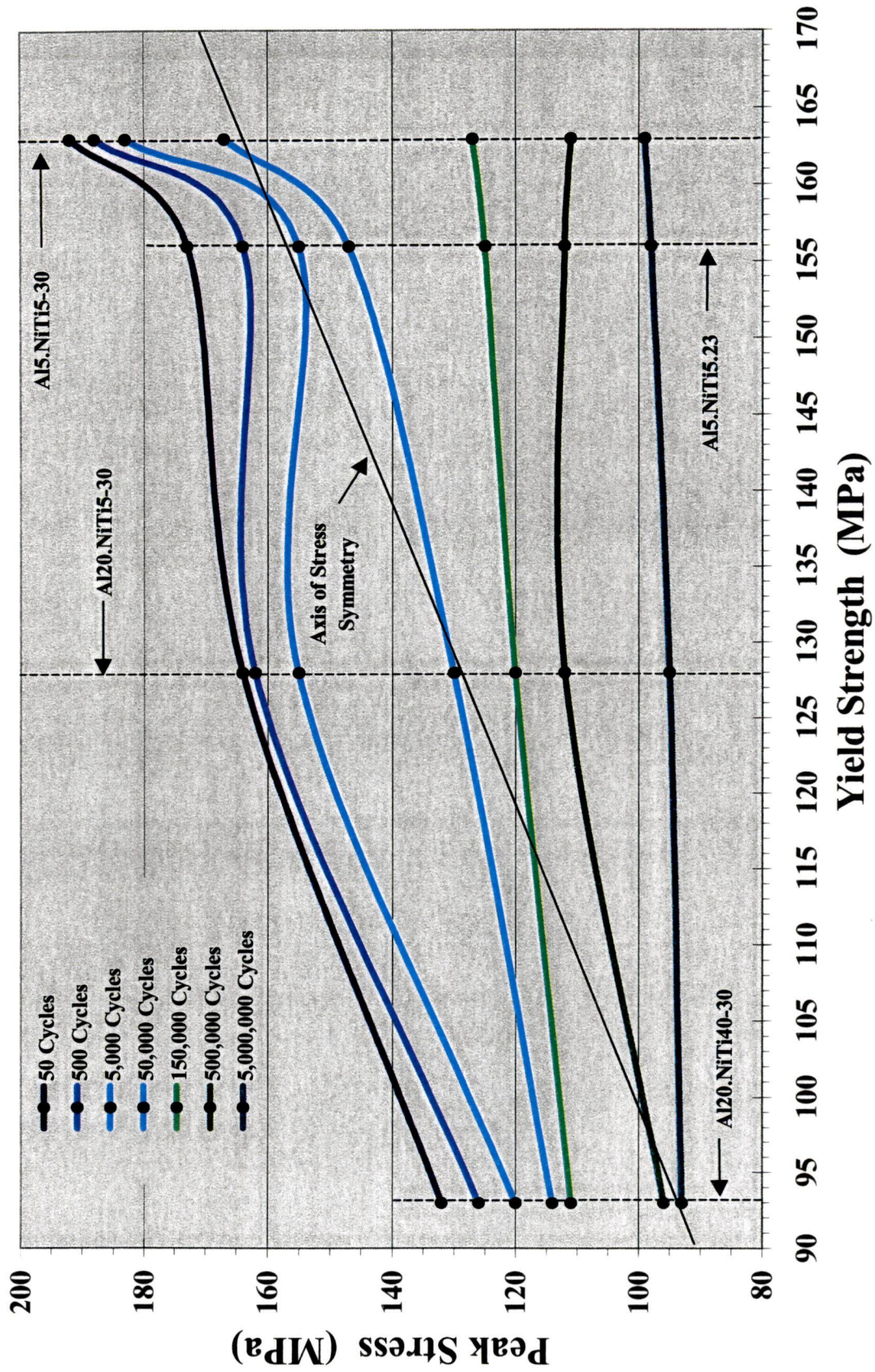
Figure 4.3.5: Peak stress corresponding to a given number of fatigue life cycles vs. yield strength, for the nickel-titanium shape-memory alloy reinforced aluminum composite materials. (Some data points have been extrapolated.)

119
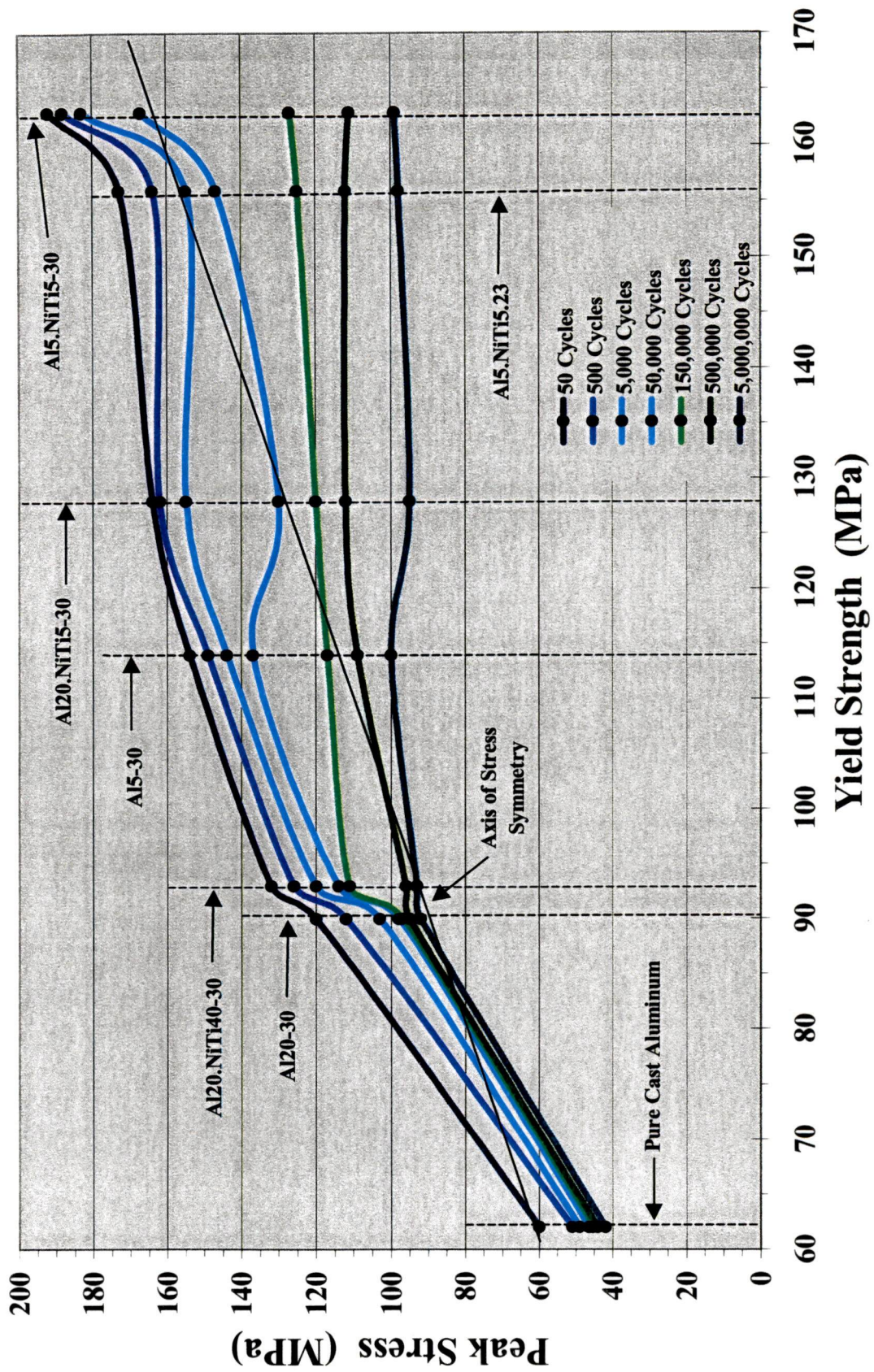
Figure 4.3.6: Peak stress corresponding to a given number of fatigue life cycles vs. yield strength, for all materials tested. (Some data points have been extrapolated.)

The Influence of the NiTi Reinforcement

In Figure 4.3.1, it can be seen that the NiTi reinforced, 5 μm sized aluminum particle materials have a clear benefit in the fatigue life as compared to the matrix material, especially at higher stress levels. The S-N curve for the composite material deformed at room temperature (Al5.NiTi 5.23) has a similar shape as that of the matrix material (Al5-30), only it generally falls near a 10 MPa greater peak-stress range. However, the same material deformed below the M_s temperature (Al5.NiTi-30) displays a remarkable improvement in the peak-stress capability and the fatigue life, over both the matrix material, and the composite material deformed at room temperature.

It is interesting to note in Figure 4.3.1, that the curves for the composite materials (Al5.NiTi 5.23 and Al5.NiTi-30), are congruent at stresses below 125 MPa (18.125 ksi). All the curves converge at cycles greater than approximately 600,000. The corresponding stress for this value is about 110 MPa (15.95 ksi). This is just below the yield stress for the matrix material (114 MPa or 16.53 ksi). It is thought that these are related, as will be discussed later. At stress levels above this, the composite materials have a marked advantage over the unreinforced material, and the material deformed below the martensitic starting temperature (Al5.NiTi5-30), has far superior lifetime characteristics, averaging between two to three orders of magnitude better than the unreinforced aluminum material.

In Figure 4.3.2, the materials made with the 20 μm sized aluminum powders have similar behaviors as those of the 5 μm sized aluminum powders, although at slightly lower peak stresses, as shown in Figure 4.3.3. Despite the fact that the composite material made with the 40 μm NiTi particles (Al20.NiTi40-30) only provided a 3% increase in the yield strength, as compared to the matrix material (Al20-30), the fatigue resistance has improved approximately two orders of magnitude at peak stresses above 100 MPa. The composite material made with the mechanically milled NiTi powders (Al20.NiTi5-30) displays a remarkable amplification of both the peak-stress capability and the fatigue life, for the entire tested range of values. Especially at the peak stress of 120 MPa, where the matrix material can only withstand 50 cycles until failure, the composite material made with the mechanically milled NiTi powders retains its integrity for 150,000 cycles.

The S-N curve (Figure 4.3.2) for the material made with the 40 μm NiTi powder (Al20.NiTi40-30) converges with that of the matrix material (Al20-30) at just over 300,000 cycles and upwards. The corresponding stress for this value is about 95 MPa (13.78 ksi). This is just above the yield stress for the matrix material (90 MPa or 13.05 ksi). It is thought that these are related, and will be discussed later. The S-N curve for the material made with the 5 μm NiTi powder (Al20.NiTi5-30) converges with that of the matrix material at 8,000,000 cycles with a corresponding stress level of 93 MPa (13.49 ksi), again just above the yield stress for the matrix material. For numbers of cycles greater than 10,000,000, it is thought that the curves approach the yield strength value of the matrix (90 MPa or 13.05 ksi) asymptotically. For the higher stress levels, the

composite materials have a decidedly longer life than the unreinforced material, and the material containing the mechanically-milled NiTi powders (Al20.NiTi5-30), has a greatly improved lifetime characteristic, which is four orders of magnitude better than the matrix material (Al5-30) at 155 MPa (22.48 ksi).

The Influence of the Particle Size

Figure 4.3.3 may present a generalized comparison between the materials made with the 5 μm sized aluminum powders, and the materials made with the 20 μm sized aluminum powders. However, these differences can be made increasingly obvious by use of the P-L curves, shown in Figures 4.3.4 through 4.3.6. Figure 4.3.4 displays the peak-stress corresponding to a given number of fatigue life cycles vs. the yield strength for the pure aluminum materials. Figure 4.3.5 is this relationship for the composite materials, and Figure 4.3.6, for all the materials tested. The general trend is that the peak-stress at failure increases directly with the yield strength. However, this relationship only holds true for high stress, (i.e. short life), conditions. As the peak stress is lowered, (i.e. for longer life conditions), this effect diminishes under the accumulation of fatigue. (Note the axis of stress-symmetry, which indicates the specimens which have failed above the yield strength, and which ones have failed below.) This trend indicates a greater fatigue resistance in the composite materials, as compared to the matrix materials, especially at higher stress levels, thus, producing a longer fatigue life in the composites.

Figure 4.3.4 reveals that if a smaller aluminum particle size is used in the fabrication of the material, the peak-stress corresponding to a given number of fatigue life

cycles will increase. This behavior may be due to the presence of more aluminum oxides or impurities, or perhaps because of the smaller grain size formed, as a result of the smaller particles being used. It is of interest to observe that the pure cast aluminum materials all failed below the yield strength, due to the softness of the material and the incredible ease of slip. The material produced by P/M processing (Al20-30) fared much better, having required stresses greater than the yield strength to induce fatigue failure. Interestingly, the material made with the 5 μm sized aluminum powders failed at peak stresses below the yield strength at cycles greater than around 300,000.

This behavior is similar for the NiTi reinforced composite materials (see Figure 4.3.5), although the required stress to cause failure at a given fatigue life cycle, falls further below the yield strength as the cycles are increased. Composite materials made with the 5 μm sized aluminum powders (Al5.NiTi5.23 and Al5.NiTi5-30) have much higher yield strengths than the materials made with the 20 μm sized aluminum powders (Al20.NiTi40-30 and Al20.NiTi5-30). However, the required stress to cause a fatigue failure also increases proportionately, except under conditions greater than 150,000 cycles, in which the peak stress required to induce failure does not change appreciably between one composite material and another. It is thought that this phenomenon is caused by the weakness of the matrix material. This characteristic will be discussed in more detail, in the section covering the *Patterns of Fracture Mechanisms*.

The Influence of the Shape-Memory Effect

In Figure 4.3.5, it can be seen that the NiTi reinforced composite material, which has been deformed below the M_s temperature (Al5.NiTi5-30), not only has a greater yield strength than the same material deformed at room temperature (Al5.NiTi5.23), but it also requires much higher peak stresses in order to induce the failure of the material, even higher than the yield strength in some instances (at fatigue lives between 5,000 and 50,000 cycles). This gain in mechanical properties is most probably due to the cold rolling of the material at the lower temperature, in which the NiTi particles are in the martensitic phase during the deformation.

Scanning Electron Microscope Fractography

After testing, the broken fatigue samples were marked and mounted erect, and the fracture surfaces were examined using a scanning electron microscope. Other broken samples were mounted in an epoxy base and polished, following a standard metallographic practice using diamond pastes. The microstructures of these samples were then examined carefully, using the SEM, to determine NiTi particle size and distribution characteristics. Voids and other impurities (though few) could be seen as well. Crack interfaces were inspected in order to characterize fracture mechanisms, which will be discussed later. The SEM used in this study is a Hitachi Model S-800, operating between 20 and 25 kV.

Figure 4.3.7 is a macroscopic, birds-eye view of the fracture surface of a pure aluminum P/M sample, WX-10, produced by fatigue loading. The particle size of the powder used for this material is 20 μm. The maximum stress for this sample is 94 MPa. This particular sample (WX-10a) endured 5,657,850 cycles before failure. The crack initiation site and propagation area at the top left corner (circled) are clearly visible because of their large size. Figure 4.3.8 represents a better view of this area. It is interesting to note that in the massive failure region, a plane-strain failure mechanism dominates, resulting in a relatively flat fracture surface. This surface exhibits signs of fracture due to void growth and coalescence. Necking in the failure region is extensive.

Figure 4.3.9 displays the most interesting fracture of a pure aluminum P/M sample (WX-10) produced by fatigue loading. This material is identical to that in the previous photo, with an aluminum powder size of 20 μm. The maximum stress for this sample is 105 MPa. This particular sample (WX-10b) endured 13,459 cycles before failure. The fracture begins with the initiation of a crack tip at the lower right-hand corner (circled), but after a critical crack size has been attained, the massive failure occurs in a plane 45° from the primary applied stress. In plane-stress shear, the massive crack-tip branches at an angle from the original fatigue crack *surface - not the tip* - leaving the original crack tip partially hidden. This is most probably resulting from the weakening of the material due to void coalescence, in the plane of the maximum shear stress in the sample. The process of failure due to void coalescence is discussed in greater detail in a later section, and also the degree of deformation due to necking. A better view of this crack tip is portrayed in Figure 4.3.10. Figure 4.3.11 portrays a greater detail of the
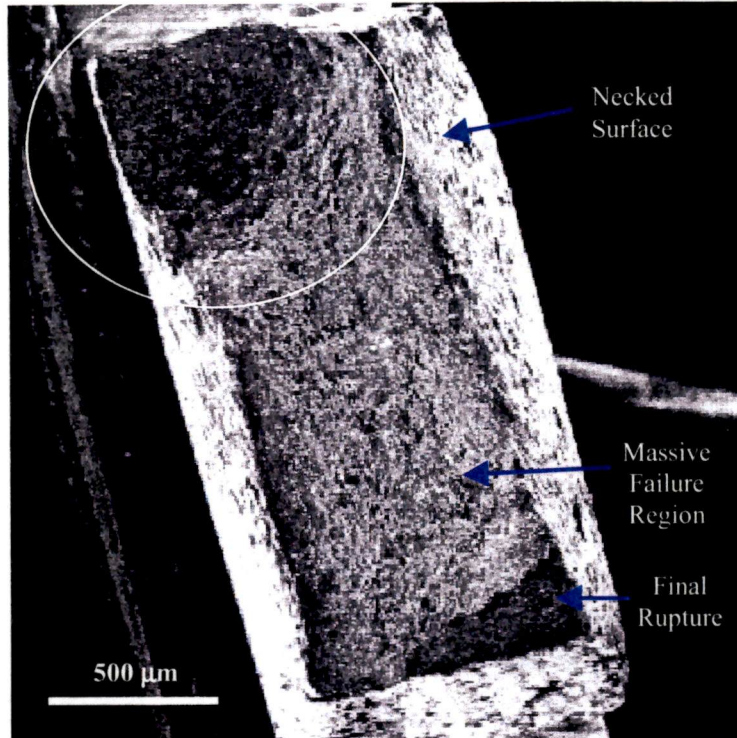
Figure 4.3.7: A macroscopic view of the fatigue fracture surface of a pure aluminum P/M sample, WX-10a, made with 20 µm sized aluminum powders. The maximum stress is 94 MPa. Notice the crack initiation site (circled) in the upper left corner.
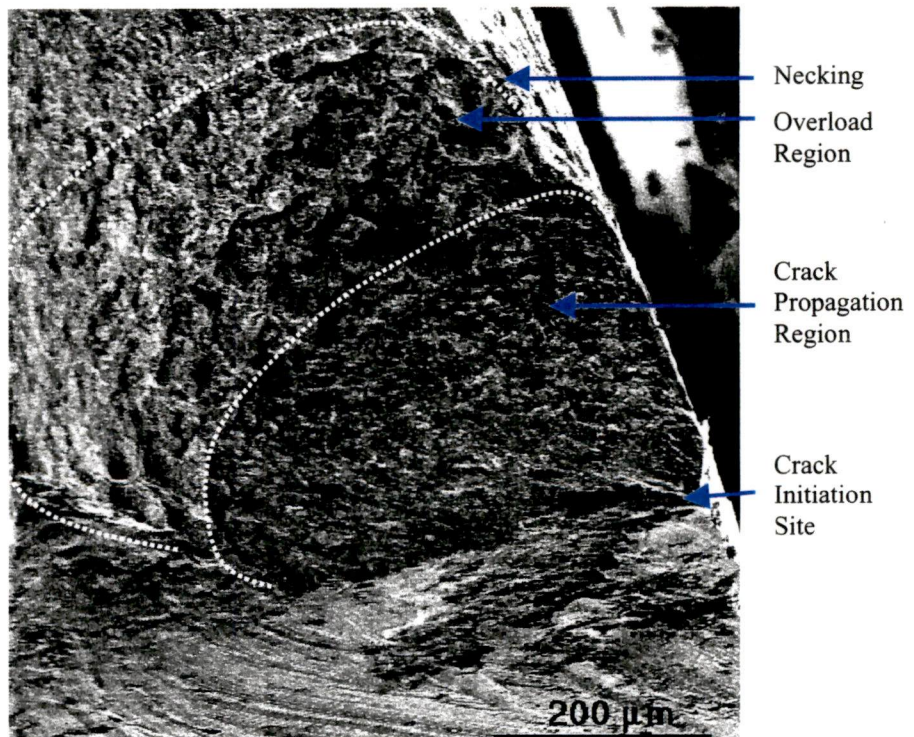
Figure 4.3.8: A close-up view of the crack initiation site pictured above.
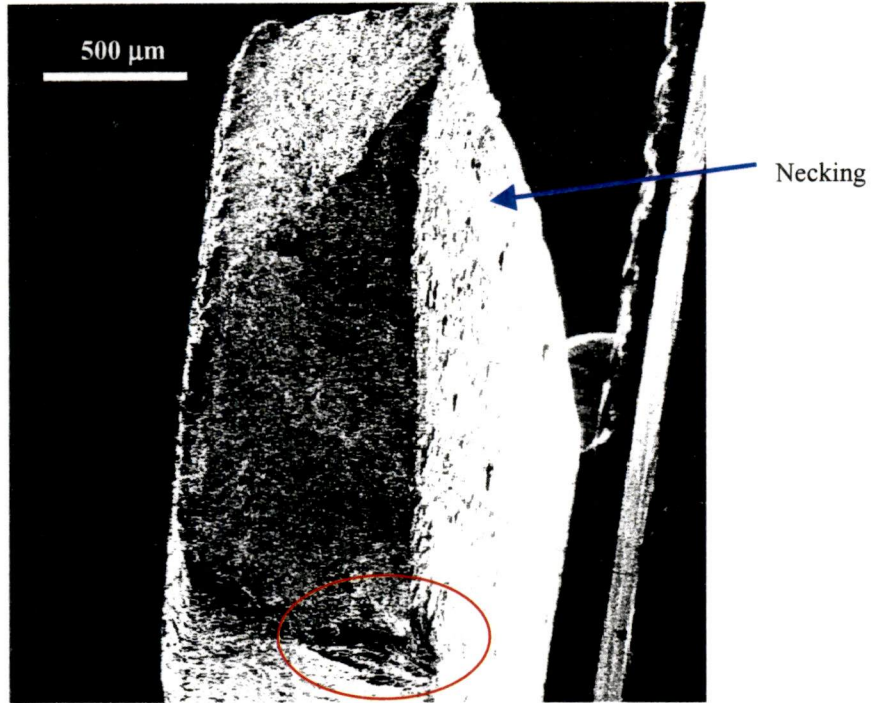
Figure 4.3.9: A macroscopic view of the fatigue fracture surface of a pure aluminum P/M sample, WX-10b. The maximum stress is 105 MPa. Notice the crack initiation site (circled) at the lower right corner, and the severe amount of necking.
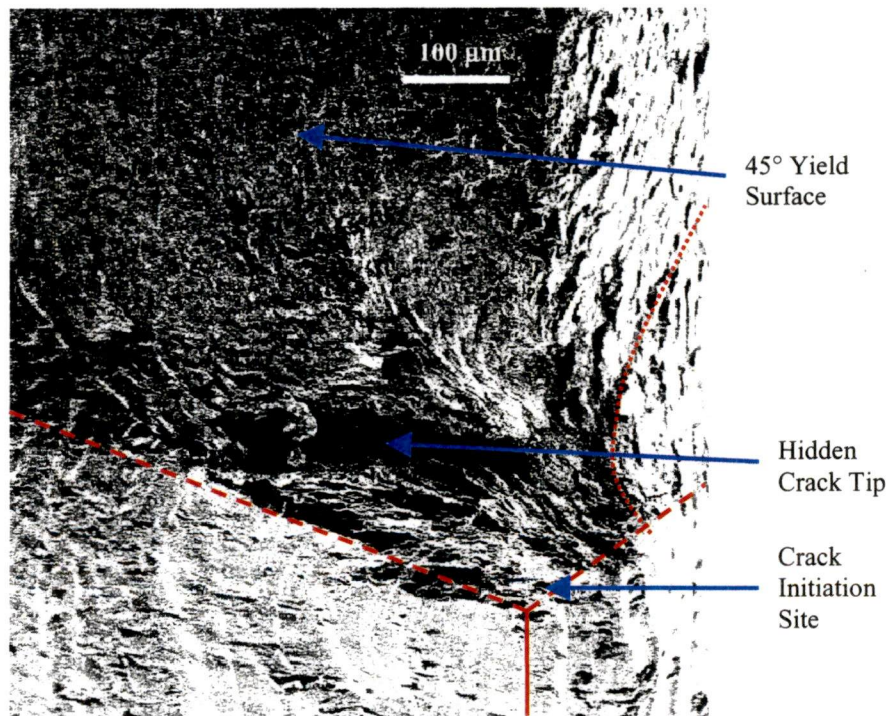
Figure 4.3.10: The crack initiation site of the above sample, WX-10b, magnified. The dashed lines indicate a circumscribed line perpendicular to the loading direction. The dotted line is the line displacement by necking. The solid line is the edge of the specimen.
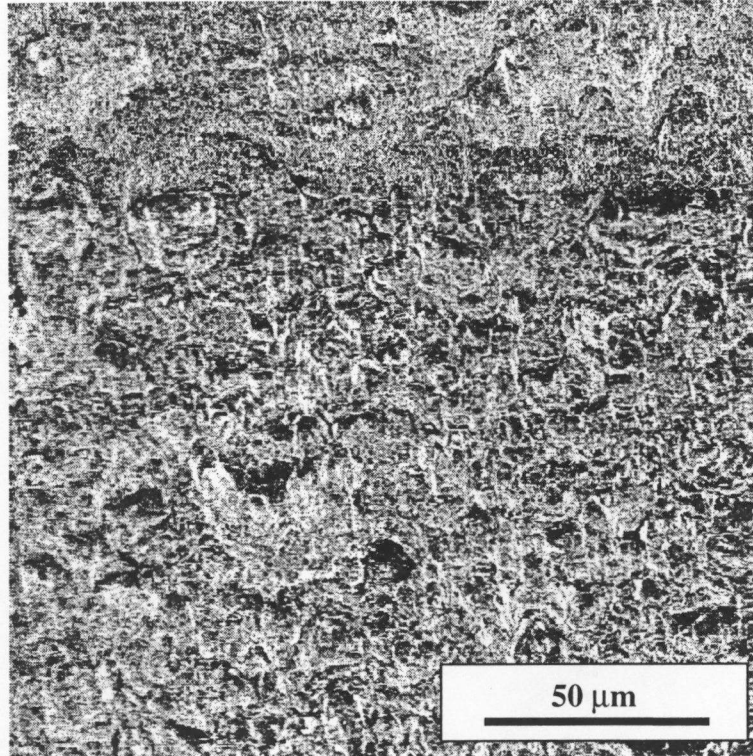
Figure 4.3.11: Fracture surface of the above sample, WX-10b, pure aluminum made by P/M processing.

fracture surface. There is a some evidence of void growth, although it is limited. This surface shows the growth of a crack tip that has been repeatedly blunted.

Figure 4.3.12 is a macroscopic, birds-eye view of the fracture surface of a pure aluminum P/M sample (WX-10) produced by fatigue loading. The particle size of the powder used for this material is 20 μm. The maximum stress for this sample is 116 MPa (16.82 ksi). This particular sample (WX-10c) endured 283 cycles before failure. It is difficult to see from the photo, but the surface is V-shaped, indicating plane-stress shear. The photo does show the crack initiation site at the top left corner (circled), and also the degree of deformation due to necking. The fracture surface of this sample is revealed in Figure 4.3.13. This surface does not indicate signs of fracture due to void growth.
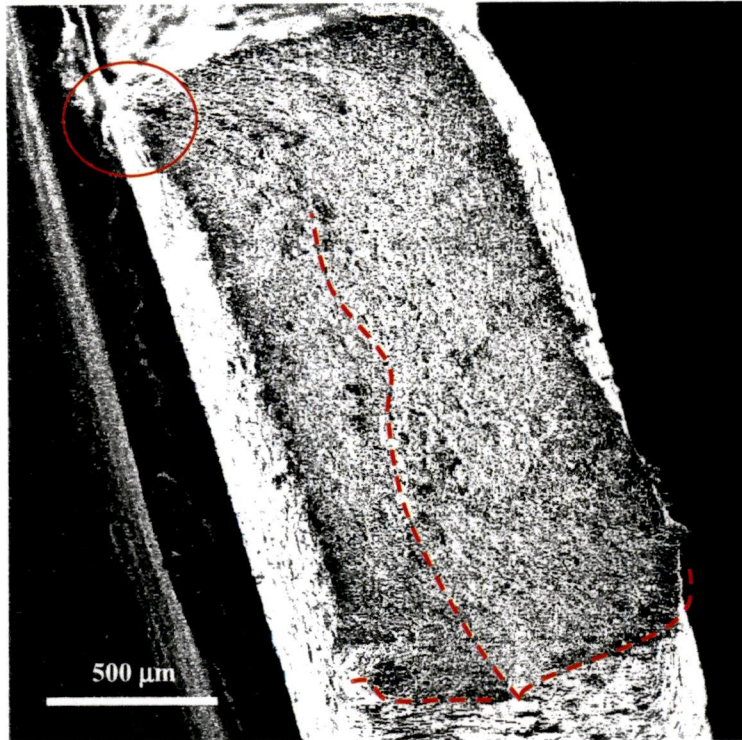
Figure 4.3.12: A macroscopic view of the fatigue fracture surface of a pure aluminum P/M sample (WX-10c). The maximum stress is 116 MPa. Notice the crack initiation site (circled) at the upper left corner. The dashed lines indicate the V-shaped surface.
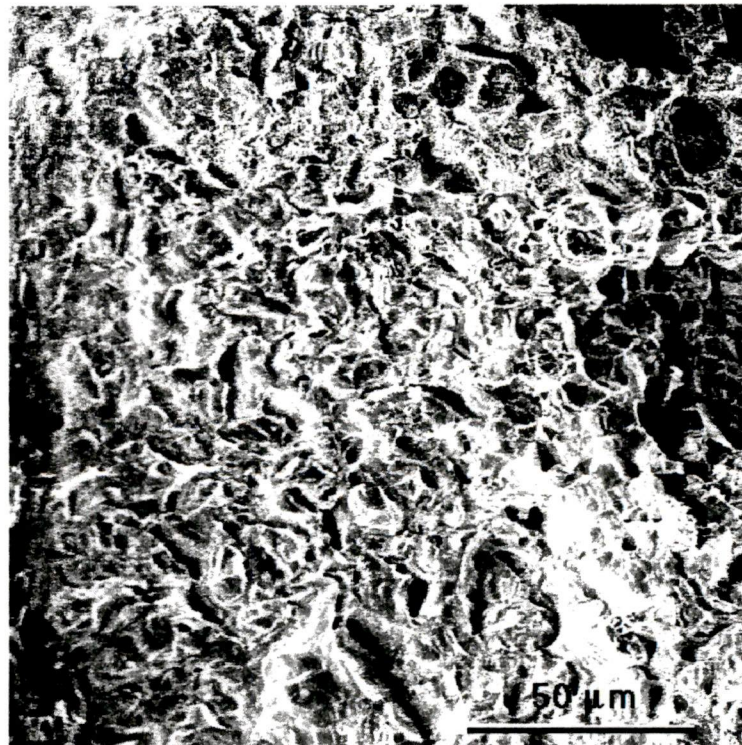
Figure 4.3.13: The fracture surface of the pure aluminum sample (WX-10c).

130

Figure 4.3.14: The fracture surface of a NiTi/Al composite fatigue sample (WX-11a), made with NiTi particles with a diameter of 5 µm. The maximum stress is 99 MPa.

Figure 4.3.14 identifies the fracture surface of a NiTi/Al composite fatigue sample, made with NiTi particles with a diameter of 5 µm, also produced by fatigue loading. The particle size of the aluminum powder used for this material is 20 µm. The maximum stress for this sample is 99 MPa, which is the lowest stress level tested for this material. This particular sample (WX-11a) endured 2,673,129 cycles before failure. This example is different from most others, because the crack originated from the side surface of the specimen, instead of the edge or corner, as is usually seen. As is seen in the previous specimen, the crack propagation region is flat, at a 90° angle, while the overload region rises sharply at a 45° angle. However, the massive failure region levels somewhat to about 30°.

Figure 4.3.15: The fracture surface of a NiTi/Al composite fatigue sample (WX-11b), made with NiTi particles with a diameter of 5 μm. The maximum stress is 116 MPa.

Figure 4.3.15 exhibits the fracture surface of a NiTi/Al composite fatigue sample, made with NiTi particles with a diameter of 5 μm, also produced by fatigue loading. The particle size of the aluminum powder used for this material is 20 μm. The maximum stress for this sample is 116 MPa (16.82 ksi). This particular sample (WX-11b) endured 202,870 cycles before failure. As is seen in the previous specimen, the crack propagation region is flat, at a 90° angle from the loading direction, and the massive failure region is about 30°. The fracture mechanism is largely plane-strain, as seen by the flat fracture surfaces.

Figure 4.3.16: The fracture surface of a NiTi/Al composite fatigue sample (WX-11c), made with NiTi particles with a diameter of 5 μm. The maximum stress is 163 MPa. Notice that the plane of fracture is located at a 45° angle from the direction of applied loading.

Figure 4.3.16 is another fracture surface of a NiTi/Al composite fatigue sample, made of NiTi particles with a diameter of 5 μm (WX-11c). This sample experienced 139 cycles before failure, with a maximum stress of 163 MPa (23.6 ksi). The presence of a high stress level has caused an entirely different mode of failure from the others. The crack initiation region is so minute, that it could not be located. The entire fracture surface is a flat, plane-strain, massive failure region, located at a 45° angle from the direction of applied loading. Figure 4.3.17 reveals the fracture surface at a higher magnification. There is some evidence of failure from void coalescence, however, the ridges lack a prominent edge, indicating a brisk force during separation, which would prohibit a sharp edge from maturing.
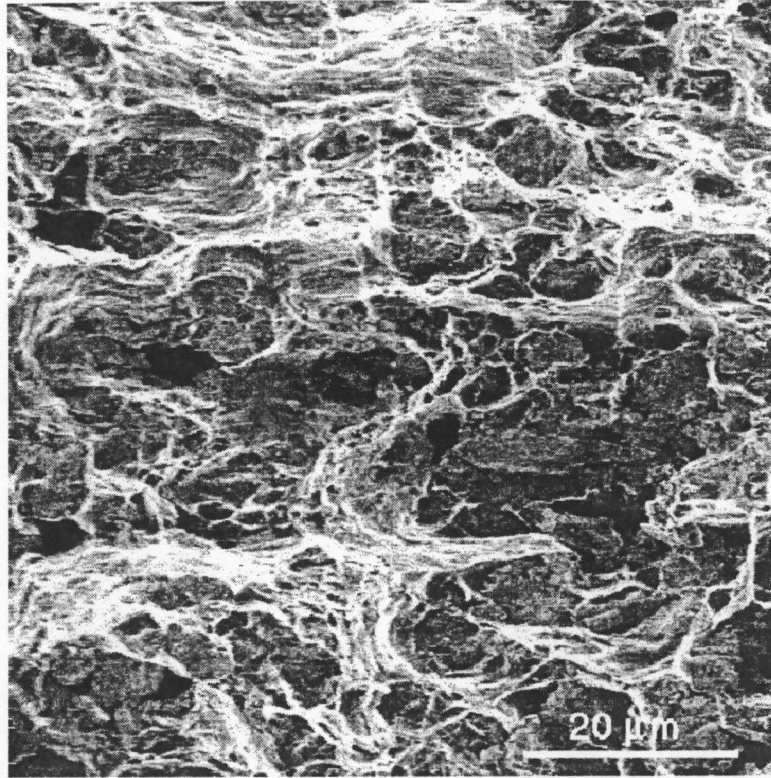
Figure 4.3.17: The fracture surface of the composite sample pictured in Figure 4.3.16.

Figure 4.3.18 is an example of the fracture surface of a NiTi/Al composite fatigue sample, made with NiTi particles with a diameter of 40 μm (WX-12a). The aluminum powder used for the matrix material is 20 μm in size. The maximum stress is 94 MPa. This particular sample endured 1,827,311 cycles before failure. Figure 4.3.19 depicts a peculiar cleft along the edge of the crack propagation region, which is believed to be the crack initiation site. The lower half of the photo is the surface of the side of the specimen. A closer view of the surface in the crack propagation region of this sample is shown in Figure 4.3.20. The formation of the crater at the top left corner was due to the presence of a NiTi particle, which seems to have pulled away from the interface. In Figure 4.3.21, the surface of the massive failure region shows sharp ridges, which indicate very mature void growth.
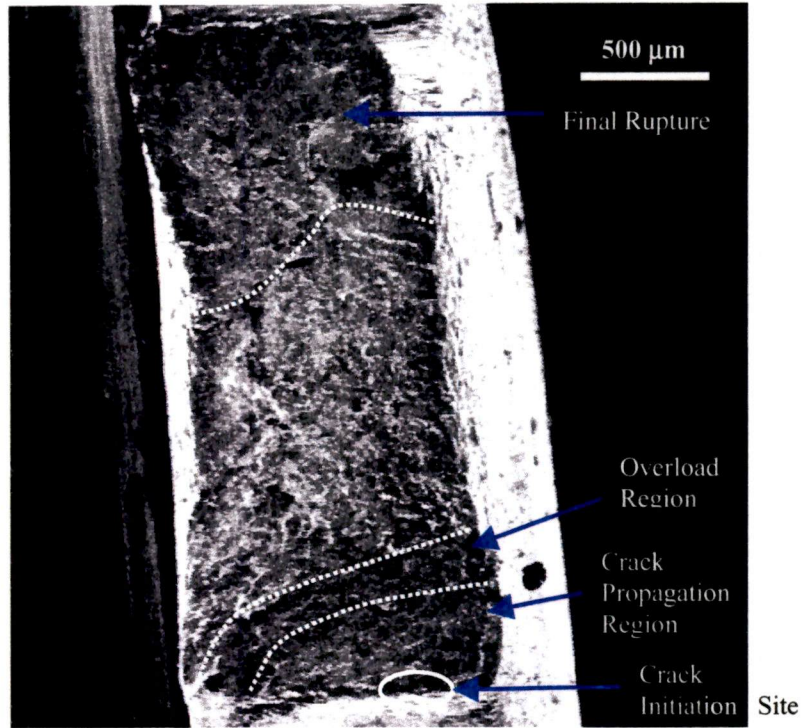
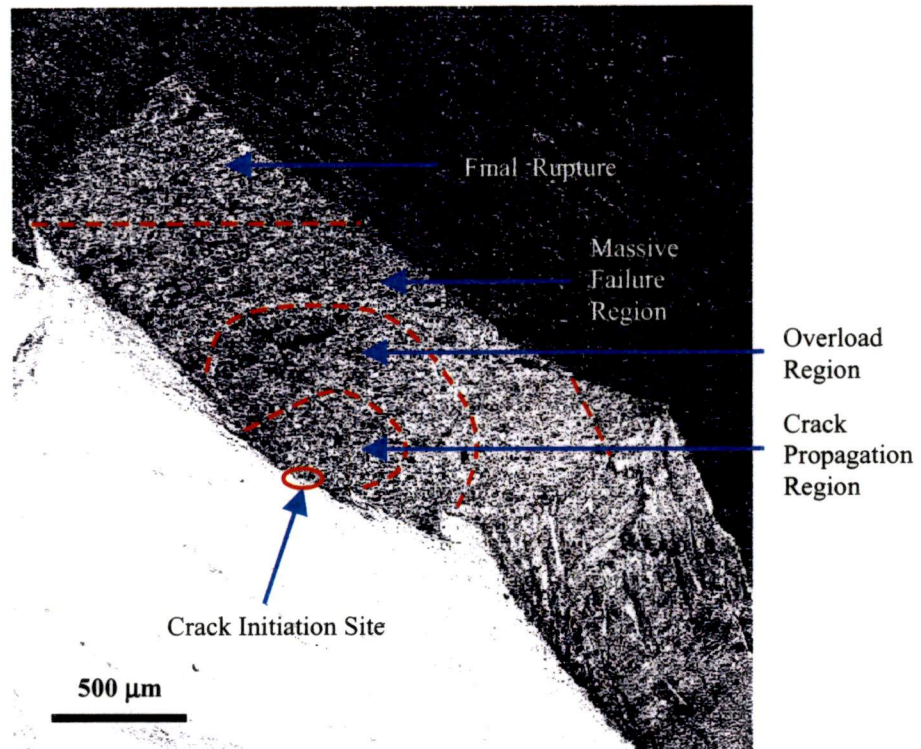Figure 4.3.18: The fracture surface of a NiTi/Al composite fatigue sample (WX-12a), made with NiTi particles of a diameter of 40 µm. The maximum stress is 94 MPa.
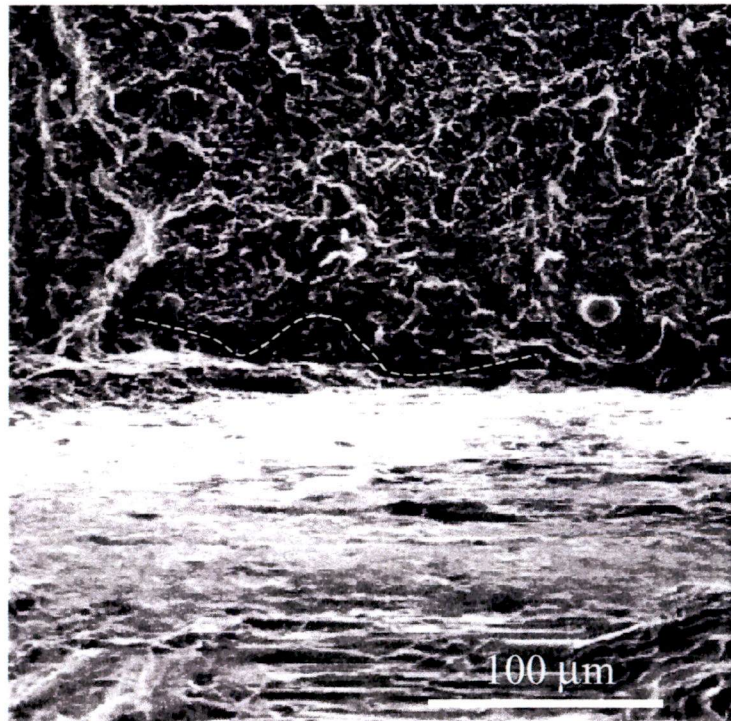
Figure 4.3.19: A strange cleft (indicated by the dotted line) along the edge of the crack propagation region, what is believed to be the crack initiation site. The lower half of the photo is the side surface of the specimen (WX-12a).
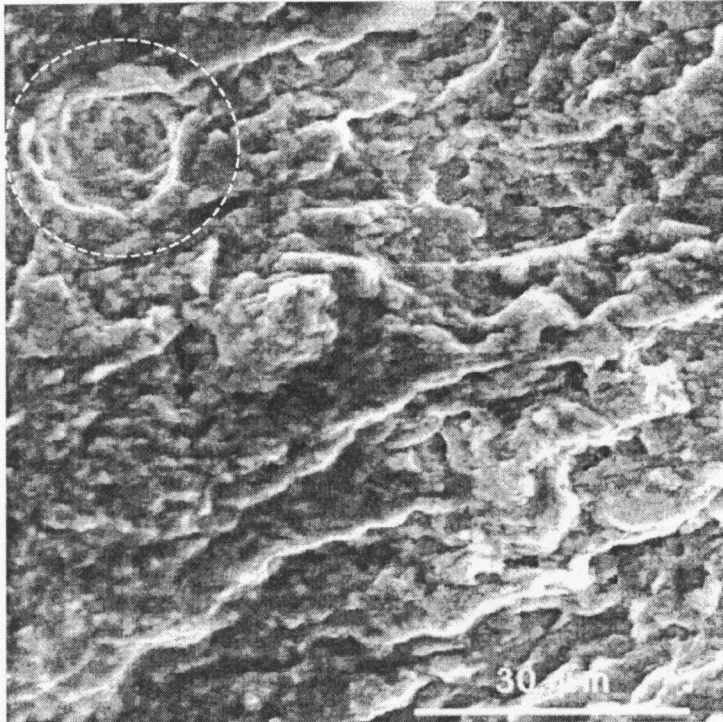
Figure 4.3.20: A closer view of the surface of the crack propagation region of the above sample. The formation of the crater at the top left corner (circled by a dotted line) was due to the presence of a NiTi particle.
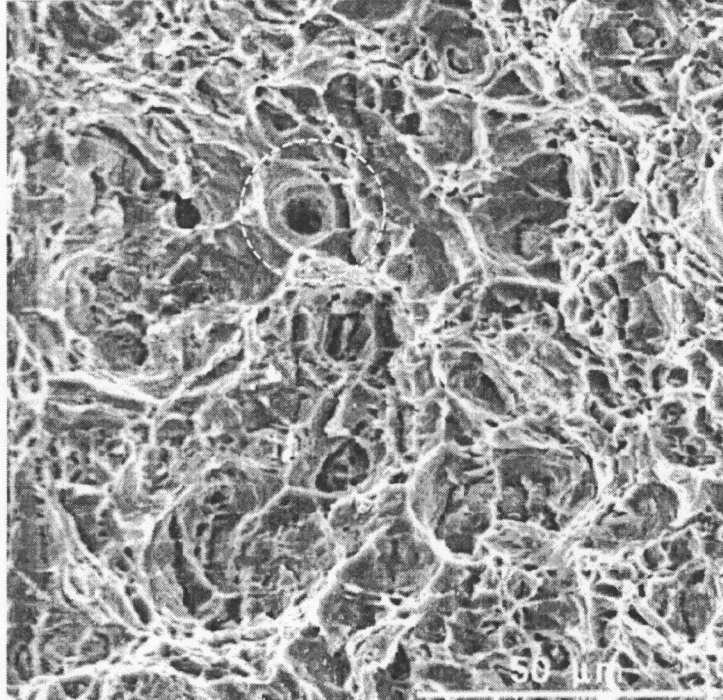
Figure 4.3.21: The surface of the massive failure region showing sharp ridges, which indicate very mature void growth. One pore has grown to an especially large size (circled by a dotted line).
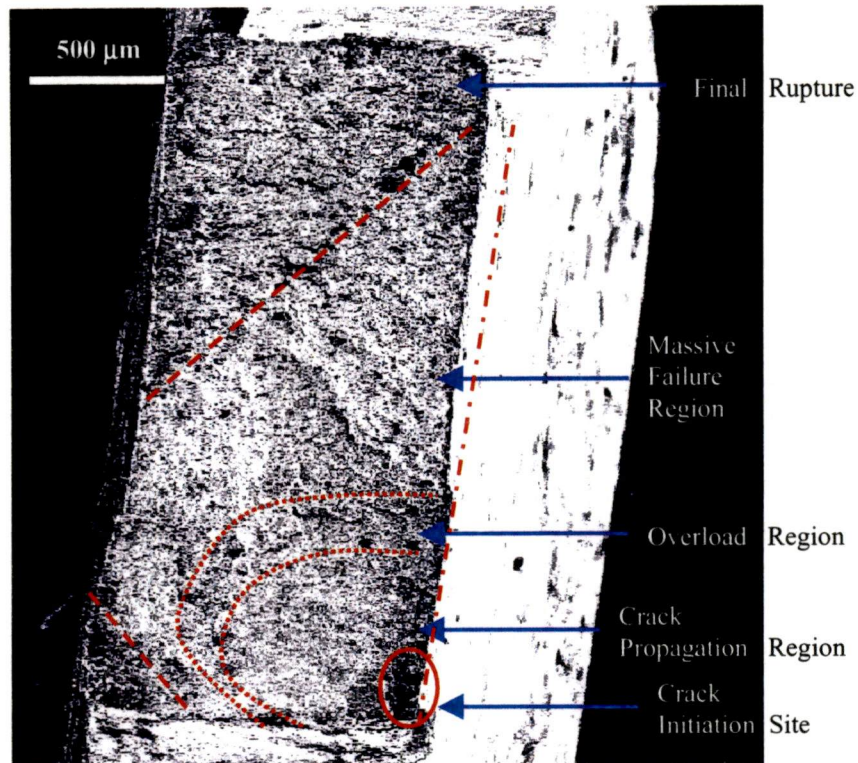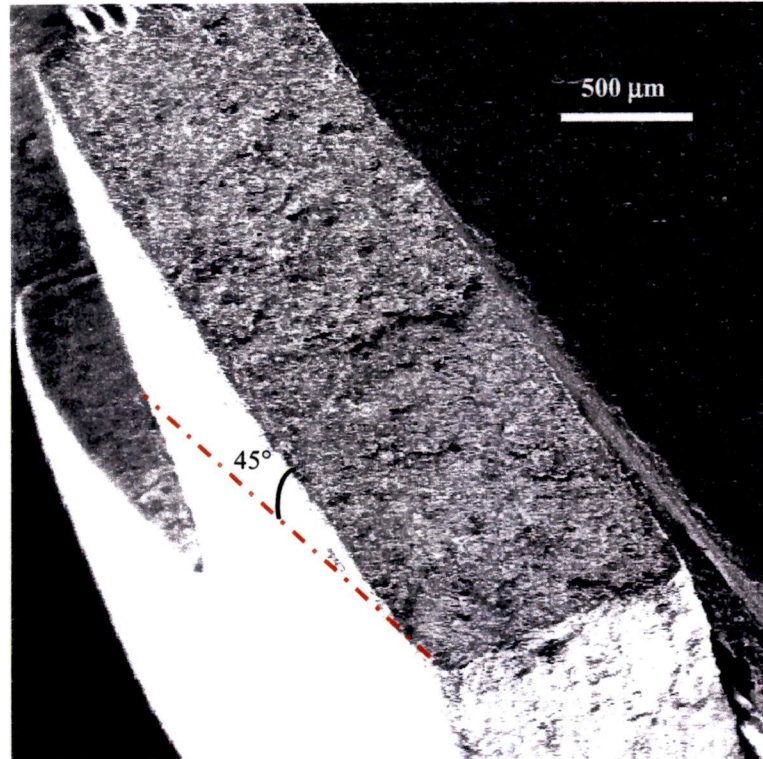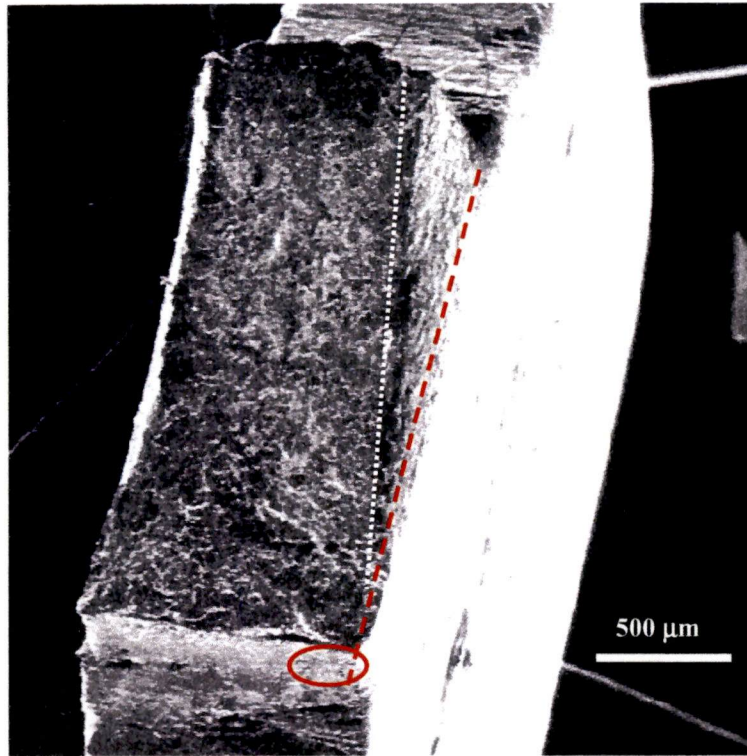
Figure 4.3.22: Fracture surface of a NiTi/Al composite fatigue sample (WX-12b), made with NiTi particles of a diameter of 40 µm. The maximum stress is 105 MPa. The crack initiation site is circled. The dashed line indicates the normal plane. A dotted line follows the edge of fracture, and defines the degree of necking.

Figure 4.3.22 exhibits the fracture surface of a NiTi/Al composite fatigue sample, containing NiTi particles with a diameter of 40 µm. The particle size of the powder used for this material is 20 µm. The maximum stress is 105 MPa (15.23 ksi). This particular sample (WX-12b) endured 364,599 cycles before failure. The dashed line indicates the plane normal to the loading direction, while the dotted line follows the edge of fracture, and defines the extended degree of necking. The crack initiation site is circled, and the fracture surface from this area is magnified in Figure 4.3.23. Also note that a plane-strain failure mechanism dominates in the massive failure region, resulting in a relatively flat fracture surface. This surface exhibits signs of fracture due to void growth and coalescence, as depicted in Figure 4.3.24.
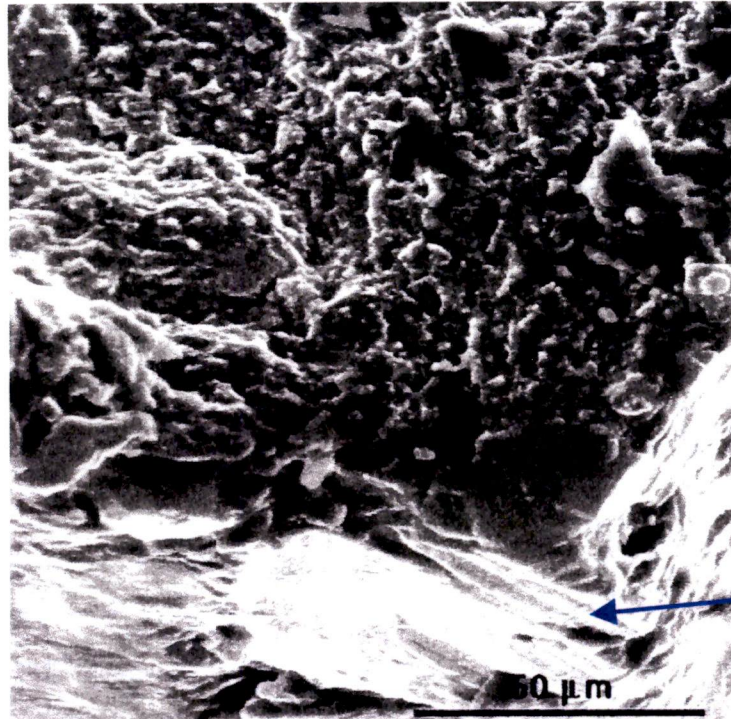
Surface
check from
the stamping
operation

Figure 4.3.23: The crack initiation site of the described sample (WX-12b), which seems to be a check in the surface due to the stamping procedure.
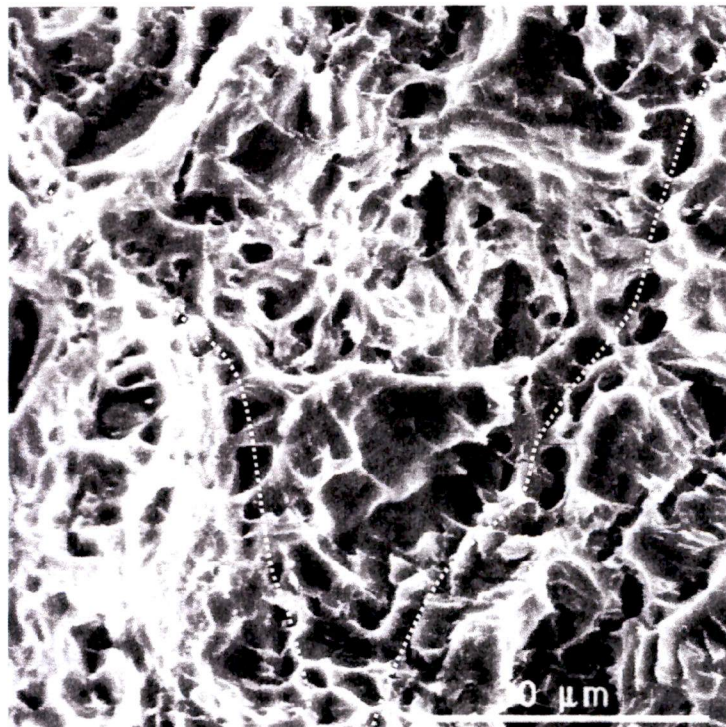
Figure 4.3.24: The massive failure region showing extremely mature void growth, with a linear array of voids, as indicated by dotted lines, which presents an excellent pictoral example of the growth of cracks due to the void coalescence fracture process.

Modes of Failure

After an inspection of the fracture surfaces, three common fracture morphologies in the materials were observed. Therefore, the maximum stress level has been divided into three ranges. Since these stress levels vary with the yield strength of each material, these levels have been defined according to the fatigue life results. A low stress level represents those samples enduring a lifespan greater than 1,000,000 cycles. A high stress level indicates those samples withstanding a lifespan under 10,000 cycles. An intermediate stress level envelopes the samples with a lifespan between these two values.

For low stress levels (usually $\leq \sigma_y$), cracks were most often nucleated from an inclusion or a surface defect, but were occasionally due to a conglomeration of NiTi particles that were not sufficiently separated after the 800°C (1470°C) heat treatment which follows the mechanical-milling procedure. In this case, the NiTi particles were not sufficiently bonded to each other since they were not in contact with the aluminum matrix. The poor bonding characteristics produced voids between the NiTi particles in the matrix, which became crack initiation sites upon loading.

After initiating, these cracks grew with an increasing number of cycles, due to localized stress concentration, until a plane-strain failure of the remaining cross-section occurred. Since much of the fatigue life involved the slow growth of the crack initiation, the composite material showed very little fatigue improvement over the matrix material

for low stress levels, as depicted in the S-N curves (Figures 4.3.1 through 4.3.3), and in the P-L curves (Figures 4.3.4 through 4.3.6).

At higher stress levels, the NiTi reinforcement played a large role as a matrix stiffener. There was much more extensive strain deformation in the unreinforced aluminum matrix materials than in the composite materials. In the composite materials, there was much less deformation that occurred. The material was weakened through the formation and growth of voids in the matrix, until a catastrophic plane-stress fracture causes failure. There were very few voids near the NiTi particles, whose growth contributed to failure. This was due to the excellent bonding between the particles and the matrix, and perhaps also due to stress interactions stemming from the shape-memory effect, or the associated stress-induced martensite phenomenon.

For intermediate stress levels, there was a combination of the previously mentioned failure mechanisms. A crack initiated from an inclusion or surface defect, and quickly grew. However, it did not grow to failure so soon as to prevent a general weakening of the total cross section of the sample. Both were happening simultaneously. When the crack reached a critical size, the material has already been weakened from void growth to allow a partially-ductile fracture. This resulted in a combination of plane-stress and plane-strain failures.

Table 4.3.2 summarizes the basic fracture properties of the pure aluminum P/M matrix materials. Table 4.3.3 delineates the various fracture and deformation characteristics for the NiTi reinforced aluminum matrix composite materials.

Table 4.3.2: A summary of fracture and deformation characteristics for the aluminum matrix materials with no reinforcement.

* Angle is measured from the axis of loading
† V-morphology is in either the transverse or the through-thickness direction.

Stress Level	Property	Propagation Region	Overload Region	Massive Failure Region
Low (N > 10⁶ cycles)	Fracture Mode	Cleavage	Combination of Shear and Cleavage	Shear
	Type of Fracture	Plane-Stress	Combination of Plane-Stress and Plane-Strain	Plane-Strain
	Fracture Morphology and angle*	Large, Flat/90°	45°	30°
Intermediate (10⁴ cycles < N < 10⁶ cycles)	Fracture Mode	Cleavage	Combination of Shear and Cleavage	Shear
	Type of Fracture	Plane-Stress	Combination of Plane-Stress and Plane-Strain	Plane-Strain
	Fracture Morphology and angle*	Small, Flat/90°	Combination of Plane-Stress and Plane-Strain	45°
High (N <10⁴ cycles)	Fracture Mode	Cleavage	Combination of Shear and Cleavage	Shear
	Type of Fracture	Plane-Stress	Combination of Plane-Stress and Plane-Strain	Plane-Strain
	Fracture Morphology and angle*	~	V/45°†	V/45°†

141

Table 4.3.3: A summary of fracture and deformation characteristics for the nickel-titanium shape-memory alloy reinforced aluminum composite materials.

* Angle is measured from the axis of loading

Stress Level	Property	Propagation Region	Overload Region	Massive Failure Region
Low (N > 10⁶ cycles)	Fracture Mode	Cleavage	Combination of Cleavage and Void Coalescence	Void Coalescence
	Type of Fracture	Plane-Stress	Combination of Plane-Stress and Plane-Strain	Plane-Strain
	Fracture Morphology and angle*	Large, Flat/90°	Large, Concave/45°	Flat/30°
Intermediate (10⁴ cycles < N < 10⁶ cycles)	Fracture Mode	Cleavage	Combination of Cleavage and Shear	Combination of Shear and Void Coalescence
	Type of Fracture	Plane-Stress	Combination of Plane-Stress and Plane-Strain	Combination of Plane-Stress and Plane-Strain
	Fracture Morphology and angle*	Small, Flat/90°	Small, Concave/45°	Flat/30°
High (N <10⁴ cycles)	Fracture Mode	Cleavage	Combination of Cleavage and Shear	Shear
	Type of Fracture	Plane-Stress	Plane-Stress	Plane-Stress
	Fracture Morphology and angle*	Extremely Small	Flat/45°	Flat/45°

Patterns of Fracture Mechanisms

After tensile and fatigue tests were conducted, the fracture surfaces were examined using SEM. It was found that there were two fracture mechanisms occurring simultaneously in the material during loading, especially during cyclic loading, that contrubuted toward failure. These mechanisms are;

1. General crack initiation and propagation
2. Void coalescence

The crack propagation mechanism is dependent on slip bands around the crack tip, which allow the crack to open and propagate, thus increasing the stress concentration and the rate of failure with each progressive cycle. The greater part of the fatigue life of a specimen is spent in nucleating a crack tip and the slow propagation of this crack tip. A specimen may require a few million cycles to accomplish this, while the overload region may only last a few thousand cycles. With this damage already done, the massive failure region of a fracture may only require a few hundred more cycles to complete the failure. The rate of crack growth for the mechanism of crack propagation, can be governed by the Paris relationship (Equations 4.3.1 through 4.3.3). The major contributing factor to the rate of the first mechanism is the stress concentration around the crack tip. It is the magnitude of this stress, which causes the crack to grow slowly or quickly. Therefore, a higher stress would lead to the failure of the material in a short time, whereas a lower stress would not cause the crack to propagate as rapidly, thus increasing the life of the material. The crack growth rate of the propagation mechanism is governed by the stress

intensity factor range, ΔK, around a crack tip of length, a, according to the modified Paris equation,[34,39]

$$\frac{da}{dN} = \frac{A(\Delta K)^p}{(1-R)K_c - \Delta K}$$

(Eq. 4.3.1)

where N is the number of loading cycles, A is a constant, p is a constant that ranges between three and four, K_c is the fracture toughness of the material, and R is the stress ratio, defined by,

$$R = \frac{\sigma_{min}}{\sigma_{max}} = \frac{K_{min}}{K_{max}}$$

(Eq. 4.3.2)

The ΔK value around the crack tip is further defined by,

$$\Delta K = \sigma_{max}\sqrt{\pi a} - \sigma_{min}\sqrt{\pi a} = \sigma_r\sqrt{\pi a}$$

(Eq. 4.3.3)

where σ_r is the stress range. It is generally true that as the crack grows in length, so does ΔK, thus compounding the rate of failure.

In contrast, the failure due to the coalescence mechanism is directly dependent on the formation and growth of voids throughout the matrix. The growth rate of these voids may also depend on the Paris relationships. During the process of void coalescence, a shear strain will cause a defect to open up into a void, or perhaps there are already voids present in the material due to porosity. With the continued slip and deformation of the material local to the voids, these voids grow larger. As these voids increase in size, the overall cross section of material diminishes, creating higher stress concentrations around

144

the voids, and thus, increasing the rate of failure. Eventually these voids join together to form a "dimpled" fracture surface.

The difference between these two mechanisms is that the first one, crack propagation, concerns one large crack, which forms and grows due to slip, leading to failure. The second mechanism is caused by a multitude of tiny cracks, or voids, which slowly grow, thus weakening the entire cross section of the material. The first mechanism is primarily responsible for the crack propagation region, thus determining the majority of the life of the sample. However, both of these mechanisms simultaneously contribute to the massive failure of the sample, because as the crack grows, the crack tip will seek out the growing voids, which become a part of the crack surface, as the crack proceeds through the material.

At high loads, the stress concentration factor will likewise be very high, leading to a very imminent failure due to the first mechanism of crack propagation. The obvious 45° angle of the fracture surfaces of these samples exemplify the magnitudes of stresses which cause this behavior. Since the fatigue crack grows at a much faster rate at high stress levels, the material is short lived in comparison, and there is very little time for voids to nucleate and grow, As a result, the massive failure surfaces show little evidence of void coalescence for high-stress loading conditions. Crack initiation and propagation are the main mode of failure, causing the material to fracture before any voids have a chance to grow to a size which may have an impact on the overall strength.

At low stress levels, the stress concentration factor around the fatigue crack tip is too low to cause a rapid crack growth. The crack remains small for the majority of the duration of the fatigue test, ranging from 80,000 to 200,000 cycles for the composites made with the 5 μm sized aluminum powder, and 200,000 to 400,000 cycles for the 20 μm sized aluminum powder in the matrix. After this stage in crack growth, the crack begins to grow at a much faster rate. This transition is marked by a sharp hook in the S-N curve for some of the materials, as indicated in Figures 4.3.1 through 4.3.3. At this transition, it is thought that the matrix-oriented voids have grown to a considerable size to begin affecting the overall strength of the material, and the rate of crack growth. The material soon fails afterward. The initiation of the massive failure is predominantly due to the overall weakening of the material, resulting from the second, void-coalescence mechanism, which enhances the rate of the crack propagation in the first mechanism. Since these voids are matrix-contained, and since the corresponding materials displaying this behavior share a common matrix material, this may explain why the S-N curves converge at low stress levels.

Void coalescence is the most common mode of failure in P/M materials. This is not surprising, since it is known that internal voids are common in P/M materials. However, for all stress levels in the NiTi/Al composite material, there happens to be an interesting deviation to the usual process of fracture due to void coalescence. In most engineering alloys which fail by void coalescence, the voids first form at the second-phase particles. However, when the broken NiTi/Al composite samples were mounted and polished, a surprising phenomenon was discovered. The voids, which resulted in the

formation of the massive failure surface, were expected to form around the second-phase NiTi particles in some way, but this was not the case. Large voids near the NiTi particles were extremely rare. Consequently, the fracture surface is almost totally matrix-contained.

A SEM technique, known as Z-imaging, can detect compositional differences on the surface of a specimen. The Z-value of an element is its atomic number on the periodic table of the elements, i.e., aluminum is 13, titanium is 22, and nickel is 28. This technique utilizes the fact that elements of a higher Z-value tend to produce more backscattered electrons upon exposure to the electron beam. With the use of a special backscattered electron detector, which hovers closely above the surface of the sample during the scanning, a generated image will show elements of a higher Z-value to be of a lighter shade of gray than those elements of a lower Z-value. Hence, the NiTi particles will appear as white spots on the gray aluminum matrix. A Z-imaging examination of the open fracture surface, resulting from SEM backscattering techniques, showed that no nickel or titanium were present on the surface of the fracture (see Figure 4.3.25). This evidence further endorses the supposition that the crack paths avoid the NiTi particles in the matrix. This may result in a more tortuous crack path, or it may also require more intra-matrix deformation surrounding the crack tip, to enable the continuation of the fracture. This trend could promote strong fatigue resistance in the composite, as compared to the matrix material alone. The aluminum matrix itself is also very ductile, lending the possibility of a vast amount of deformation, thus, absorbing much of the energy invested into the fracture.
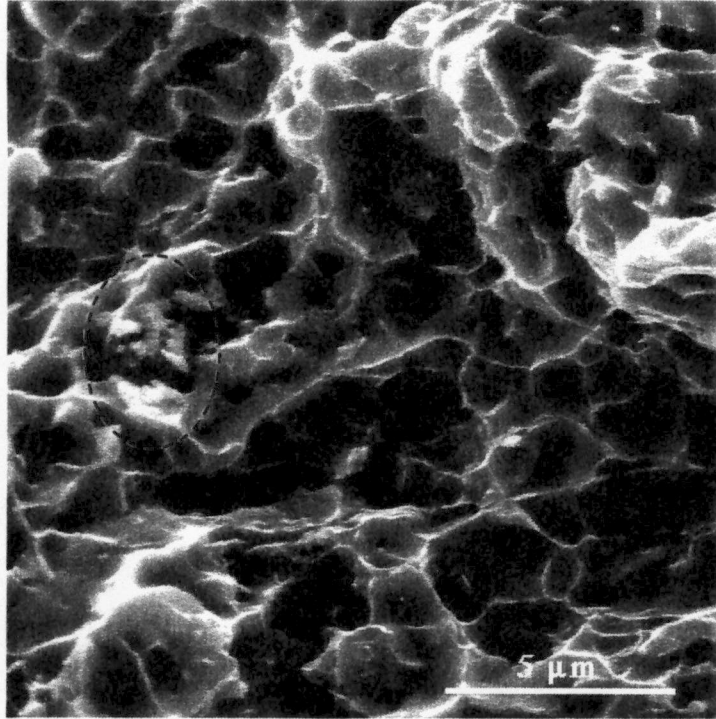
Figure 4.3.25: The fracture surface of the SMA MMC (WX-8). Particle sizes for both the NiTi and Al are 5 μm. The circled area is a clump of NiTi particles that were not sufficiently separated before pressing. Note the cusps and dimples, which are characteristic of failure due to void coalescence.

Figure 4.3.26 displays such a crack path, which has few NiTi particles exposed to the surface. The fracture, rather, is almost totally matrix-contained. Note that the mounting epoxy in the sample will collect charge from the electron beam during SEM imaging, producing the light colored streaks in the open fracture area of the photomicrograph. A quantitative technique for measuring variations in crack paths, in relation to variations in microstructure, was developed in the early eighties, and has recently been used by Wu at the University of Alabama.[40] In this technique, a single, straight line, parallel to the crack, such as the one illustrated in Figure 4.3.26, is drawn at random across a photomicrograph of the microstructure, and the number of particles lying along that line is counted. Alternatively, the lengths of the segments of that line which intersect areas of the second phase may be summated. This data is then compared

148
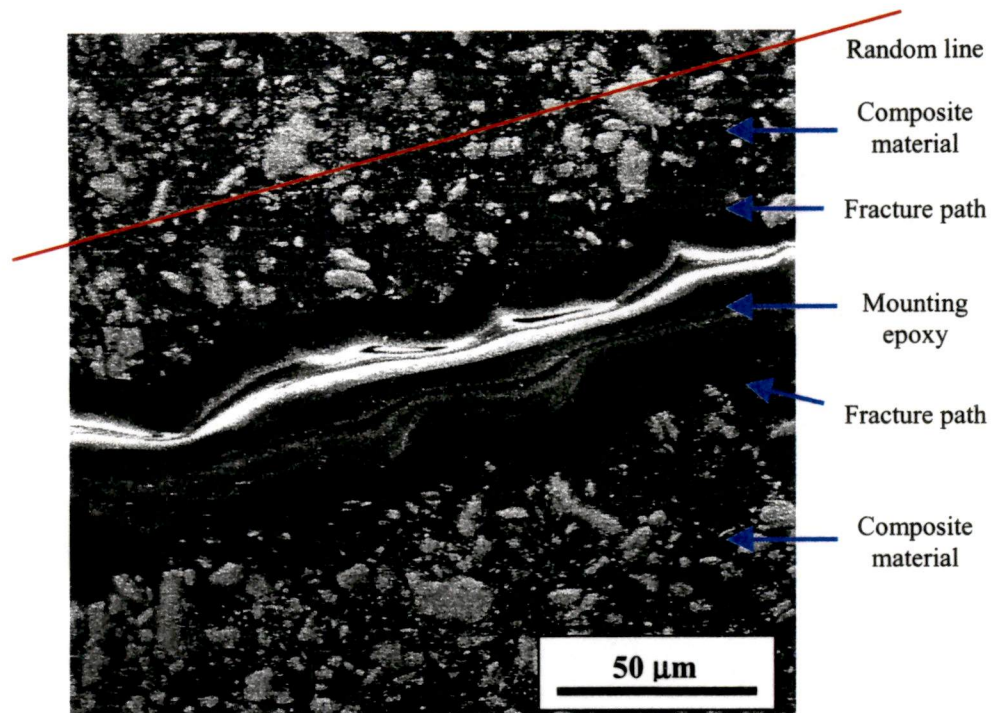
Figure 4.3.26: A fatigue crack in a Al5.NiTi5-30 material, which shows very little failure along the NiTi particles. The majority of failure is due to the matrix material.

to the number of particles found along a fracture path. The data for an Al5.NiTi5-30 material is enumerated in Table 4.3.4. The line length is 190 μm.

As indicated by the data, the crack faces only possess about 42% of the number of NiTi particles that the matrix material contains. This difference is enhanced by the fact that the crack faces are approximately 25% longer than the random lines, due to the irregularity in their shapes. Regardless of the stress level at which the different materials were tested, this behavior remained virtually consistent for all the nickel-titanium reinforced-aluminum composite materials. Crack paths progressed through the matrix material and tended to avoid the NiTi phases. It is thought that the excellent bonding between the particles and the matrix is largely responsible for this behavior. Recall that the titanium oxide layer on the surfaces of the NiTi particles will react with the aluminum

Table 4.3.4: NiTi particle/crack path interaction data for an Al5.NiTi5-30 material.

All composite materials display a similar behavior
* Line lengths are 190 μm, except for crack faces, which extend approximately 25% longer, due to the irregularity in shape

Line #	Distance from Crack Face (μm)	# of NiTi Particles Along a 190 μm Line*	NiTi Particle Concentration (Particles/mm)	Average NiTi Particle Concentration in the Matrix (Particles/mm)	Average NiTi Particle Concentration Along Crack Faces (Particles/mm)
1	40	15	78 9		
2	32	16	84.2		
3	24	14	73 7		
4	16	14	73.7		
5	8	13	68 4		
Upper Crack Face	0	6	31 6	**80.5**	**34.2**
Lower Crack Face	0	7	36.8		
6	8	13	68 4		
7	16	12	63.2		
8	24	18	94.7		
9	32	20	105.3		
10	40	18	94 7		

to produce aluminum oxide, among a number of other phases. Fortunately, there is a minimum of the formation of these second phases, but a strong particle-to-matrix bond is established from those reactions.

Figure 4.3.27 is a schematic diagram of the crack growth process in the massive failure region, due to void coalescence in NiTi/Al composite materials. The composite material is subjected to a strain under loading conditions. The voids in the matrix grow larger due to deformation and slip mechanisms. However, the voids surrounding the NiTi particles undergo a strictly limited growth rate, as indicated by the figure. The voids grow in size as the material continues to be subjected to strain. The voids eventually join together, decreasing the total amount of the cross-sectional area of the specimen. Because of this, localized stress concentrations increase in magnitude, accelerating the rate of the fracture process. The voids continue to form, grow in size, and join together, until the massive failure occurs. Since the voids contained in the matrix grow, and the voids located near particles do not, then only the matrix-oriented voids will contribute to the fracture mechanism.

There may be two reasons why voids in the vicinity of the NiTi particles did not grow as quickly as those which are wholly matrix-contained. As discussed earlier, voids require strain in the material in order to grow. A NiTi particle in the austenitic phase, which is also coated with an oxide layer, will exhibit a much higher modulus than the aluminum material. This high modulus, combined with excellent bonding characteristics, may have inhibited high rates of strain in the matrix material in the vicinity of the NiTi

1. Composite material

   Subjected to strain...

2. Voids in the matrix grow larger due to deformation and slip mechanisms, whereas the voids situated next to the NiTi particles remain virtually unchanged.

   Continued to be subjected to strain...

3. Voids eventually join

   Stress concentrations increase, voids continue to form, grow in size, and join together, until...

4. Failure occurs

   Note that those voids situated near the NiTi particles have not grown considerably.

NiTi Particles   Voids
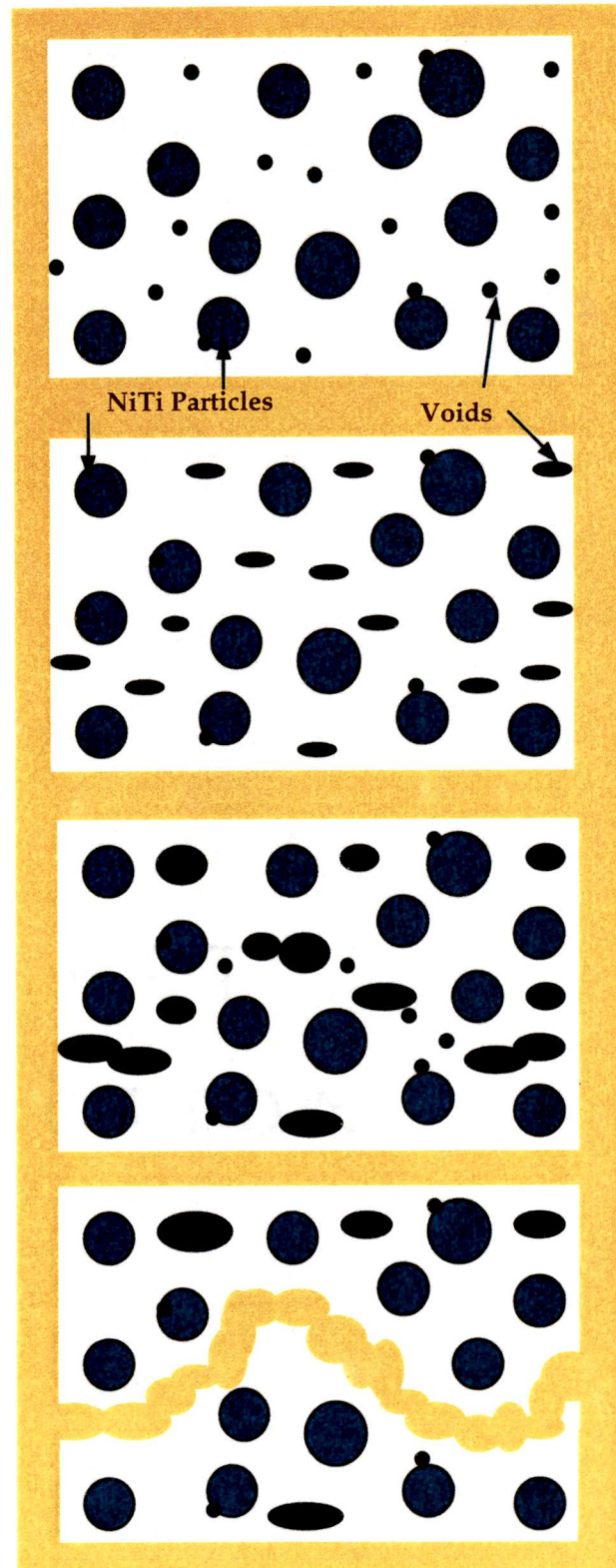
Figure 4.3.27: A schematic diagram of the process of failure, due to void coalescence in the massive failure region, for NiTi/Al composite materials.

particle during loading. This, in turn, would slow the rate of void growth.

Another possibility is the shape-memory property of the NiTi, which may have induced stress fields that somehow absorb the strain around the particle. Again, the reduction of strain would decrease the rate of void formation and growth. It remains unclear exactly how the shape-memory effect may affect crack propagation in reality, although theoretically, there should be certain stress fields around each particle, which would promote crack branching. Theory also shows that there should also be a compressive stress normal to a tensile stress around each particle, which would create more ductility in the surrounding matrix material. The relief of this stress combination, which might occur under loading conditions, would decrease the ductility and increase the resistance to crack propagation.

PART V.

FINAL CONCLUSIONS

5.1 A Summary of The NiTi/Al Composite Material Properties

The nickel-titanium shape-memory alloy reinforced aluminum composite, with 10 volume percent NiTi, has been successfully fabricated using powder metallurgy techniques. Densities have surpassed 99% for most materials. The mechanical-milling of the NiTi powders, has reduced the particle sizes from 40 μm, to approximately 5 μm in diameter. This process roughens the surface texture and enhances the matrix bonding interface. A subsequent heat-treatment has allowed the phase transformation, associated with the shape-memory effect, to be recovered from the mechanical-milling process, which leaves the material in a high free-energy, amorphous condition. This same heat-treatment also deposits a thin oxide layer on the surfaces of the NiTi particles, which inhibits diffusion, and allows the shape-memory effect to be preserved through the hot-pressing procedure.

The presence of the NiTi particles in the matrix provide the possibility for the shape-memory properties to produce residual stresses in the matrix. It is assumed that the NiTi particles in the composite material attempt to resume their original shape as the phase transformation is induced, after the deformation. The degree to which this actually happens is unknown, although residual stresses are expected to generate in the vicinity of the particle/matrix interface. Upon generation, however, these stresses may restrain the phase transformation, and cause martensite to remain in the particle, thus relieving the surrounding stress fields. This behavior is termed *stress-induced martensite* (SIM), and is a phenomenon which may be quite possible in the work described. It is difficult to

155

determine the exact mechanism by which the shape-memory effect induces these stresses in the matrix. A theory needs to be developed and tested in order to present a legitimate understanding of the phenomenon.

Monotonic tensile tests, conducted at the University of Tennessee, have proven that the composite material has achieved an elevation in the yield strengths and ultimate strengths, as compared to the aluminum matrix material. Some materials have exhibited a 43% gain in the yield strength, however, the elongation is sharply reduced. Some materials have revealed an interesting decrease in the Young's modulus with the addition of the NiTi powders. This behavior is supposedly caused by a phenomenon called *stress-induced martensite*, in which the application of a pressure forces the shape-memory alloy to return to the martensitic phase. As a result, the hardness and modulus of these particles may be reduced, thus affecting the composite as a whole.

Mechanical testing has revealed that a better fatigue life performance has been achieved in the NiTi SMA reinforced aluminum composite material. At higher stress levels, especially those above the yield strength of the material, the improvement on the fatigue life of the composite material is outstanding, averaging between two to three orders of magnitude, and up to four orders of magnitude in some materials. However, at lower stress levels, the fatigue life remains virtually unchanged. All the tested materials show a strong convergence in the S-N curves near the yield strength. Usually, the effects of microstructure on fatigue life tend to be stronger at lower stresses, but this is the opposite of what has been found in the present case. It can be seen from the SEM study, that the overall cross-section of the sample is weakened from the continual void

formation during the extended period of cyclic loading. As a result, the prime mode of crack propagation is largely matrix-dominated, due to void coalescence through the matrix material. However, as evidenced by the SEM study of the crack faces, the stresses which cause the crack propagation vary for different load levels. For high stress levels, the primary stresses leading to a brittle failure are shear stresses, whereas for low stress levels, normal stresses contribute most towards a ductile type of fracture. It is, therefore, thought that much of the failure at high stress levels, as contrasted with the increase in fatigue life, is intrinsically linked to stress fields interacting with strain barriers, as described by the Peach-Koehler relation. In the present case at this time, it is difficult to quantitatively determine the exact mechanism by which the shape-memory alloy affects crack growth, but it may be possible that the increased fatigue life at higher stress levels, is due to a stress-induced phase transformation in the shape-memory particles. A deeper understanding of the relationship cannot be ascertained without some additional experimentation.

5.2 Suggested Future Research

Further research is necessary to determine the extent of the effect of the shape-memory particles on the matrix. The present research has shown that the NiTi particles and the shape-memory effect do indeed have an effect on the aluminum matrix and the properties of the material. Some of the most notable effects include an increase in yield strength and a decrease in elastic modulus. It is unknown how the particles interact with the matrix concerning the stress fields surrounding the NiTi particles, however, these stress fields are expected to take the form of residual stresses caused by the shape-memory effect or by differences in coefficients of thermal expansion. There may also be variations in these stress fields caused by the *stress-induced martensite* phenomenon. These variations may become especially pronounced under loading conditions and may have a direct influence on the rates and modes of crack growth. The present research has found enough evidence to postulate these basic principles, however, the natures of these ideas are essentially theoretical, and need to be supported by further experimental evidence.

At the present time, several experiments are being conducted in order to discover the nature of the shape-memory effect, detect the presence of residual stresses around the NiTi particles, and pinpoint the effects on the matrix, especially during mechanical testing. With the help of Dr. George M. Pharr, nanoindentation tests are being done to measure the existence and precise location of martensite in the NiTi particles. X-ray diffraction studies have been considered, and neutron scattering techniques are also being

utilized, in cooperation with Dr. Cam Hubbard, of the High Temperature Materials Laboratory (HTML) at ORNL, in an effort to discern the magnitudes of any residual stresses in the materials. With the exciting results from these tests, it may be possible to develop a more detailed model of strengthening in the nickel-titanium shape-memory alloy reinforced aluminum composite material.

PART VI.

ACKNOWLEDGEMENTS

6.1 The University of Tennessee, Knoxville

I am greatly indebted to my major professor, Prof. Peter K. Liaw, for his advice in tensile/fatigue testing, and also for encouraging me to "work hard, write good papers, publish excellent results, and 'become rich and famous'."

Grateful acknowledgements are due to Prof. Ray Buchanan and Prof. Thomas Meek for agreeing to be on my advisory committee. I am also thankful for their suggestions and encouraging words.

I would like to thank Dr. Miinshiou Huang for his continued mentoring instruction concerning computer usage and fatigue analysis. His continued friendship has been tireless and sacrificial, and I owe much of my success to him.

Dr. Jiahong Zhu stands in special regard for his mentorship and guidance in writing proposals and thesis papers, and also Dr. Yue-Hui He and his wife, Dr. Qiu-Hua Rao, for their endearing friendship.

Mr. Liang Jiang is highly esteemed for his knowledgeable and considerate support in conducting MTS fatigue tests.

I am in great appreciation of Prof. David Joy for his expertise in SEM instruction and usage.

I would also like to thank Mr. Mike Neal for his technical aid with computer hardware and slide presentations.

Many thanks are due to Mr. Doug Fielden and Mr. Greg Jones for their help in fabricating and maintaining the testing equiptment. Mr. Fielden was enthusiastic enough to specially machine the unique tensile test grips that were needed for the sample coupons.

6.2 The Oak Ridge National Laboratory

My gratitude is due to Dr. Terry N. Tiegs for providing me the opportunity to conduct research in the area of shape-memory alloys and aluminum matrix composites, and for providing two years of financial support. He is also responsible for the idea of a NiTi SMA/Al P/M MMC, and has faithfully offered expert theory and technical guidance throughout the course of research.

I am thankful to Prof. Kwang-Hsi Wu, a visiting Professor from Florida International University, who offered much support and concern during his stay. He continually went out of his way to offer many detailed instructions. He also conducted extensive research on the mechanical milling of NiTi powders and the heat treatment of the composite material. He discovered systematic inconsistencies in the temperature measurement methods and devised a working, alternative method for an accurate temperature control during hot pressing.

It has been a great pleasure working with Drs. Fred Montgomery and Rene Androsch, who are responsible for technical analyses, especially in detecting powder coatings and measuring phase transformations.

Mr. Paul Menchhofer is greatly valued for the technical assistance he contributed towards hot pressing, and Dr. Mike Santella for providing access to mechanical deformation machinery.

Many thanks to Mr. Tom Geer, our distinguished metallographist, and to Mr. Charles Justice for technical support.

6.3 The Southeastern Universities Research Association

I would like to give an extended appreciation to Prof. Tom Hutchinson for his continued support in the course of the research.

6.4 The National Science Foundation

Many thanks and a special appreciation are acknowledged for Dr. Delcie Durham and Ms. Mary Poats of the National Science Foundation.

REFERENCES

1. C. M. Wayman, Shape Memory Alloys, MRS Bulletin, pp. 49-56, April 1993.

2. Z. Nishiyama, Martensitic Transformation, Academic Press, Inc., New York, 1978.

3. T. Tiegs, K. Alexander, and P. Becher, Shape Memory Alloy Reinforcement of Metals, Oak Ridge National Laboratory, Metals and Ceramics Division, Oak Ridge, TN 1996.

4. I. P. Lipscomb and L. D. M. Nokes, The Application of Shape Memory Alloys in Medicine, Antony Rowe Ltd., 1996.

5. W. D. Armstrong, T. Lorentzen, P. Brondsted, and P. H. Larsen, An Experimental and Modeling Investigation of the External Strain, Internal Stress and Fiber Phase Transformation Behavior of a NiTi Actuated Aluminum Metal Matrix Composite, Acta Materialia, Vol. 46, No. 10, pp. 3455-3466, June, 1998.

6. Z. G. Wei, C. Y. Tang, W. B. Lee, L. S. Cui, and D. Z. Yang, Preparation of a Smart Composite Material with TiNiCu Shape-Memory Particulates in an Aluminum Matrix, Materials Letters, Vol. 32, pp. 313-317, 1997.

7. ASM Specialty Handbook®, Aluminum and Aluminum Alloys, ASM International®, 1994.

8. D. A. Porter and K. E. Easterling, Phase Transformations in Metals and Alloys, 2nd ed., Chapman & Hall, London, 1995.

9. L. Salvo, M. Suery, and F. Decomps, Age Hardening of Al-matrix Composites Containing Various Types of Reinforcements, ASM Journal; Fabrication of Particulates Reinforced Metal Composites, pp. 139-144, 1990.

10. T.G. Nieh and R.F. Karlack, Aging Characteristics of B₄C Reinforced 6061 Aluminum, Scripta Met. Vol. 18, No. 1, pp. 25-28, 1984.

11. I. J. Van Humbeeck, From a Seed to a Need: the Growth of Shape Memory Applications in Europe. Materials Research Society Symposium Proceedings, Vol. 246, 1992.

12. C. M. Jackson, H. J. Wagner, and R. J. Wasilewski, 55-Nitinol – The Alloy With A Memory: Its Physical Metallurgy, Properties and Applications, a report for the National Aeronautics and Space Administration (NASA), 1972.

13. D. R. Gaskell, Introduction to Metallurgical Thermodynamics, Taylor and Francis Publishers, 1981.

14. H. Tobushi, K. Tanaka, T. Hori, T. Sawada, and T. Hattori, Pseudoelasticity of NiTi Shape Memory Alloy (Dependence on Maximum Strain and Temperature), Japan Society of Mechanical Engineering, Series A, Vol. 36, No. 3, pp. 314-318, 1993.

15. J. Verhoeven, Fundamentals of Physical Metallurgy, John Wiley & Sons, 1975.

16. G. Deiter, Mechanical Metallurgy, McGraw-Hill Publishers, 1986.

17. E. Nembach, Particle Strengthening of Metals and Alloys, John Wiley & Sons, 1997.

18. Composites I: The Basics (A study course booklet), Vol. 2 on Matrix Materials, American Society of Metals, 1984.

19. A. L. Geiger and J. A. Walker, The Processing and Properties of Discontinuously Reinforced Aluminum Composites, JOM, pp. 8-15, August 1991.

20. Z. Hashin and S. Shrtikman, J. Mech. Phys. Solids, vol. 11, p. 127, 1963.

21. Y. Furuya, A. Sasaki, and M. Taya, Enhanced Mechanical Properties of NiTi Shape Memory Fiber/Al Matrix Composite, Materials Transactions, JIM, Vol. 34, No. 3, pp. 224-227, 1993.

22. Y. Furuya, Intelligent Material Design Using Shape Memory Alloy, Mat. Res. Soc. Symp. Proc., Vol. 360, Materials Research Society, 1995.

23. D. J. Lloyd, Particle Reinforced Aluminum and Magnesium Matrix Composites, International Materials Reviews, Vol. 39, No. 1, pp. 1-23, 1994.

24. G. A. Porter, P. K. Liaw, T. N. Tiegs, and K. H. Wu, Shape-Memory Alloy Reinforced Aluminum Composites, Final Report for the Southeast Universities Research Association (SURA), October, 1999.

25. Y. W. Kim, W. M. Griffith, and F. H. Froes, Surface Oxides in Powder Metallurgy Aluminum Alloys, JOM, pp. 27-33, August 1985.

26. J. L. Estrada and J. Duszczyk, Relationship Between Degassing Conditions and Tensile Properties of Al-20Si-X P/M Products, Journal of Materials Science, Vol. 26, pp. 4203-4207, 1991.

27. H. Chung and B. Kim, <u>Powder Metallurgy at KIMM, Korea</u>, The International Journal of Powder Metallurgy, Vol. 32, No. 2, pp. 137-143, 1996.

28. F. H. Froes and D. Eylon, <u>Powder Metallurgy of Titanium Alloys</u>, International Materials Reviews, Vol. 35, No. 3, pp. 162-182, 1990.

29. R. M. German, <u>Powder Metallurgy Science</u>, Metal Powder Industries Federation, Princeton N.J., 1989.

30. S. Zhang, L. Lu, and M. O. Lai, <u>Cu-Based Shape Memory Powder Preparation Using the Mechanical Alloying Technique</u>, Materials Science and Engineering, A171, pp. 257-262, 1993.

31. S. M. Green, D. M. Grant, and J. V. Wood, <u>XPS Characterization of Surface Modified NiTi Shape Memory Alloy</u>, Materials Science and Engineering, A224, pp. 21-26, 1997.

32. <u>CRC Handbook of Chemistry and Physics</u>, 1st Student Edition, CRC Press, 1988.

33. ASM Handbook, Vol. 3, <u>Alloy Phase Diagrams</u>, ASM International, Materials Park, Ohio, 1992.

34. R. W. Hertzberg, <u>Deformation and Fracture Mechanics of Engineering Materials</u>, John Wiley and Sons, Inc., New York, 1996.

35. Y. V. R. K. Prasad, H. L. Gegel, S. M. Doraivelu, J. C. Malas, J. T. Morgan, K. A. Lark, and D. R. Barker, <u>Modeling of Dynamic Material Behavior in Hot Deformation: Forging of Ti-6242</u>, Metallurgical Transactions A, Vol. 15A, pp. 1883-1892, Oct. 1984.

36. J. R. Pickens, T. J. Langan, R. O. England, and M. Liebson, <u>A Study of the Hot-Working Behavior of SiC-Al Alloy Composites and Their Matrix Alloys by Hot Torsion Testing</u>, Metallurgical Transactions A, Vol. 18A, pp. 303-310, Feb. 1987.

37. T. S. Hutchison and D. C. Baird, <u>The Physics of Engineering Solids</u>, Royal Military College of Canada, New York and London, John Wiley and Sons, Inc., 1963.

38. ASTM (American Society for Testing and Materials) Standard (E8M-91), "<u>Standard Test Methods of Tension Testing of Metallic Materials,</u>" 1996.

39. H. Tada, P. C. Paris, and G. R. Irwin, <u>The Stress analysis of Cracks Handbook</u>, Del Research Corporation, Hellertown PA, 1973.

40. S. H. Wu, B. R. Patterson, and M. K. Ferber, <u>Influence of Crack Path on Fracture Toughness of Ceramic Matrix Composites,</u> 100th Annual Meeting of the American Ceramics Society, Cincinnati, OH, 1998

41. M. S. Huang, <u>A Multivariant Model for Shape Memory Alloys,</u> Ph.D. dissertation, Northwestern University, Evanston, IL, December 1997.

42. Y. Liu, Z. Xie, J. Van Humbeeck, and L. Delaey, <u>Asymmetry of Stress-Strain Curves Under Tension and Compression for NiTi Shape Memory Alloys,</u> Acta Met, Vol. 46. No. 12. pp. 4325-4338, 1998.

43. Y. Liu and P. G. Mc Cormick, <u>Criteria of Transformation Sequences in NiTi Shape Memory Alloys,</u> Materials Transactions, JIM, Vol. 37, No. 4, pp. 691-696, 1996.

44. M. Kawaguchi, Y. Ohashi, and H. Tobushi, <u>Cyclic Characteristics of Pseudoelasticity of NiTi Alloys (Effect of Maximum Strain, Test Temperature and Shape Memory Processing Temperature),</u> Japan Society of Mechanical Engineering, Series I, Vol. 34, No. 1, pp. 76-82, 1991.

45. H. Tobushi and K. Tanaka, <u>Deformation of a Shape Memory Alloy Helical Spring (Analysis Based on Stress-Strain-Temperature Relation),</u> Japan Society of Mechanical Engineering, Series I, Vol. 34, No. 1, pp. 83-89, 1991.

46. T. Sawada, H. Tobushi, K. Kimura, T. Hattori, K. Tanaka, and P. H. Lin, <u>Stress-Strain-Temperature Relationship Associated with the R-Phase Transformation in NiTi Shape Memory Alloy (Influence of Shape Memory Processing Temperature),</u> Japan Society of Mechanical Engineering, Series A, Vol. 36, No. 4, pp. 395-401, 1993.

47. P. H. Lin, H. Tobushi, K. Tanaka, and A. Ikai, <u>Deformation Properties of NiTi Shape Memory Alloy,</u> Japan Society of Mechanical Engineering, Series A, Vol. 39, No. 1, pp. 108-116, 1996.

48. P. H. Lin, H. Tobushi, K. Tanaka, and A. Ikai, <u>Influence of Strain Rate on Deformation Properties of NiTi Shape Memory Alloy,</u> Japan Society of Mechanical Engineering, Series A, Vol. 39, No. 1, pp. 117-123, 1996.

49. R. E. Newnham, <u>Molecular Mechanisms in Smart Materials,</u> MRS Bulletin, pp. 20-34, May, 1997.

50. I. E. Campbell and E. M. Sherwood, <u>High-Temperature Materials and Technology,</u> The Electrochemical Society, Inc., John Wiley & Sons.

Glen Andrew Porter was born in Columbus, Ohio, in the United States, on March 5, 1972. As a child, he took a great interest in the fine arts, especially in drawing and sculpture. He attended the *Columbus College of Art and Design* - Saturday School Program for eight years, winning full scholarships in merit of his work for seven of those years, and a partial scholarship for one year. He received his high-school education at *Madison Plains High School*, in London, Ohio, in which he learned the art of drafting, welding and metalsmithing, among other crafts. Finding a great interest and talent in these fields, he held several related positions following graduation. Glen endured a formal training as a die-makers apprentice under Karl Kuzela at the *Superior Die, Tool and Machine Co.* He was tutored in the fine art of hammer-mill body-working techniques, by the esteemed Greg Brickles, while professionally restoring antique automobiles. He also served as an assembly line welder at *Tomasco Mulciber Inc.*, a subsidiary of the *Honda Motor Co.*, producing hanger beams; a safety part having high standards for tolerances.

Following these endeavors, Glen pursued his further education at *Carson-Newman College*, in Jefferson City, Tennessee, and graduated with his Bachelor of Arts degree, with a major in Physics, in May, 1997. He enrolled at the *University of Tennessee* in Knoxville, that fall, and obtained his Master of Science Degree in Metallurgical Engineering, in May, 2000, under the advisory supervision of Prof. Peter K. Liaw. Glen performed research work at the Oak Ridge National Laboratory, in Oak Ridge, Tennessee, under Dr. Terry N. Tiegs, as part of his Thesis requirements. In doing so, he has delivered two Metallurgical Society presentations and has written over five publications concerning shape-memory alloy reinforced aluminum composites.